



12-2013

Synthesis and Characterization of 2,2-cis-  
[Rh<sub>2</sub>(NPhCOCH<sub>3</sub>)<sub>4</sub>]•NCC<sub>6</sub>H<sub>4</sub>R where R = H,  
2-CH<sub>3</sub>, 3-CH<sub>3</sub>, 4-CH<sub>3</sub> and  
[Rh<sub>2</sub>(O<sub>2</sub>CCH<sub>3</sub>)(NPhCOCF<sub>3</sub>)<sub>3</sub>]

Fredricka F. Quarshie  
East Tennessee State University

Follow this and additional works at: <https://dc.etsu.edu/etd>

 Part of the [Inorganic Chemistry Commons](#)

#### Recommended Citation

Quarshie, Fredricka F., "Synthesis and Characterization of 2,2-cis-[Rh<sub>2</sub>(NPhCOCH<sub>3</sub>)<sub>4</sub>]•NCC<sub>6</sub>H<sub>4</sub>R where R = H, 2-CH<sub>3</sub>, 3-CH<sub>3</sub>, 4-CH<sub>3</sub> and [Rh<sub>2</sub>(O<sub>2</sub>CCH<sub>3</sub>)(NPhCOCF<sub>3</sub>)<sub>3</sub>]" (2013). *Electronic Theses and Dissertations*. Paper 2289. <https://dc.etsu.edu/etd/2289>

This Thesis - Open Access is brought to you for free and open access by the Student Works at Digital Commons @ East Tennessee State University. It has been accepted for inclusion in Electronic Theses and Dissertations by an authorized administrator of Digital Commons @ East Tennessee State University. For more information, please contact [digilib@etsu.edu](mailto:digilib@etsu.edu).

Synthesis and Characterization of 2,2-*cis*-[Rh<sub>2</sub>(NPhCOCH<sub>3</sub>)<sub>4</sub>]•NCC<sub>6</sub>H<sub>4</sub>R where R = H, 2-CH<sub>3</sub>, 3-CH<sub>3</sub>, 4-CH<sub>3</sub> and [Rh<sub>2</sub>(O<sub>2</sub>CCH<sub>3</sub>)(NPhCOCF<sub>3</sub>)<sub>3</sub>]

---

A thesis

presented to

the Faculty of the Department of Chemistry

East Tennessee State University

In partial Fulfillment

of the requirements for the degree

Master of Science in Chemistry

---

by

Fredricka Francisca Quarshie

December 2013

---

Dr. Cassandra T. Eagle, Chair

Dr. Ismail Kady

Dr. Ningfeng Zhao

Keywords: X-ray Crystal structure, Dirhodium, Phenylacetamide, dimeric rhodium, Rh<sub>2</sub>L<sub>4</sub>,  
nitriles

## ABSTRACT

Synthesis and Characterization of 2,2-*cis*-[Rh<sub>2</sub>(NPhCOCH<sub>3</sub>)<sub>4</sub>]•NCC<sub>6</sub>H<sub>4</sub>R where R = H, 2-CH<sub>3</sub>, 3-CH<sub>3</sub>, 4-CH<sub>3</sub> and [Rh<sub>2</sub>(O<sub>2</sub>CCH<sub>3</sub>)(NPhCOCF<sub>3</sub>)<sub>3</sub>]

by

Fredricka Francisca Quarshie

Five novel compounds were synthesized and characterized. Crystal structures were determined using Rigaku Mercury 375/MCCD(XtaLAB mini) diffractometer with graphite monochromated MoK $\alpha$  radiation. The crystal structures of [Rh<sub>2</sub>(NPhCOCH<sub>3</sub>)<sub>4</sub>]•xNCC<sub>6</sub>H<sub>4</sub>R where x = 1 or 2 and R=H, 2-CH<sub>3</sub>,3-CH<sub>3</sub> and 4-CH<sub>3</sub> were solved to an R<sub>1</sub> value of less than 5 (R<sub>1</sub>= $\Sigma||F_o| - |F_c|| / \Sigma |F_o|$ ). In each of the nitrile complexes, the rhodium is five or six coordinate and possesses pseudo D<sub>4h</sub> symmetry. The complexes were also characterized by NMR and IR spectroscopy.

[Rh<sub>2</sub>(CO<sub>2</sub>CCH<sub>3</sub>)(PhCOCF<sub>3</sub>)<sub>3</sub>] was also synthesized. In this complex, each rhodium atom is six coordinate, thus each rhodium is in an octahedral environment. Details of each synthesized complex are discussed.

## DEDICATION

I dedicate this work to the Almighty God and to my dear daughter Huldah.

## ACKNOWLEDEMENTS

I am thankful to Almighty God for His guidance and protection over my life and especially for granting me the opportunity to have my graduate studies at ETSU.

I am very grateful to my supervisor, Dr. Cassandra T Eagle, for her professional guidance and mentorship of this research. My sincere gratitude also goes to Dr. Ismail Kady and Dr. Ningfeng Zhao for serving on my committee and for their advice and suggestions on this work. I am grateful to Dr. Jeff Wardeska for his help. I thank the faculty and staff of the department of Chemistry ETSU, especially Dr. Reza Mohseni, Miss Jillian Quirante, and Mr. Ryan Alexander. I am grateful to Dr. Lee Daniels of Rigaku Americas for all the help he gave me in solving crystal structures.

My gratitude goes to my late dad and my sweet mum who made me realize the value of education. Mum, I say thank you so much for your immense prayer support and words of encouragement that has inspired me to come this far. My love goes to my dearest fiancé Andrew and my daughter Huldah for their love and prayers during my studies.

I also thank my Godparents Dr. and Mrs. Nyarambi and their family for their encouragement, prayer, support, and guidance throughout my course. I thank all the graduate students in the chemistry department. You have been awesome!

Finally, I thank Kenneth Kpogo, Nkongho Atem-Tambe, Megan Ketron, Cragin Harris and John Jordan for shared ideas in the Eagle research group.

## TABLE OF CONTENTS

	Page
ABSTRACT.....	2
DEDICATION.....	3
ACKNOWLEDGEMENTS.....	4
LIST OF TABLES.....	9
LIST OF FIGURES.....	11
Chapter	
1. INTRODUCTION.....	16
Practical Application of Rhodium Acetate Complexes.....	22
Preparative Methods and Classification.....	23
Tetrakis Carboxamidato Dirhodium (II) (Rhodium Carboxamidate).....	24
2.EXPERIMENTAL.....	30
Reagents.....	30
Instruments.....	30
Synthesis of $[\text{Rh}_2(\text{O}_2\text{CCH}_3)(\text{NPhCOCF}_3)_3]$ .....	30
Glassware.....	30
Observation .....	32
Thin-Layer Chromatography.....	33
Evaporation of Chlorobenzene.....	34
Flash Column Chromatography .....	35
Synthesis of 2,2- <i>cis</i> - $[\text{Rh}_2(\text{NPhCOCH}_4)_4]$ ·Nitrile.....	37
Benzonitrile Complex and Crystallization.....	37

Vapor Diffusion Method .....	38
<i>O</i> -Tolunitrile Complex and Crystallization.....	38
<i>M</i> -Tolunitrile Complex and Crystallization .....	38
<i>P</i> -Tolunitrile Complex and Crystallization .....	39
Synthesis of 200 equivalents of Nitriles .....	39
Synthesis of $[\text{Rh}_2(\text{O}_2\text{CCH}_3)(\text{NPhCOCF}_3)_3] \cdot \text{NCC}_6\text{H}_5$ complex .....	39
X-ray Crystallographic Studies.....	40
Data Collection.....	40
<i>2,2-cis</i> - $[\text{Rh}_2(\text{NPhCOCH}_4)_4] \cdot 2\text{NCC}_6\text{H}_5$ complex .....	40
Benzonitrile (Two Equivalents) .....	40
<i>2,2-cis</i> - $[\text{Rh}_2(\text{NPhCOCH}_4)_4] \cdot \text{NC}(\{2\text{-CH}_3\}\text{C}_6\text{H}_4)$ complex.....	40
<i>O</i> -Tolunitrile (One Equivalents) .....	40
<i>2,2-cis</i> - $[\text{Rh}_2(\text{NPhCOCH}_4)_4] \cdot \text{NC}(\{3\text{-CH}_3\}\text{C}_6\text{H}_4)$ complex.....	41
<i>M</i> -Tolunitrile (One Equivalent).....	41
<i>2,2-cis</i> - $[\text{Rh}_2(\text{NPhCOCH}_4)_4] \cdot \text{NC}(\{4\text{-CH}_3\}\text{C}_6\text{H}_4)$ complex.....	41
<i>P</i> -Tolunitrile (Two Equivalents) .....	41
<i>2,2-cis</i> - $[\text{Rh}_2(\text{NPhCOCH}_4)_4] \cdot \text{NC}(\{2\text{-CH}_3\}\text{C}_6\text{H}_4)$ complex.....	41
<i>O</i> -Tolunitrile (Two Equivalents) .....	41

2,2- <i>cis</i> -[Rh <sub>2</sub> (NPhCOCH <sub>4</sub> ) <sub>4</sub> ]·NC({3-CH <sub>3</sub> }C <sub>6</sub> H <sub>4</sub> ) complex.....	42
<i>M</i> -Tolunitrile (Two Equivalents) .....	42
[Rh <sub>2</sub> (O <sub>2</sub> CCH <sub>3</sub> )(NPhCOCF <sub>3</sub> ) <sub>3</sub> ]·NCC <sub>6</sub> H <sub>5</sub> complex.....	42
<b>3. RESULTS AND DISCUSSION .....</b>	<b>43</b>
Fourier Transform Infrared Spectrometer (FTIR) Data.....	43
<sup>1</sup> H NMR Data .....	54
X-ray Results .....	111
2,2- <i>cis</i> -[Rh <sub>2</sub> (NPhCOCH <sub>4</sub> ) <sub>4</sub> ]·2NCC <sub>6</sub> H <sub>5</sub> complex .....	111
Benzonitrile (Two Equivalents) .....	111
2,2- <i>cis</i> -[Rh <sub>2</sub> (NPhCOCH <sub>4</sub> ) <sub>4</sub> ]·NC({2-CH <sub>3</sub> }C <sub>6</sub> H <sub>4</sub> ) complex.....	115
<i>O</i> -Tolunitrile (One Equivalent) .....	115
2,2- <i>cis</i> -[Rh <sub>2</sub> (NPhCOCH <sub>4</sub> ) <sub>4</sub> ]·NC({3-CH <sub>3</sub> }C <sub>6</sub> H <sub>4</sub> ) complex.....	119
<i>M</i> -Tolunitrile (One Equivalent).....	119
2,2- <i>cis</i> -[Rh <sub>2</sub> (NPhCOCH <sub>4</sub> ) <sub>4</sub> ]·NC({4-CH <sub>3</sub> }C <sub>6</sub> H <sub>4</sub> ) complex.....	122
<i>P</i> -Tolunitrile (Two Equivalents) .....	122
2,2- <i>cis</i> -[Rh <sub>2</sub> (NPhCOCH <sub>4</sub> ) <sub>4</sub> ]·NC({2-CH <sub>3</sub> }C <sub>6</sub> H <sub>4</sub> ) complex.....	126
<i>O</i> -Tolunitrile (Two Equivalents) .....	126



2,2- <i>cis</i> -[Rh <sub>2</sub> (NPhCOCH <sub>4</sub> ) <sub>4</sub> ]·NC({3-CH <sub>3</sub> }C <sub>6</sub> H <sub>4</sub> ) complex.....	129
<i>M</i> -Tolunitrile (Two Equivalents) .....	129
[Rh <sub>2</sub> (O <sub>2</sub> CCH <sub>3</sub> )(NPhCOCF <sub>3</sub> ) <sub>3</sub> ] complex.....	135
4.CONCLUSION.....	140
REFERENCES.....	143
VITA.....	146

## LIST OF TABLES

Table	Page
Table 3.1: Phenyl Peak Positions and Protons for Uncomplexed Benzonitrile.....	56
Table 3.2: Phenyl Peak Positions and Protons for 2,2- <i>cis</i> -[Rh <sub>2</sub> (NPhCOCH <sub>4</sub> ) <sub>4</sub> ]·2NCC <sub>6</sub> H <sub>5</sub> complex.....	60
Table 3.3: Phenyl Peak Positions and Protons for Uncomplexed <i>o</i> -tolunitrile.....	65
Table 3.4: Phenyl Peak Positions and Protons for 2,2- <i>cis</i> -[Rh <sub>2</sub> (NPhCOCH <sub>4</sub> ) <sub>4</sub> ]·NC({2-CH <sub>3</sub> }C <sub>6</sub> H <sub>4</sub> ) complex.....	72
Table 3.5: Phenyl Peak Positions and Protons for Uncomplexed <i>m</i> -tolunitrile .....	77
Table 3.6: Phenyl Peak Positions and Protons for 2,2- <i>cis</i> -[Rh <sub>2</sub> (NPhCOCH <sub>4</sub> ) <sub>4</sub> ]·NC({3-CH <sub>3</sub> }C <sub>6</sub> H <sub>4</sub> ) complex.....	83
Table 3.7: Phenyl Peak Positions and Protons for Uncomplexed <i>p</i> -tolunitrile.....	89
Table 3.8: Phenyl Peak Positions and Protons for 2,2- <i>cis</i> -[Rh <sub>2</sub> (NPhCOCH <sub>4</sub> ) <sub>4</sub> ]·NC({4-CH <sub>3</sub> }C <sub>6</sub> H <sub>4</sub> ) complex.....	95
Table 3.9: Phenyl Peak Positions and Protons for 2,2,2-trifluoro-N-phenylacetamide (NPhCOCF <sub>3</sub> ).....	101
Table 3.10: Phenyl Peak Positions and Protons for [Rh <sub>2</sub> (O <sub>2</sub> CCH <sub>3</sub> )(NPhCOCH <sub>3</sub> ) <sub>3</sub> ]·2NCC <sub>6</sub> H <sub>5</sub> complex .....	107
Table 3.11: Crystallographic Data of 2,2- <i>cis</i> -[Rh <sub>2</sub> (NPhCOCH <sub>4</sub> ) <sub>4</sub> ]·2NCC <sub>6</sub> H <sub>5</sub> .....	113
Table 3.12: Crystallographic Data of 2,2- <i>cis</i> -[Rh <sub>2</sub> (NPhCOCH <sub>4</sub> ) <sub>4</sub> ]·NC({2-CH <sub>3</sub> }C <sub>6</sub> H <sub>4</sub> ) complex.....	117
Table 3.13: Crystallographic Data of 2,2- <i>cis</i> -[Rh <sub>2</sub> (NPhCOCH <sub>4</sub> ) <sub>4</sub> ]·NC({3-CH <sub>3</sub> }C <sub>6</sub> H <sub>4</sub> ) complex.....	120

Table 3.14: Crystallographic Data of 2,2- <i>cis</i> -[Rh <sub>2</sub> (NPhCOCH <sub>4</sub> ) <sub>4</sub> ]·NC({4-CH <sub>3</sub> }C <sub>6</sub> H <sub>4</sub> ) complex.....	124
Table 3.15: Crystallographic Data of 2,2- <i>cis</i> -[Rh <sub>2</sub> (NPhCOCH <sub>4</sub> ) <sub>4</sub> ]·NC({2-CH <sub>3</sub> }C <sub>6</sub> H <sub>4</sub> ) complex.....	127
Table 3.16: Crystallographic Data of 2,2- <i>cis</i> -[Rh <sub>2</sub> (NPhCOCH <sub>4</sub> ) <sub>4</sub> ]·NC({3-CH <sub>3</sub> }C <sub>6</sub> H <sub>4</sub> ) complex.....	131
Table 3.17: The Bond Angles and Bond Lengths of Interest in Complexes of 2,2- <i>cis</i> - [Rh <sub>2</sub> (N(C <sub>6</sub> H <sub>5</sub> )COCH <sub>3</sub> ) <sub>4</sub> ].....	135
Table 3.18: Crystallographic Data of [Rh <sub>2</sub> (O <sub>2</sub> CCH <sub>3</sub> )(NPhCOCH <sub>3</sub> ) <sub>3</sub> ]·2NCC <sub>6</sub> H <sub>5</sub> complex.....	138

## LIST OF FIGURES

Figure	Page
Figure 1.1: The overlaps of $d_z^2$ and the resulting energy levels.....	18
Figure 1.2: The overlaps of $d_{xz}$ and the resulting energy levels.....	18
Figure 1.3: The overlaps of $d_{yz}$ and the resulting energy levels.....	18
Figure 1.4: The overlaps of $d_x^2, d_y^2$ and the resulting energy levels.....	19
Figure 1.5: The overlaps of $d_{xy}$ and the resulting energy levels.....	19
Figure 1.6: Molecular orbital diagram of rhodium acetate ( $Rh_2OAc_4$ ).....	20
Figure 1.7: $\sigma$ - Bonding .....	21
Figure 1.8: $\pi$ - Back- Bonding.....	21
Figure 1.9: Scheme of rhodium carboxamidate .....	25
Figure 1.10: Picture of rhodium carboxamidate .....	25
Figure 1.11: Diagrammatic representation of the paddlewheel structure around a Rh-Rh Axi.....	26
Figure 2.1: Set-up of the synthesis of $[Rh_2(O_2CCH_3)(NPhCOCF_3)_3]$ .....	33
Figure 2.2: Rotary evaporation of Chlorobenzene from reaction mixture .....	34
Figure 2.3: Set-up for Flash Column Chromatography.....	36
Figure 2.4: IR of Uncomplexed benzonitrile ( $NCC_6H_5$ ) .....	44
Figure 3.2: IR of 2,2- <i>cis</i> - $[Rh_2(NPhCOCH_4)_4] \cdot 2NCC_6H_5$ complex .....	45
Figure 3.3: IR of Uncomplexed <i>o</i> - tolunitrile ( $NCC_7H_7$ ) .....	46
Figure 3.4: IR of 2,2- <i>cis</i> - $[Rh_2(NPhCOCH_4)_4] \cdot NC(\{2-CH_3\}C_6H_4)$ complex .....	47
Figure 3.5: IR of Uncomplexed <i>m</i> - tolunitrile ( $NCC_7H_7$ ) .....	48

Figure 3.6: IR of 2,2- <i>cis</i> -[Rh <sub>2</sub> (NPhCOCH <sub>4</sub> ) <sub>4</sub> ]·NC({3-CH <sub>3</sub> }C <sub>6</sub> H <sub>4</sub> ) complex .....	49
Figure 3.7: IR of Uncomplexed <i>p</i> -tolunitrile (NCC <sub>7</sub> H <sub>7</sub> ).....	50
Figure 3.8: IR of 2,2- <i>cis</i> -[Rh <sub>2</sub> (NPhCOCH <sub>4</sub> ) <sub>4</sub> ]·NC({4-CH <sub>3</sub> }C <sub>6</sub> H <sub>4</sub> ) complex .....	51
Figure 3.9: IR of [Rh <sub>2</sub> (O <sub>2</sub> CCH <sub>3</sub> )(NPhCOCF <sub>3</sub> ) <sub>3</sub> ]·NCC <sub>6</sub> H <sub>5</sub> complex .....	52
Figure 3.10: <sup>1</sup> H labels of Uncomplexed benzonitrile.....	55
Figure 3.11: <sup>1</sup> HNMR spectrum of Uncomplexed benzonitrile.....	57
Figure 3.12: <sup>1</sup> H labels of 2,2- <i>cis</i> -[Rh <sub>2</sub> (NPhCOCH <sub>4</sub> ) <sub>4</sub> ]·2NCC <sub>6</sub> H <sub>5</sub> complex.....	59
Figure 3.13: <sup>1</sup> HNMR spectrum of 2,2- <i>cis</i> -[Rh <sub>2</sub> (NPhCOCH <sub>4</sub> ) <sub>4</sub> ]·2NCC <sub>6</sub> H <sub>5</sub> complex.....	61
Figure 3.14: <sup>1</sup> HNMR spectrum of 2,2- <i>cis</i> -[Rh <sub>2</sub> (NPhCOCH <sub>4</sub> ) <sub>4</sub> ]·2NCC <sub>6</sub> H <sub>5</sub> complex (Expanded region 1.2ppm -2.7ppm).....	62
Figure 3.15: <sup>1</sup> HNMR spectrum of 2,2- <i>cis</i> -[Rh <sub>2</sub> (NPhCOCH <sub>4</sub> ) <sub>4</sub> ]·2NCC <sub>6</sub> H <sub>5</sub> complex (Expanded region 6.6ppm -7.7ppm).....	63
Figure 3.16: <sup>1</sup> H labels of Uncomplexed <i>o</i> -tolunitrile.....	64
Figure 3.17: <sup>1</sup> HNMR spectrum of Uncomplexed <i>o</i> -tolunitrile.....	66
Figure 3.18: <sup>1</sup> HNMR spectrum of Uncomplexed <i>o</i> -tolunitrile (expanded region 1.8ppm-2.6ppm).....	67
Figure 3.19: <sup>1</sup> HNMR spectrum of Uncomplexed <i>o</i> -tolunitrile (expanded region 1.2ppm-2.6ppm).....	68
Figure 3.20: <sup>1</sup> H labels of Uncomplexed <i>o</i> -tolunitrile (expanded region 7.0ppm-7.8ppm).....	69
Figure 3.21: <sup>1</sup> H labels of 2,2- <i>cis</i> -[Rh <sub>2</sub> (NPhCOCH <sub>4</sub> ) <sub>4</sub> ]·NC({2-CH <sub>3</sub> }C <sub>6</sub> H <sub>4</sub> ) complex .....	71
Figure 3.22: <sup>1</sup> HNMR spectrum of 2,2- <i>cis</i> -[Rh <sub>2</sub> (NPhCOCH <sub>4</sub> ) <sub>4</sub> ]·NC({2-CH <sub>3</sub> }C <sub>6</sub> H <sub>4</sub> ) complex.....	73

Figure 3.23: $^1\text{H}$ NMR spectrum of 2,2- <i>cis</i> - $[\text{Rh}_2(\text{NPhCOCH}_3)_4]\cdot\text{NC}(\{2\text{-CH}_3\}\text{C}_6\text{H}_4)$ complex (expanded region 1.2ppm-2.6ppm).....	74
Figure 3.24: $^1\text{H}$ NMR spectrum of 2,2- <i>cis</i> - $[\text{Rh}_2(\text{NPhCOCH}_3)_4]\cdot\text{NC}(\{2\text{-CH}_3\}\text{C}_6\text{H}_4)$ complex (expanded region 6.7ppm-7.6ppm) .....	76
Figure 3.25: $^1\text{H}$ labels of Uncomplexed <i>m</i> -tolunitrile .....	76
Figure 3.26: $^1\text{H}$ NMR spectrum of Uncomplexed <i>m</i> -tolunitrile .....	78
Figure 3.27: $^1\text{H}$ NMR spectrum of Uncomplexed <i>m</i> -tolunitrile (expanded region 1.6ppm- 2.9ppm).....	79
Figure 3.28: $^1\text{H}$ NMR spectrum of Uncomplexed <i>m</i> -tolunitrile (expanded region 7.2ppm- 7.6ppm).....	80
Figure 3.29: $^1\text{H}$ labels of 2,2- <i>cis</i> - $[\text{Rh}_2(\text{NPhCOCH}_3)_4]\cdot\text{NC}(\{3\text{-CH}_3\}\text{C}_6\text{H}_4)$ complex.....	82
Figure 3.30: $^1\text{H}$ NMR spectrum of 2,2- <i>cis</i> - $[\text{Rh}_2(\text{NPhCOCH}_3)_4]\cdot\text{NC}(\{3\text{-CH}_3\}\text{C}_6\text{H}_4)$ complex.....	84
Figure 3.31: $^1\text{H}$ NMR spectrum of 2,2- <i>cis</i> - $[\text{Rh}_2(\text{NPhCOCH}_3)_4]\cdot\text{NC}(\{3\text{-CH}_3\}\text{C}_6\text{H}_4)$ complex(expanded region 1.1ppm-1.7ppm).....	85
Figure 3.32: $^1\text{H}$ NMR spectrum of 2,2- <i>cis</i> - $[\text{Rh}_2(\text{NPhCOCH}_3)_4]\cdot\text{NC}(\{3\text{-CH}_3\}\text{C}_6\text{H}_4)$ complex(expanded region 1.8ppm-2.5ppm).....	86
Figure 3.33: $^1\text{H}$ NMR spectrum of 2,2- <i>cis</i> - $[\text{Rh}_2(\text{NPhCOCH}_3)_4]\cdot\text{NC}(\{3\text{-CH}_3\}\text{C}_6\text{H}_4)$ complex(expanded region 6.9ppm-7.5ppm).....	87
Figure 3.34: $^1\text{H}$ labels of Uncomplexed <i>p</i> -tolunitrile .....	88
Figure 3.35: $^1\text{H}$ NMR spectrum of Uncomplexed <i>p</i> -tolunitrile.....	90
Figure 3.36: $^1\text{H}$ NMR spectrum of Uncomplexed <i>p</i> -tolunitrile (expanded region 1.6ppm- 2.5ppm).....	91

Figure 3.37: $^1\text{H}$ NMR spectrum of Uncomplexed <i>p</i> -tolunitrile (expanded region 6.8ppm-7.0ppm).....	92
Figure 3.38: $^1\text{H}$ labels of 2,2- <i>cis</i> - $[\text{Rh}_2(\text{NPhCOCH}_4)_4]\cdot\text{NC}(\{4\text{-CH}_3\}\text{C}_6\text{H}_4)$ complex.....	94
Figure 3.39: $^1\text{H}$ NMR spectrum of 2,2- <i>cis</i> - $[\text{Rh}_2(\text{NPhCOCH}_4)_4]\cdot\text{NC}(\{4\text{-CH}_3\}\text{C}_6\text{H}_4)$ complex.....	96
Figure 3.40: $^1\text{H}$ NMR spectrum of 2, 2- <i>cis</i> - $[\text{Rh}_2(\text{NPhCOCH}_4)_4]\cdot\text{NC}(\{4\text{CH}_3\}\text{C}_6\text{H}_4)$ complex.....	97
Figure 3.41: $^1\text{H}$ NMR spectrum of 2,2- <i>cis</i> - $[\text{Rh}_2(\text{NPhCOCH}_4)_4]\cdot\text{NC}(\{4\text{-CH}_3\}\text{C}_6\text{H}_4)$ complex(expanded region 1.0ppm-6.0ppm) .....	98
Figure 3.42: $^1\text{H}$ NMR spectrum of 2, 2- <i>cis</i> - $[\text{Rh}_2(\text{NPhCOCH}_4)_4]\cdot\text{NC}(\{4\text{-CH}_3\}\text{C}_6\text{H}_4)$ complex(expanded region 1.0ppm-8.0ppm).....	99
Figure 3.43: $^1\text{H}$ labels for 2,2,2-trifluoro-N-phenylacetamide ( $\text{NPhCOCF}_3$ ).....	100
Figure 3.44: $^1\text{H}$ NMR for 2,2,2-trifluoro-N-phenylacetamide ( $\text{NPhCOCF}_3$ ).....	102
Figure 3.45: $^1\text{H}$ NMR for 2,2,2-trifluoro-N-phenylacetamide ( $\text{NPhCOCF}_3$ )(expanded region 1.8ppm-2.3ppm).....	103
Figure 3.46: $^1\text{H}$ NMR for 2,2,2-trifluoro-N-phenylacetamide ( $\text{NPhCOCF}_3$ )(expanded region 7.2ppm-7.6ppm).....	104
Figure 3.47: $^1\text{H}$ labels for $[\text{Rh}_2(\text{O}_2\text{CCH}_3)(\text{NPhCOCF}_3)_3]\cdot\text{NCC}_6\text{H}_5$ complex.....	106
Figure 3.48: $^1\text{H}$ NMR for $[\text{Rh}_2(\text{O}_2\text{CCH}_3)(\text{NPhCOCF}_3)_3]\cdot\text{NCC}_6\text{H}_5$ complex.....	108
Figure 3.49: $^1\text{H}$ NMR for $[\text{Rh}_2(\text{O}_2\text{CCH}_3)(\text{NPhCOCF}_3)_3]\cdot\text{NCC}_6\text{H}_5$ complex(expanded region 0.4ppm-2.5ppm).....	109
Figure 3.50: $^1\text{H}$ NMR for $[\text{Rh}_2(\text{O}_2\text{CCH}_3)(\text{NPhCOCF}_3)_3]\cdot\text{NCC}_6\text{H}_5$ complex(expanded region 6.0ppm-8.1ppm).....	110

Figure 3.51: ORTEP of 2,2- <i>cis</i> -[Rh <sub>2</sub> (NPhCOCH <sub>4</sub> ) <sub>4</sub> ] $\cdot$ 2NCC <sub>6</sub> H <sub>5</sub> complex.....	114
Figure 3.52: Packing diagram of 2,2- <i>cis</i> -[Rh <sub>2</sub> (NPhCOCH <sub>4</sub> ) <sub>4</sub> ] $\cdot$ 2NCC <sub>6</sub> H <sub>5</sub> complex looking along the b-axis.....	114
Figure 3.53: ORTEP of 2,2- <i>cis</i> -[Rh <sub>2</sub> (NPhCOCH <sub>4</sub> ) <sub>4</sub> ] $\cdot$ NC({2-CH <sub>3</sub> }C <sub>6</sub> H <sub>4</sub> ) complex.....	118
Figure 3.54: Packing diagram of 2,2- <i>cis</i> -[Rh <sub>2</sub> (NPhCOCH <sub>4</sub> ) <sub>4</sub> ] $\cdot$ NC({2-CH <sub>3</sub> }C <sub>6</sub> H <sub>4</sub> ) complex Looking along the b-axes.....	118
Figure 3.55: ORTEP of 2,2- <i>cis</i> -[Rh <sub>2</sub> (NPhCOCH <sub>4</sub> ) <sub>4</sub> ] $\cdot$ NC({3-CH <sub>3</sub> }C <sub>6</sub> H <sub>4</sub> ) complex.....	121
Figure 3.56: Packing diagram of 2,2- <i>cis</i> -[Rh <sub>2</sub> (NPhCOCH <sub>4</sub> ) <sub>4</sub> ] $\cdot$ NC({3-CH <sub>3</sub> }C <sub>6</sub> H <sub>4</sub> ) complex looking along the b- axes.....	122
Figure 3.57: ORTEP of 2,2- <i>cis</i> -[Rh <sub>2</sub> (NPhCOCH <sub>4</sub> ) <sub>4</sub> ] $\cdot$ NC({4-CH <sub>3</sub> }C <sub>6</sub> H <sub>4</sub> ) complex.....	125
Figure 3.58: Packing diagram of 2,2- <i>cis</i> -[Rh <sub>2</sub> (NPhCOCH <sub>4</sub> ) <sub>4</sub> ] $\cdot$ NC({4-CH <sub>3</sub> }C <sub>6</sub> H <sub>4</sub> ) complex looking along the b-axes.....	125
Figure 3.59: ORTEP of 2,2- <i>cis</i> -[Rh <sub>2</sub> (NPhCOCH <sub>4</sub> ) <sub>4</sub> ] $\cdot$ NC({2-CH <sub>3</sub> }C <sub>6</sub> H <sub>4</sub> ) complex. ....	129
Figure 3.60: Packing diagram of 2,2- <i>cis</i> -[Rh <sub>2</sub> (NPhCOCH <sub>4</sub> ) <sub>4</sub> ] $\cdot$ NC({2-CH <sub>3</sub> }C <sub>6</sub> H <sub>4</sub> ) complex looking along the b- axes.....	129
Figure 3.61: ORTEP of 2,2- <i>cis</i> -[Rh <sub>2</sub> (NPhCOCH <sub>4</sub> ) <sub>4</sub> ] $\cdot$ NC({3-CH <sub>3</sub> }C <sub>6</sub> H <sub>4</sub> ) complex.....	132
Figure 3.62: Packing diagram of 2,2- <i>cis</i> -[Rh <sub>2</sub> (NPhCOCH <sub>4</sub> ) <sub>4</sub> ] $\cdot$ NC({3-CH <sub>3</sub> }C <sub>6</sub> H <sub>4</sub> ) complex looking along the b- axes.....	133
Figure 3.63: ORTEP of [Rh <sub>2</sub> (O <sub>2</sub> CCH <sub>3</sub> )(NPhCOCH <sub>3</sub> ) <sub>3</sub> ] $\cdot$ 2NCC <sub>6</sub> H <sub>5</sub> complex.....	139
Figure 3.64: Packing diagram of [Rh <sub>2</sub> (O <sub>2</sub> CCH <sub>3</sub> )(NPhCOCH <sub>3</sub> ) <sub>3</sub> ] $\cdot$ 2NCC <sub>6</sub> H <sub>5</sub> complex looking along the b-axes.....	139



## CHAPTER 1

### INTRODUCTION

The d-orbitals present in transition complexes allow for the formation of up to four bonds. An example of a complex formed from these bonds is tetrakis(acetato) dichromium(II) (chromium acetate), which is the first compound containing a quadruple bond to be synthesized.<sup>1</sup> Other transition metals, like rhodium, have been shown to have similar bonding capabilities to chromium.

When two metal atoms approach each other, only five non zero overlaps between pairs of d-orbitals in the two atoms are possible because of its symmetry properties<sup>2</sup>.

These overlaps are formed between corresponding pairs of d-orbitals as described below: The positive overlap of two  $d_z^2$  orbitals:  $d_z^{2(1)} + d_z^{2(2)}$  gives rise to a  $\sigma$  bond orbital which has a corresponding antibonding  $\sigma^*$  orbital formed by negative overlap,  $d_z^{2(1)} - d_z^{2(2)}$ . This is shown in Figure 1.1 below. The  $d_{xz}^{(1)} + d_{xz}^{(2)}$  and  $d_{yz}^{(1)} + d_{yz}^{(2)}$  can each give rise to a  $\pi$  bond which are equivalent but orthogonal, thus constituting a degenerate pair. There are corresponding  $\pi^*$  orbitals resulting from the negative overlaps<sup>2</sup>. This is shown in Figure 1.2 below.

In addition to these, there are bonding and anti-bonding ( $\delta$  and  $\delta^*$ ) combinations of the  $d_{xy}$  - orbitals. The remaining pair of d-orbitals,  $d_{x^2-y^2}$  on each metal atom, can also overlap to form  $\delta$  and  $\delta^*$  bonding and antibonding combinations<sup>2</sup>. These are shown in Figures 1.3 and 1.4 below. The  $dx^2-dy^2$  orbital is involved in metal to ligand bonding and is thus unavailable for metal-metal bonding. The involvement of the  $d_{x^2-y^2}$  in metal to ligand bonding is because acetate ligands also bond to the metal along the x and y axes. Therefore electrons in the acetate ligands overlap with electron density in  $d_{x^2-y^2}$  to form metal to ligand bonding.

Studies done in the past reveal that chromium forms compounds with multiple bonds in the sense that there are four occupied molecular orbitals in  $\text{Cr}_2\text{L}_4$  that can be identified as one  $\sigma$ , two  $\pi$  and one  $\delta$  interactions. The chromium acetate complex,  $[\text{Cr}_2(\text{O}_2\text{CCH}_3)_4]$ , has a formal bond order of four while the maximum bond order of the rhodium acetate is one. Thus, the rhodium acetate has a single bond and chromium acetate has a quadruple bond.

These bond orders are deduced from the formula:

$$\frac{\text{Number of bonding electrons} - \text{Number of anti-bonding electrons}}{2} = \text{bond order}$$

Tetrakis(acetato) dirhodium (II) (rhodium acetate), however is the compound of interest. The rhodium atom has an atomic number of 45 and an electronic configuration of  $[\text{Kr}] 5s^2 4d^7$ . However, in the condensed state its electronic configuration is  $[\text{Kr}] 4d^9 5s^0$  thus when a rhodium atom is oxidized, electrons come out of the highest quantum number (4d) first. Each acetate group has a charge of -1, and because there are four acetates bridging two rhodium atoms, there is a total of -4 charges on the acetates and the  $\text{Rh}_2$  core shares a +4 charge resulting in each rhodium atom having a +2 charge. Rhodium (Rh) is now  $\text{Rh}^{2+}$  with electronic configuration,  $[\text{Kr}] 4d^7$  (showing that there are 7 electrons in the outer shell)

In the rhodium acetate ( $\text{Rh}_2\text{OAc}_4$ ) complex, two atoms of the rhodium (each having 7 electrons) are required to combine with 4 ions of the acetate ( $\text{OAc}^-$ ), therefore, making a total of 14 electrons. The simplified form of the molecular orbital picture shows that eight of the 14 electrons are distributed in the  $\sigma$ ,  $\pi$ ,  $\delta$ - and the remaining six are in  $\pi^*$  and  $\delta^*$  orbitals with a net Rh-Rh bond order of one and no unpaired electrons. Figures 1.1, 1.2, 1.3, 1.4, and 1.5 are molecular orbital (MO) diagrams, which gives a better representation of this. Figure 1.6 on the other hand shows the energy axis for these MO diagrams.

## Diagrammatic Representation of Molecular Orbitals

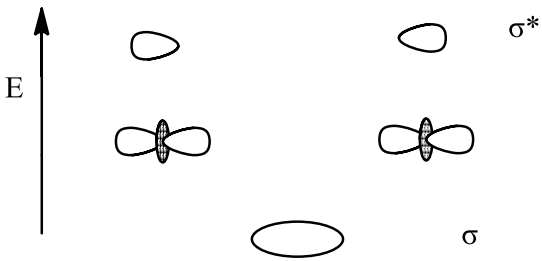


**Figure 1.1:** The overlaps of  $d_{z^2}$  and the resulting energy levels.

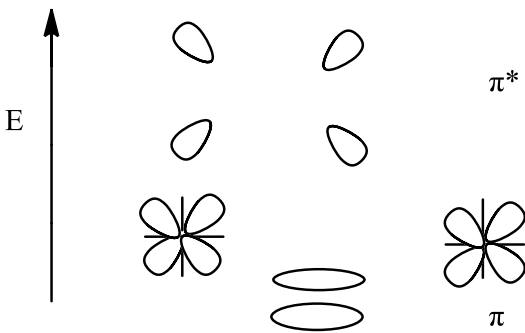


**Figure 1.2:** The overlaps of  $d_{xz}$  and the resulting energy levels.

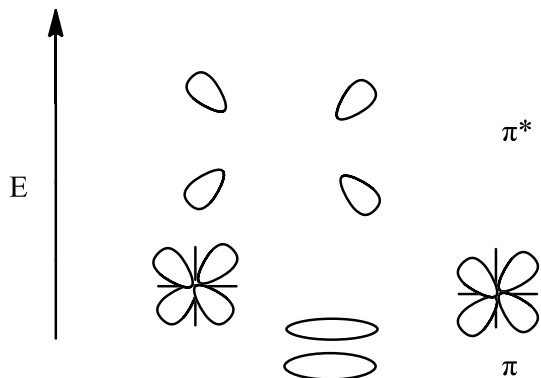


**Figure 1.3:** The overlaps of  $d_{yz}$  and the resulting energy levels.

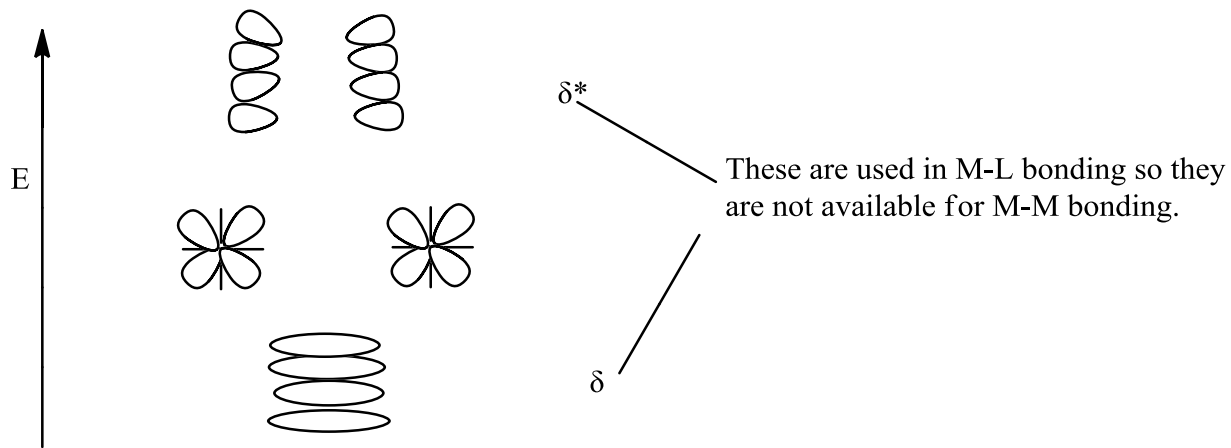


**Figure 1.4:** The overlaps of  $d_x^2-d_y^2$  and the resulting energy levels.

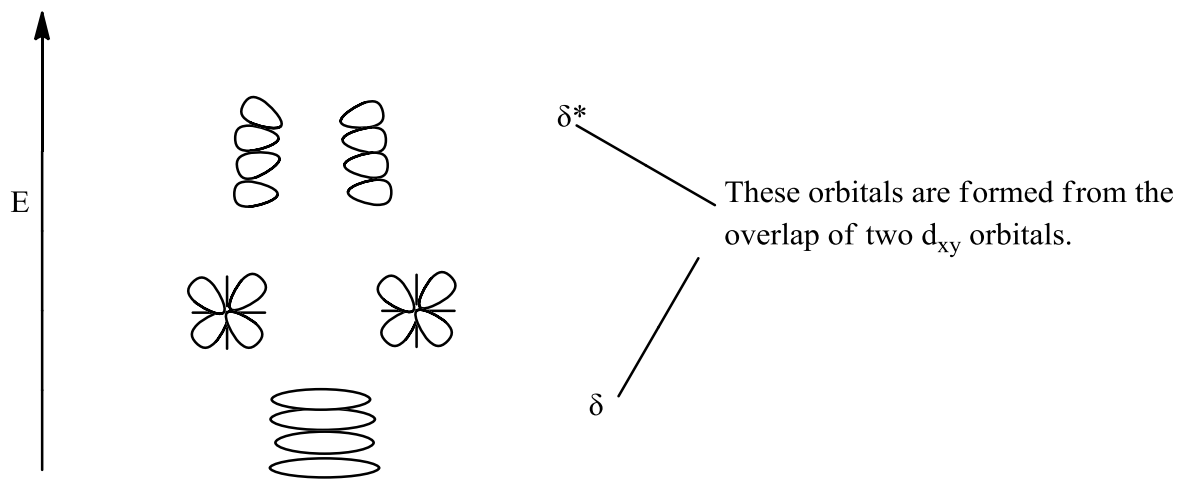
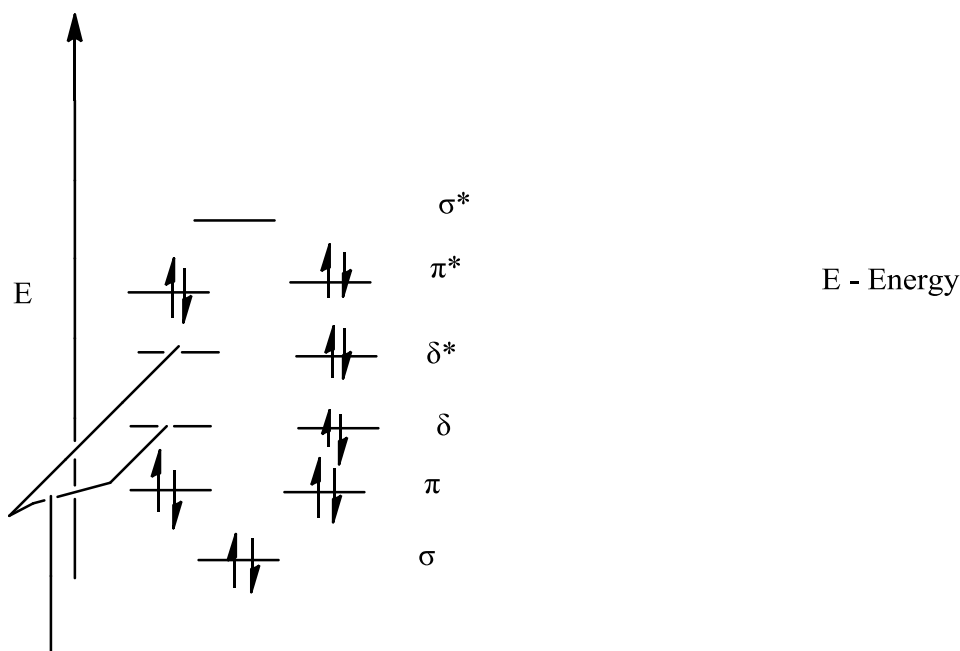


**Figure 1.5:** The overlaps of  $d_{xy}$  and the resulting energy levels.



**These set of orbitals resulting from  $d_{x^2-y^2}$  overlap are not available for M-M bonding**

**Figure 1.6:** Molecular orbital diagram of rhodium acetate ( $\text{Rh}_2\text{OAc}_4$ )

The single Rh-Rh bond varies in length in the range of (2.35-2.45) Å.

There are two types of bonding that occur when  $\text{Rh}_2\text{L}_4$  binds to a ligand in the axial site: sigma ( $\sigma$ -bonding) and pi-back-bonding ( $\pi$ -back-bonding).

$\sigma$ -bonding occurs when a filled orbital of a  $\sigma$ -type of a ligand (e.g.  $\text{C}\equiv\text{N}$ ) donates or transfers electron density into an empty  $\sigma^*$  orbital of a  $\text{Rh}_2\text{L}_4$ .

$\pi$ -back-bonding, on the other hand, occurs when electrons from a full  $\pi^*$  orbital of a rhodium metal atom are transferred into an empty  $\pi^*$  orbital of a ligand. Electron density is usually transferred from the d-orbital of the rhodium metal and placed into an anti-bonding molecular orbital of the ligand that causes the metal to metal bond order to decrease and the metal to ligand bond order to increase.<sup>3</sup>

Figures 1.7 and 1.8 below show a diagrammatic representation of the  $\sigma$ - and  $\pi$ - back-bonds.

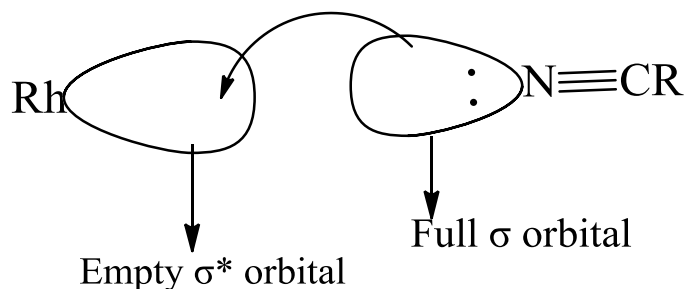


**Figure 1.7:**  $\sigma$  Bonding

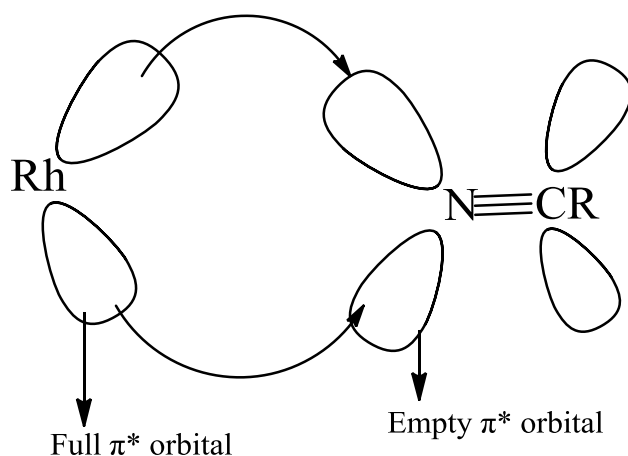


**Figure 1.8:**  $\pi$ - Back-bonding

Complexes containing multiple bonds between metal atoms are most often characterized by X-ray crystallography which is an experimental technique used in studying the structure of a crystal through X-ray diffraction. When atoms in a crystal are bathed in X-rays, they absorb some of the radiation and emit it again in all directions, thus causing each atom to become a tiny X-ray source. The emission of X-rays from these atoms is in-phase in some directions but out-of-phase in other directions. This phenomenon of in-phase (constructive) and out of phase (destructive) interferences is called diffraction.

There are several numbers of atoms in a crystal that are evenly spaced throughout the lattice. When a beam of X-rays strike a crystal, the radiation is diffracted (the electrons are diffracting the X-rays) due to constructive interference and appears only in specific directions. No X-rays appear in other directions due to destructive interference.

When X-rays coming from a crystal fall on a photographic film, the diffracted beams form a diffraction pattern. Certain conditions are necessary to obtain a constructive interference of X-rays from successive layers of atoms in a crystal. A beam of X-rays having a wavelength,  $\lambda$  strikes the layers at an angle  $\Theta$ .

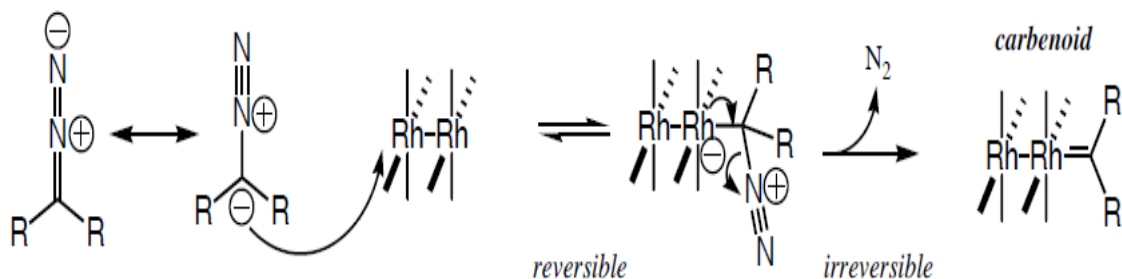
However, determination of the structure of a crystal is done by measuring the angle  $\Theta$  at which diffracted X-ray beams emerge from a crystal. These measured angles are used to calculate the distances between the various planes of atoms in the crystal. The calculated distances are then used to identify the locations of the atoms in the crystal.

Since 1912, several scientists have worked on improving this technique until 1960 when the capabilities of X-ray crystallography were greatly improved by the computerized system. Modern X-ray crystallography provides the most accurate and powerful method for determining single crystal structure.

Practical application of rhodium acetate complexes

Rhodium acetate complexes are very useful and as such are among the most well studied  $M_2(O_2CR)_4L_n$  ( $n = 1$  or  $2$ ;  $L =$  axial ligand).<sup>4</sup>

Studies have revealed that these complexes are involved in catalyzing organic transformations by the decomposition of diazo compounds to form rhodium stabilized carbenes as shown below;



The decomposition of diazo compounds has emerged as the most effective and widely utilized approach in reactions involving carbene insertions.<sup>5</sup>

There are several organic transformations that the rhodium atom can be involved in some of which are: cyclopropanation, O-H insertion and C-H insertion. During C-H insertion the metal does not interact directly with the C-H bond. However, coordination of chiral ligands to the dirhodium complex can still induce highly enantioselective insertions under catalytic conditions.<sup>1</sup>

Another example is its use as a catalyst in the synthesis of tetrahydrofurans by O-H insertion. In this synthesis, studies have revealed that there is an efficient Rh(II)-catalyzed intramolecular O-H insertion reaction of  $\alpha$ -diazo- $\beta$ -ketoesters that produced tetrahydrofuran in quantitative yield.

#### Preparative methods and classification

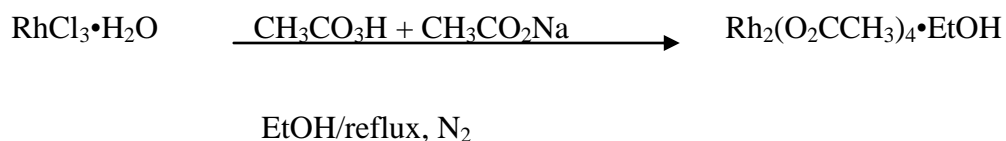
Complexes of rhodium acetate are mostly obtained by reduction of Rh(III) compounds in alcohols which is presumed to act as a reducing agent but mechanically determined details are not known.<sup>6</sup>

Compounds of the general type  $\text{Rh}_2(\text{O}_2\text{CR})_4\text{L}_n$  ( $n=1$  or  $2$ ) were first obtained by refluxing salts of  $[\text{RhCl}_6]^{3-}$  in aqueous formic acid. This reaction gave a dark-green product



$\text{Rh}_2(\text{O}_2\text{CH})_4(\text{H}_2\text{O})$ . This compound is believed to exhibit a structure consisting of  $\text{Rh}_2(\text{OCH})_4(\text{H}_2\text{O})_2$  units and  $\text{Rh}_2(\text{O}_2\text{CH})_4$  chains.<sup>6</sup>

The most efficient general synthetic method for rhodium acetate involves refluxing  $\text{RhCl}_3 \cdot 3\text{H}_2\text{O}$  under  $\text{N}_2$  in a mixture of sodium acetate, acetic acid and ethanol as illustrated in the following equation:<sup>6</sup>



Amongst the most studied  $\text{M}_2(\text{O}_2\text{CR})_4\text{L}_n$  ( $n=1$  or  $2$ ) compounds are the rhodium carboxylate complexes that exhibit the paddlewheel structure.<sup>6</sup>

Tetrakis carboxamidato dirhodium (ii) (rhodium carboxamidate)

While rhodium carboxylates are electron deficient at the rhodium center, rhodium carboxamidates are electron rich as a result of the high basicity of the carboxamidate ligand.

Below in Figures 1.9 and 1.10 are the scheme and a picture of rhodium carboxamidate respectively ;

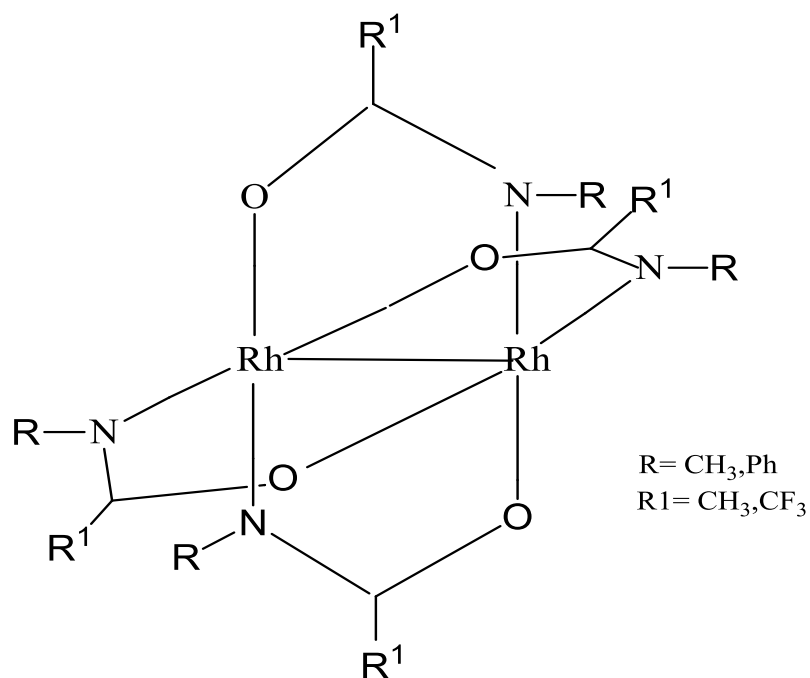


**Figure 1.9:** Scheme of rhodium carboxamidate

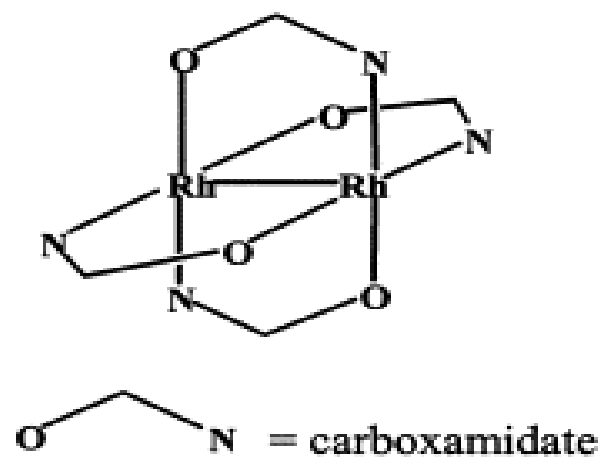


**Figure 1.10:** Picture of rhodium carboxamidate.<sup>7</sup>

Dirhodium carboxamidate complexes possess a paddlewheel structure. Paddlewheel can be described as a pseudo 4 fold rotational symmetry about the Rh-Rh axis as shown in Figure 1.11:

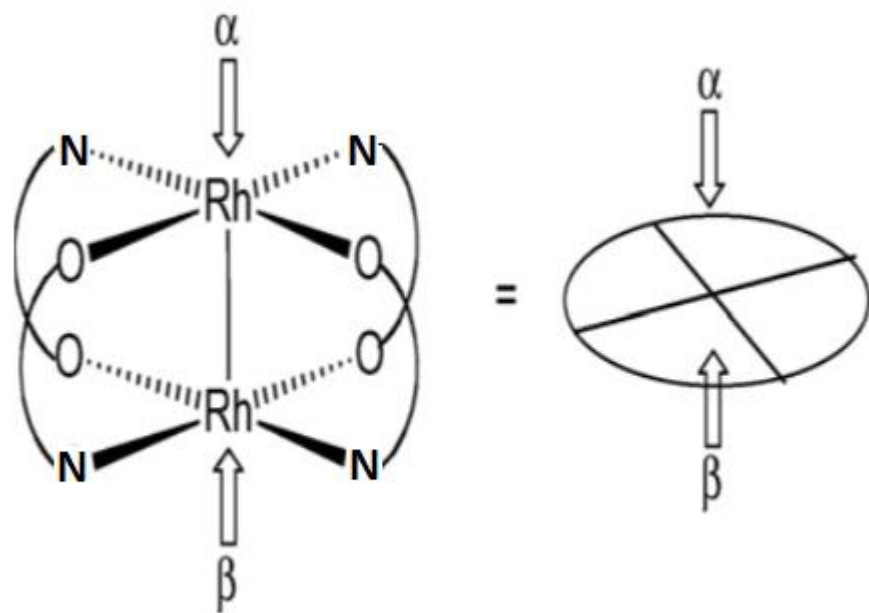
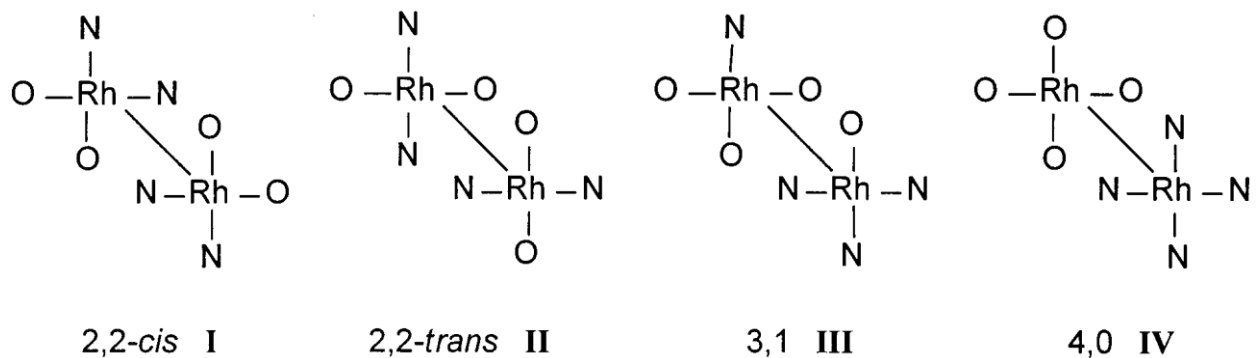


**Figure 1.11:** Diagrammatic representation of the paddlewheel structure around a Rh-Rh axis.

In the rhodium carboxamidate complex, however, the paddlewheel structure can be described by the bridging acetamide ligands around a  $\text{Rh}_2^{4+}$  core. These ligands are orthogonal to the  $\text{Rh}_2^{4+}$  core.

Although the acetate ligands can form only one isomer of rhodium acetate, four isomers of rhodium acetamide are possible; I cis-(2,2), II trans-(2,2), III (3,1), and IV (4,0) as shown below;<sup>6</sup>



Paddlewheel dirhodium compounds with  $\text{Rh}_2^{4+}$  and  $\text{Rh}_2^{5+}$  cores generally possess one or two axial ligands but the Rh-Rh bond length is essentially insensitive to the presence of  $\sigma$  donor axial ligands. This is confirmed by comparing the structural data for  $\text{Rh}_2(\text{TiPB})_4$  (TiPB is 2,4,6-triisopropyl benzoate) that lacks entirely axial interactions to  $\text{Rh}_2(\text{TiPB})_4(\text{Me}_2\text{CO})_2$ .

The Rh-Rh distance in the  $\text{Rh}_2(\text{TiPB})_4$  (2.350Å) is only slightly shorter by 0.02Å than that of the  $\text{Rh}_2(\text{TiPB})_4(\text{Me}_2\text{CO})_2$  (2.370Å) that has axial ligands.<sup>4</sup>

An exponential growth has been seen in the number of structurally characterized dirhodium compounds in the last two decades. These compounds have been classified according to the ligands that are coordinated to the dirhodium core in equatorial positions.<sup>8</sup>

By the use of cyclic voltammetry and UV– spectroscopy, Bear and co-workers characterized two dirhodium acetamidates,  $\text{Rh}_2(\text{NHCOCF}_3)_4$ <sup>9</sup> and  $\text{Rh}_2(\text{PhNCOCH}_3)_4$ .<sup>10</sup> The trifluoroacetamidate complex was synthesized as a single isomer and presumed to be the 2, 2-*cis* isomer.<sup>11</sup>

Doyle and co-workers also recently isolated and obtained solid-state structures for chiral rhodium acetamidate analogs with the 3, 1 ( $\text{Rh}_2(4S\text{-MACIM})_4$ )<sup>6</sup> and 4,0 ( $\text{Rh}_2(4S\text{-MACIM})_4$ )<sup>12</sup> isomeric orientations.

The method for synthesis of rhodium carboxamidate is by refluxing the rhodium acetate with the carboxamide in a soxhlet extraction apparatus for seven days. The acetic acid by-product is trapped in a thimble packed with 50% sodium carbonate and 50% sand. The operation of the trans effect in the ligand exchange process and the discovery of the high selectivity enhancement afforded by the carboxylate attachment are the key developments here.

The focus of this research is on non-chiral complexes specifically on 2,2-cis rhodium N-phenylacetamide with nitriles and other ligands.

Examples of these complexes are: 2,2-cis rhodium N-phenylacetamide with benzonitrile, 2, 2-cis rhodium N-phenylacetamide with *o*-tolunitrile, 2,2-cis rhodium N-phenylacetamide with *m*-tolunitrile and 2,2-cis rhodium N-phenylacetamide with *p*-tolunitrile.

This research is on the synthesis and characterization of nitrile adducts of 2,2-cis- $[\text{Rh}_2(\text{NPhCOCH}_3)_4]$  complexes. The expectation is to learn how and why ligands bond to the rhodium atom in the axial site and to analyze a variety of bond distances and angles before and after the ligand is bonded to the rhodium metal. Thus, we plan to gain information on interactions between rhodium and axial ligands that can be used later to provide insight into  $[\text{Rh}_2(\text{NPhCOCH}_3)_4]$  as a catalyst.

This research focused on two of the many possible ways of making a better dirhodium carboxamidate catalyst. These are;

- I. Synthesis of a new  $\text{Rh}_2\text{L}_4$  (where L is  $(\text{NPhCOCF}_3)_4$ ) complex and its characterization for further studies. The new  $\text{CF}_3$  complex produced was synthesized to see if there is a difference in the way the nitriles bind.

II. Synthesis of a series of  $\text{Rh}_2(\text{NPhCOCH}_3)_4$  nitrile complexes and their characterization so that a library of these complexes can be compared to each other

.

## CHAPTER 2

### EXPERIMENTAL

#### Reagents:

1. Chlorobenzene (PhCl)

Chlorobenzene was dried with magnesium sulfate ( $\text{MgSO}_4$ ) before use.

2. Rhodium Acetate

Rhodium acetate was synthesized as reported in the literature.<sup>6</sup>

3. Ligand

2,2,2-trifluoro-N-phenylacetamide was used as prepared by Landon Zink.<sup>13</sup>

4. Rhodium Phenylacetamide

Rhodium phenylacetamide was used as prepared by previous members of the Eagle research group.<sup>14</sup>

#### Instruments

1. Shimadzu IR prestige -21 Fourier transform Infrared spectrometer
2. 400 MHZ Joel Nuclear Magnetic Resonance Instrument,  $\text{CDCl}_3$ (solvent)
3. Rigaku Mercury 375R/M CCD X-talab Mini diffractometer

#### Synthesis of $[\text{Rh}_2(\text{O}_2\text{CCH}_3)(\text{NPhCOCF}_3)_3]$

#### Glassware:

Necessary apparatus included: round bottomed flask, soxhlet extractor, plastic hose, four-way adapters, 7 thimbles, condenser column, test tube, Erlenmeyer flasks, column for flash column chromatography, beakers.

All the glassware needed for the synthesis was assembled and dried in the oven of a temperature of  $110^\circ\text{C}$  for 24 hours before use.

The seven thimbles were all filled to two-thirds full with a 1:1 ratio of sand/molecular sieves and sodium carbonate. It was ensured that the sand/molecular sieves were the last to be put in the thimbles to ensure a good packing.

The NMR of the 2,2,2-trifluoro-N-phenylacetamide (ligand) was taken with 10 mg of the ligand.

0.249 g of rhodium acetate and 3 g of the ligand were weighed out and both of them put in a round bottomed flask that was set on a heating mantle connected to a Variac transformer. The heating mantle was then set on a magnetic stirrer. A Soxhlet column was fitted on the round bottomed flask (300ml). The flask was then filled to two-thirds full (200ml) with chlorobenzene through the Soxhlet extractor. One thimble (containing a mixture of 1:1 ratio of sand and sodium carbonate) was placed in the Soxhlet extractor. The condenser column was then attached to the Soxhlet extractor with a four-way adapter connected to the condenser column (which was also connected to a nitrogen gas) opened in such a way that the nitrogen gas was going through the entire set-up and there was a little bit of the nitrogen gas going through a test tube containing mineral oil that was also connected to the four-way adaptor by a plastic transparent hose. This test tube was clamped to a ring stand.

Water was connected to the condenser (in and out) to aid condensing and the magnetic stirrer was started. The power for the Variac transformer was switched on and the voltage was set to 55V. The set-up was then left for about 45 minutes.

The solution was at reflux after 45 minutes. Insulation was used to cover the set-up from the round bottomed flask to the Soxhlet extractor and left for about 24 hours. The set-up was as represented in Figure 2.1 below:





**Figure 2.1:** Set-up for the synthesis of  $[\text{Rh}_2(\text{O}_2\text{CCH}_3)(\text{NPhCOCF}_3)_3]$

#### Observation

After 24 hours the insulation was removed, the Variac transformer was turned off, and the flow of the nitrogen gas increased while the system cooled down. After the system had cooled down, the thimble was removed and replaced with a new thimble (containing a mixture of 1:1 ratio of sand and sodium carbonate). Chlorobenzene was replenished to make up for losses due to evaporation.

The set-up was then put back in place again and re-insulated. The Variac transformer was turned on again but this time the voltage was increased to 60V. It was left for about an hour after

which the solution was boiling very well. The nitrogen gas flow was then reduced and the set-up left for the next 24 hours.

The steps for observation were repeated until the seventh thimble was placed in the soxlet extractor.

#### Thin- layer chromatography

Twenty-four hours after the seventh thimble had been placed in the soxlet extractor, a sample of the solution was taken from the round bottomed flask with a glass pipette and evaporated under nitrogen. It was then redissolved with ethanol (which was also used to dissolve a sample of rhodium acetate).

Several thin layer chromatography (TLC) plates were eluted with ethyl acetate (EtOAc), using the reaction solution: rhodium acetate and the ligand were used as references.

The results from the TLC's showed that the reaction was not complete because rhodium acetate was still present. Thus, seven more thimbles were filled again with 1:1 ratio of sand/molecular sieves and sodium carbonate, dried in the oven for 24 hours, and the whole process from the synthesis to observation was repeated for seven more days. The difference was that this time around more insulation was used, which caused the solution to boil more vigorously.

After the seventh thimble had been used, another sample of the reaction mixture was taken and a thin layer chromatography was done and this time, there was no spot of rhodium acetate seen, confirming a completion of the reaction.

## Evaporation of chlorobenzene

The rotary evaporator (Figure 2.2) was used to evaporate chlorobenzene from the reaction mixture. Sublimation was then used to separate uncoordinated ligand from the product.



**Figure 2.2:** Rotary evaporation of chlorobenzene from reaction mixture

Sublimation was then used to separate the ligand (starting material) from the solid product.

## Flash column chromatography

Flash column chromatography was also used to separate the product into various fractions following the following procedure:

### PART A: PREPPING THE COLUMN

A flash column (outer diameter -4cm) was packed with (0.5 to 1.0) cm of chromatography grade sand, followed by 15cm of silica gel (Merck grade 9385, 230-400 mesh, 60 Å) and with an inch of sand on top of the silica gel.

About 300ml of 50% EtOAc/hexane (v:v) mixture was prepared and run through the packing in the column until the whole packing of sand and silica were wet. Nitrogen gas was used to pressurize the system as much as possible.

### PART B: ADDING SAMPLE

The solid product from the synthesis was dissolved in dichloromethane and put on the sand bed using a glass pipette. This was followed by the solvent (50% EtOAc/hexane), which was used to fill the column.

As the product drained down the sand bed to the silica, it started separating into different fractions which were seen by their different colors. These fractions were collected separately into different erlenmeyer flasks. It was ensured that there was enough solvent (about 1 inch from the sand bed) in the column all the time throughout the separation.

Decomposed rhodium acetate (solid) was left on the sand bed. Eight fractions were collected but the eighth fraction was rhodium acetate. This was added to the rhodium liquid residue.

While the 7<sup>th</sup> fraction was collected, an 80% ethyl acetate and 20% ethanol mixture of solvent was poured into the column. All the solvent was drained after the 8<sup>th</sup> fraction was collected and discarded. The column was then cleaned appropriately. Figure 2.3 below shows the set-up for the flash column chromatography:

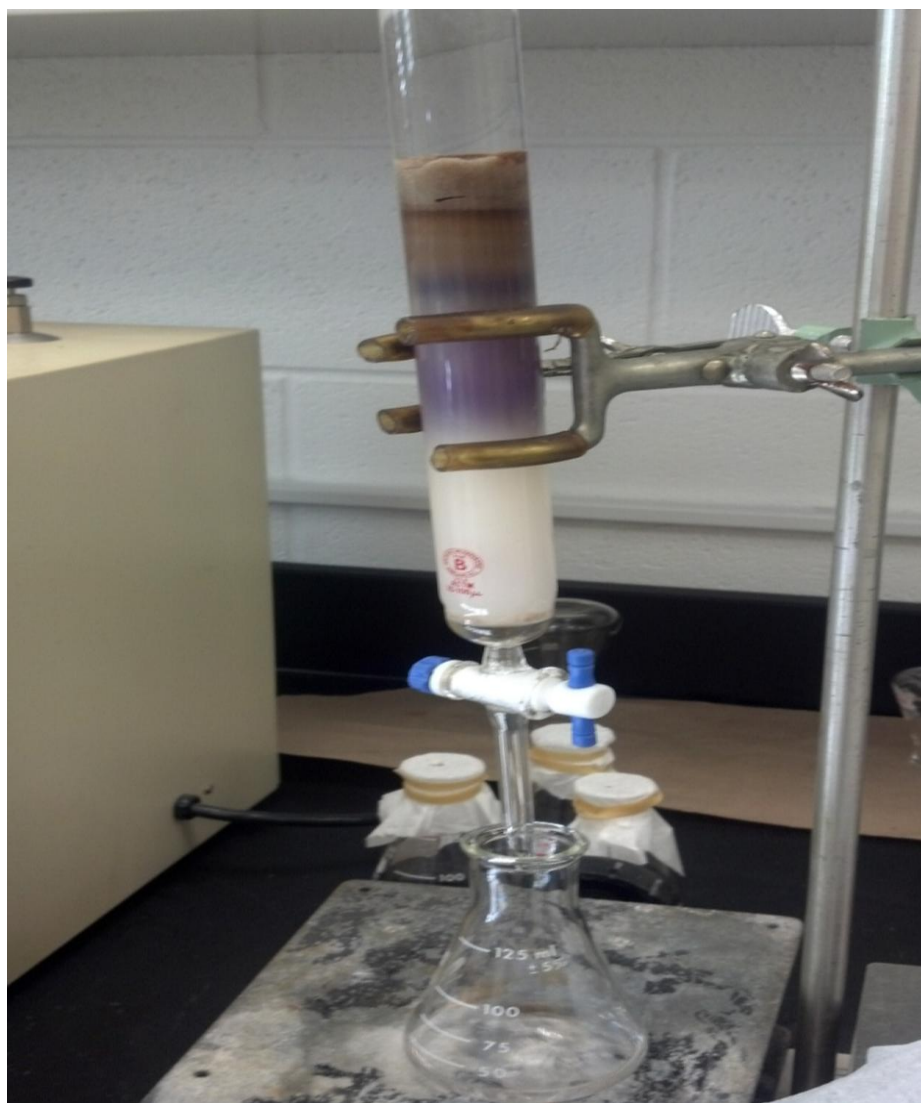


**Figure 2.3:** Set-up for flash column chromatography

A TLC was run for each of the seven fractions collected with 50% EtOAc/hexane mixture as the mobile phase. Results from TLC showed that the first fraction was a pure product, thus it

was characterized by NMR and IR spectroscopies after the solvent was evaporated and the product was dried under nitrogen gas. The rest of the fractions collected were a combination of spots; thus they were not pursued for this study.

Another column was run on a combination of fractions two and three using 10% EtOAc/hexane mixture. Fractions 13 to 16 were collected as a result of this and a TLC was run for all four fractions.

Results from the TLC showed that fraction 15 was also a pure product. This product was isolated and characterized by NMR, IR and X-ray crystallography. Fractions 13 and 14 showed a combination of spots; thus, they were not pursued for this study.

#### Synthesis of 2,2-*cis*-[Rh<sub>2</sub>(NPhCOCH<sub>3</sub>)<sub>4</sub>]·Nitrile

Complexes of 2, 2-*cis*- [Rh<sub>2</sub>(NPhCOCH<sub>3</sub>)<sub>4</sub>] were synthesized using four different nitriles, namely; benzonitrile, o-tolunitrile, p-tolunitrile, and m-tolunitrile. These complexes were then crystallized using the vapor diffusion method.

#### Benzonitrile complex and crystallization

0.01g (10mg) of 2, 2-*cis*- [Rh<sub>2</sub>(NPhCOCH<sub>3</sub>)<sub>4</sub>] were dissolved in 15 mL of dichloromethane in a 6 dram vial. The color of the solution was traffic light green. 10 μL of benzonitrile and 2 μL of acetone were added using a gas-tight syringe and the solution changed color from traffic light green to blue.

## Vapor Diffusion Method

The product solution was then transferred into seven ½ dram vials which were also placed in seven 6 dram vials each containing a different solvent. These different solvents were; methanol, ethanol, acetone, ethyl acetate, hexane, toluene, and water.

It was ensured that the ½ dram vials were placed in the center of the 6 dram vials and capped. These vials were left for about two weeks without being disturbed. After two weeks, X-ray quality crystals were formed.

### *O*-tolunitrile complex and crystallization

0.01g (10mg) of 2, 2-*cis*- [Rh<sub>2</sub>(NPhCOCH<sub>3</sub>)<sub>4</sub>] were dissolved in 15 mL of dichloromethane in a 6 dram vial. The color of the solution was traffic green. 4 μL of *o*-tolunitrile and 2 μL of acetone were added using a gas-tight syringe and the solution changed color from traffic light green to blue. The product solution was then crystallized by vapor diffusion method as described above.

### *M*-tolunitrile complex and crystallization

0.01 g (10mg) of 2, 2-*cis*-[Rh<sub>2</sub>(NPhCOCH<sub>3</sub>)<sub>4</sub>] was dissolved in 15 mL of dichloromethane in a 6 dram vial. The color of the solution was traffic green. 10 μL of benzonitrile and 2 μL of acetone were added using a gas-tight syringe and the solution changed color from traffic light green to blue. The product solution was then crystallized by vapor diffusion method.

### *P*-tolunitrile complex and crystallization

0.01 g (10 mg) of 2, 2-*cis*-[Rh<sub>2</sub>(NPhCOCH<sub>3</sub>)<sub>4</sub>] was dissolved in 15 mL of dichloromethane in a 6 dram vial. The color of the solution was traffic green. 0.004 g of *p*-tolunitrile and 2 μL of acetone were added using a gas-tight syringe and the solution changed color from traffic light green to blue. The product solution was then crystallized using the vapor diffusion method.

### Synthesis with 200 equivalents of Nitriles

0.01 g (10 mg) of 2, 2-*cis*-[Rh<sub>2</sub>(NPhCOCH<sub>3</sub>)<sub>4</sub>] was dissolved in 15 mL of dichloromethane in a 6 dram vial. The color of the solution was traffic green. 319.5 μL of *o*-tolunitrile and 2 μL of acetone were added using a gas-tight syringe and the solution changed color from traffic light green to blue. The product solution was then crystallized using the vapor diffusion method.

The procedure was repeated for *m*-tolunitrile.

### Synthesis of [Rh<sub>2</sub>(O<sub>2</sub>CCH<sub>3</sub>)(NPhCOCF<sub>3</sub>)<sub>3</sub>]·2NCC<sub>6</sub>H<sub>5</sub>

About 0.005 g (50 mg) of fraction 15, [Rh<sub>2</sub>(O<sub>2</sub>CCH<sub>3</sub>)(NPhCOCF<sub>3</sub>)<sub>3</sub>], was dissolved in 15 mL of dichloromethane in a 6 dram vial. The color of the solution was traffic light green. 10 μL of benzonitrile and 2 μL of acetone were added using a gas-tight syringe and the solution changed color from traffic green to blue. The product solution was then crystallized using vapor diffusion method.



## X-ray Crystallographic Studies

All data were collected by use of a Rigaku Mercury 375R/M CCD XtaLAB mini diffractometer (manufactured in May 2011). The X-ray source was Molybdenum K $\alpha$  radiation,  $\lambda=0.71075$  Å. The crystal-to-detector distance was 50.00 mm.

## Data Collection

2, 2-*cis*-[Rh<sub>2</sub>(NPhCOCH<sub>3</sub>)<sub>4</sub>] $\cdot$ 2 NCC<sub>6</sub>H<sub>5</sub>

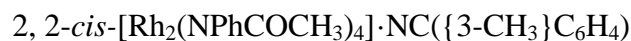
### Benzonitrile (Two Equivalents)

A red prism crystal of 2, 2-*cis*-[Rh<sub>2</sub>(NPhCOCH<sub>3</sub>)<sub>4</sub>] $\cdot$ NCC<sub>6</sub>H<sub>5</sub> having dimensions of approximately 0.354 x 0.485 x 0.158 mm was mounted on a Mitogen loop by using a mounting pin and securing the crystal onto the goniometer. The data for this crystal were collected at a temperature of -50°C with an exposure time of 15 seconds. The initial unit cell parameters were as follows: a=10.213 Å; b= 9.975 Å; c= 21.350 Å;  $\alpha=90.000^\circ$ ;  $\beta=100.950^\circ$ ;  $\gamma=90.000^\circ$

2, 2-*cis*-[Rh<sub>2</sub>(NPhCOCH<sub>3</sub>)<sub>4</sub>] $\cdot$ NC({2-CH<sub>3</sub>}C<sub>6</sub>H<sub>4</sub>)

### O-Tolunitrile (One Equivalent)

A blue chunk crystal of 2, 2-*cis*-[Rh<sub>2</sub>(NPhCOCH<sub>3</sub>)<sub>4</sub>] $\cdot$ NC({2-CH<sub>3</sub>}C<sub>6</sub>H<sub>4</sub>) having dimensions of approximately 0.279 x 0.293 x 0.179 mm was mounted on a Mitogen loop by using a mounting pin and securing the crystal onto the goniometer. The data for this crystal were collected at a temperature of -50°C with an exposure time of 15 seconds. The initial unit cell parameters were as follows: a =8.366 Å; b=9.981 Å; c=11.695 Å;  $\alpha=73.335^\circ$ ;  $\beta=86.915^\circ$ ;  $\gamma=75.621^\circ$



*M*-Tolunitrile (One Equivalent)

A green chunk crystal of 2, 2-*cis*-[Rh<sub>2</sub>(NPhCOCH<sub>3</sub>)<sub>4</sub>]·NC({3-CH<sub>3</sub>}C<sub>6</sub>H<sub>4</sub>) having dimensions of approximately 0.165 x 0.152 x 0.142 mm was mounted on a Mitogen loop by using a mounting pin and securing the crystal onto the goniometer. The data for this crystal were collected at a temperature of -50°C with an exposure time of 15 seconds. The initial unit cell parameters were as follows: a=13.006 Å; b= 15.344 Å; c= 18.322 Å; α= 90.000°; β=90.000°; γ= 90.000°



*P*-Tolunitrile (Two Equivalents)

A red chunk crystal of 2, 2-*cis*-[Rh<sub>2</sub>(NPhCOCH<sub>3</sub>)<sub>4</sub>]·NC({4-CH<sub>3</sub>}C<sub>6</sub>H<sub>4</sub>) having dimensions of approximately 0.296 x 0.279 x 0.202 mm was mounted on a Mitogen loop by using a mounting pin and securing the crystal onto the goniometer. The data for this crystal were collected at a temperature of -100°C with an exposure time of 20 seconds. The initial unit cell parameters were as follows: a=14.485 Å; b= 10.386 Å; c=19.479 Å; α= 90.000°; β=92.867°; γ= 90.000°



*O*-Tolunitrile (Two Equivalents)

A red chunk crystal of 2, 2-*cis*-[Rh<sub>2</sub>(NPhCOCH<sub>3</sub>)<sub>4</sub>]·NC({2-CH<sub>3</sub>}C<sub>6</sub>H<sub>4</sub>) having dimensions of approximately 0.235 x 0.301 x 0.160 mm was mounted on a Mitogen loop by using a mounting pin and securing the crystal onto the goniometer. The data for this crystal were

collected at a temperature of  $-50^{\circ}\text{C}$  with an exposure time of 15 seconds. The initial unit cell parameters were as follows:  $a=10.362 \text{ \AA}$ ;  $b= 10.049 \text{ \AA}$ ;  $c= 21.611 \text{ \AA}$ ;  $\alpha= 90.000^{\circ}$ ;  $\beta=100.868^{\circ}$ ;  $\gamma= 90.000^{\circ}$



*M*-Tolunitrile (Two Equivalents)

A red chunk crystal of 2, 2-*cis*- $[\text{Rh}_2(\text{NPhCOCH}_3)_4] \cdot \text{NC}(\{3\text{-CH}_3\}\text{C}_6\text{H}_4)$  having dimensions of approximately  $0.312 \times 0.365 \times 0.204 \text{ mm}$  was mounted on a Mitogen loop by using a mounting pin and securing the crystal onto the goniometer. The data for this crystal were collected at a temperature of  $-100^{\circ}\text{C}$  with an exposure time of 15 seconds. The initial unit cell parameters were as follows:  $a=10.867 \text{ \AA}$ ;  $b= 11.531 \text{ \AA}$ ;  $c= 12.363 \text{ \AA}$ ;  $\alpha= 61.666^{\circ}$ ;  $\beta=65.638^{\circ}$ ;  $\gamma= 78.288^{\circ}$



A red chunk crystal of  $[\text{Rh}_2(\text{O}_2\text{CCH}_3)(\text{NPhCOCF}_3)_3] \cdot 2\text{NCC}_6\text{H}_5$  having dimensions of approximately  $0.186 \times 0.148 \times 0.200 \text{ mm}$  was mounted on a Mitogen loop by using a mounting pin and securing the crystal onto the goniometer. The data for this crystal were collected at a temperature of  $-50^{\circ}\text{C}$  with an exposure time of 10 seconds. The initial unit cell parameters were as follows:  $a=20.822 \text{ \AA}$ ;  $b=19.928 \text{ \AA}$ ;  $c= 21.832 \text{ \AA}$ ;  $\alpha= 90.000^{\circ}$ ;  $\beta=107.150^{\circ}$ ;  $\gamma= 90.000^{\circ}$ .

## CHAPTER 3

### RESULTS AND DISCUSSION

#### Fourier Transform Infrared Spectrometer (FTIR) DATA

The FTIR data of the following compounds were obtained.

1. 2, 2-*cis*-[Rh<sub>2</sub>(NPhCOCH<sub>3</sub>)<sub>4</sub>]·2NCC<sub>6</sub>H<sub>5</sub>
2. 2, 2-*cis*-[Rh<sub>2</sub>(NPhCOCH<sub>3</sub>)<sub>4</sub>]·NC({2-CH<sub>3</sub>}C<sub>6</sub>H<sub>4</sub>)
3. 2, 2-*cis*-[Rh<sub>2</sub>(NPhCOCH<sub>3</sub>)<sub>4</sub>]·NC({3-CH<sub>3</sub>}C<sub>6</sub>H<sub>4</sub>)
4. 2, 2-*cis*-[Rh<sub>2</sub>(NPhCOCH<sub>3</sub>)<sub>4</sub>]·NC({4-CH<sub>3</sub>}C<sub>6</sub>H<sub>4</sub>)
5. Uncomplexed nitriles: benzonitrile, meta-tolunitrile, ortho-tolunitrile and para-tolunitrile
6. [Rh<sub>2</sub>(O<sub>2</sub>CCH<sub>3</sub>)(NPhCOCF<sub>3</sub>)<sub>3</sub>]·2NCC<sub>6</sub>H<sub>5</sub>

The C≡N stretching frequency when the nitrile is bound to the rhodium is indicative of the nature of the rhodium to nitrile bond. When the stretching frequency is higher than uncomplexed nitrile, σ-bonding is predominant because the bond is stronger and of a higher energy, whereas π-back-bonding is predominant when the stretching frequency is lower than uncomplexed nitrile because the bond is weaker and of a lower energy. The C≡N stretching frequency is compared for the uncomplexed nitrile and the complexed nitrile to determine whether σ or π-back-bonding is predominant. The large peaks found on uncomplexed nitriles are as a result of uncomplexed nitriles being a liquid, thus there were no competing crystallizing factors.

Figures 3.1 and 3.2 below are showing the IR (Infrared) spectra of uncomplexed NCC<sub>6</sub>H<sub>5</sub> and 2, 2-*cis*-[Rh<sub>2</sub>(NPhCOCH<sub>3</sub>)<sub>4</sub>]·2NCC<sub>6</sub>H<sub>5</sub> complex respectively. The stretching frequency for the C≡N group is located at 2227.28cm<sup>-1</sup> for the uncomplexed NCC<sub>6</sub>H<sub>5</sub> and 2229.71cm<sup>-1</sup> for 2, 2-*cis*-[Rh<sub>2</sub>(NPhCOCH<sub>3</sub>)<sub>4</sub>]·2NCC<sub>6</sub>H<sub>5</sub> complex. This is indicative that σ-bonding is predominant over

$\pi$ -back bonding because there is an increase in the stretching frequency of 2, 2-*cis*- $[\text{Rh}_2(\text{NPhCOCH}_3)_4] \cdot 2\text{NCC}_6\text{H}_5$  complex compared to uncomplexed nitrile.

The IR for the complex was taken as a solid while that of the uncomplexed nitrile was taken as a liquid. The reason for taking complex as a solid is because it was in crushed up crystalline form whereas the uncomplexed nitrile is liquid at room temperature.

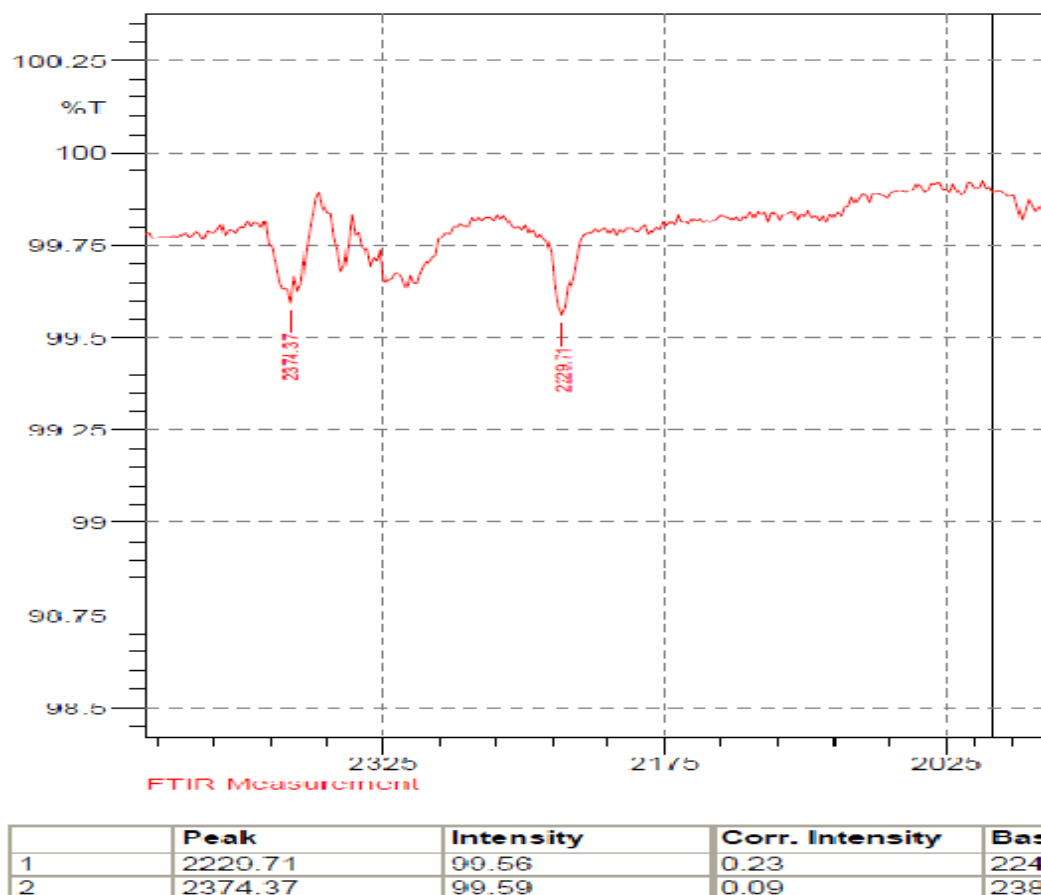
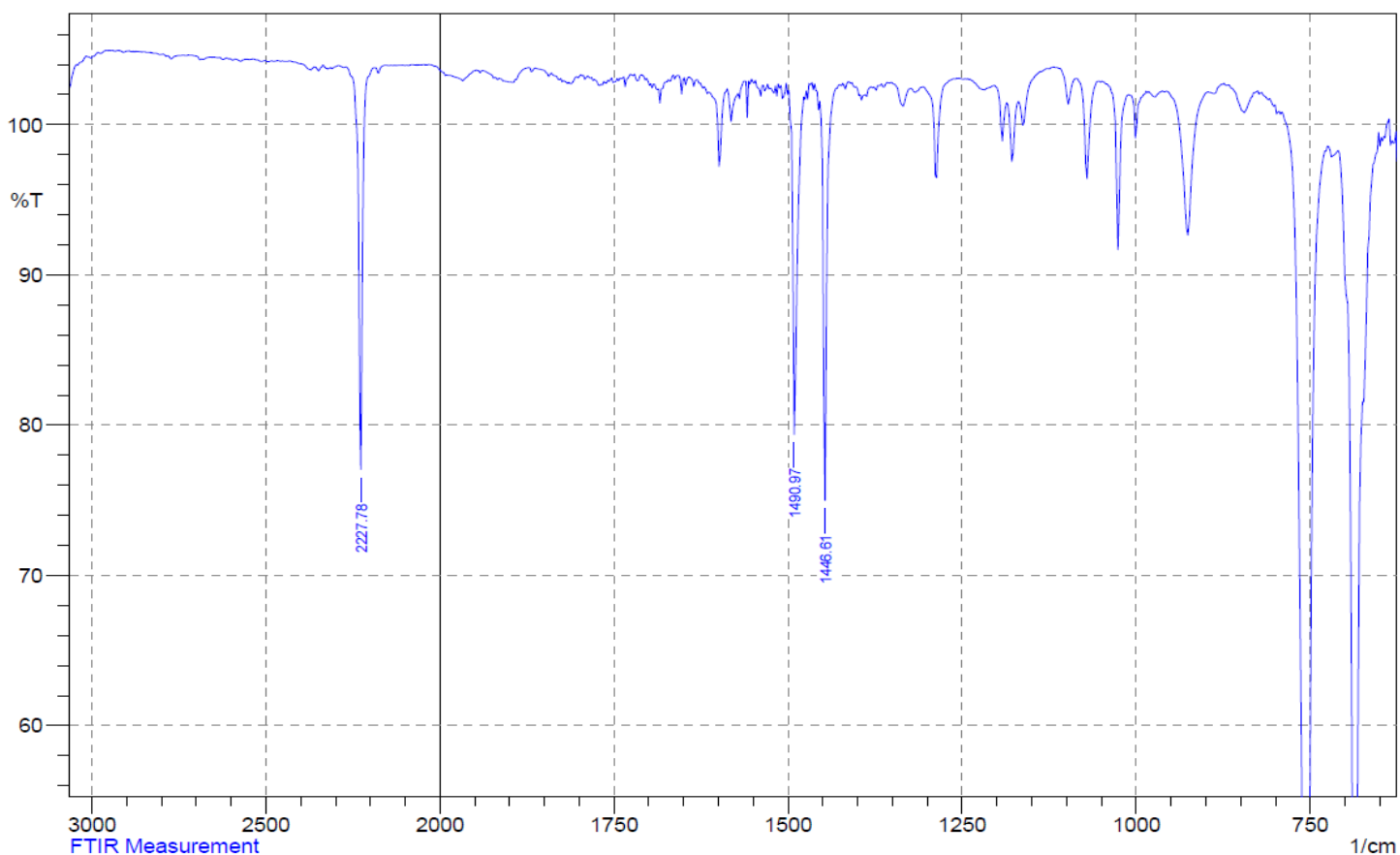


**Figure 3.1:** IR of uncomplexed benzonitrile ( $\text{NCC}_6\text{H}_5$ )



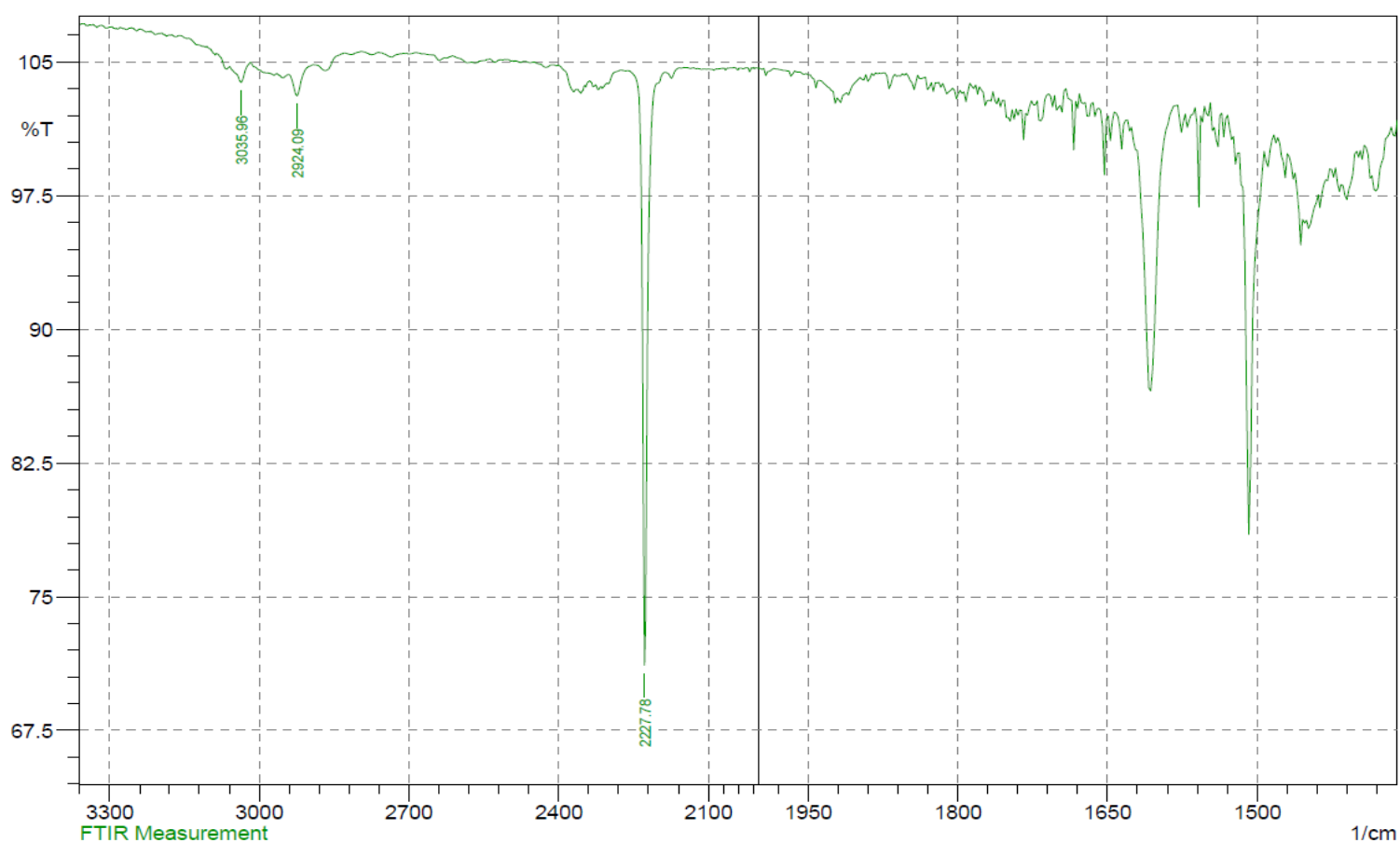
	Peak	Intensity	Corr. Intensity	Base (H)	Base (L)	Area	Corr. Area
1	1446.61	74.98	26.87	1454.33	1431.18	0.48	0.68
2	1490.97	79.39	22.72	1498.69	1477.47	0.54	0.73
3	2227.78	77.04	26.77	2270.22	2185.35	0.16	1.54
4	3064.89	102.42	1.54	3086.11	3043.67	-0.6	0.12

**Figure 3.2:** IR of 2, 2-*cis*-[Rh<sub>2</sub>(NPhCOCH<sub>3</sub>)<sub>4</sub>]·2NCC<sub>6</sub>H<sub>5</sub> complex

Figures 3.3 and 3.4 below are showing the IR (Infrared) spectra of uncomplexed *o*-tolunitrile (NC{2-CH<sub>3</sub>}C<sub>6</sub>H<sub>4</sub>) and 2, 2-*cis*-[Rh<sub>2</sub>(NPhCOCH<sub>3</sub>)<sub>4</sub>]·NC({2-CH<sub>3</sub>}C<sub>6</sub>H<sub>4</sub>) complex respectively. The stretching frequency for the C≡N group is located at 2227.28 cm<sup>-1</sup> for the uncomplexed (NC{2-CH<sub>3</sub>}C<sub>6</sub>H<sub>4</sub>) and 2320.37cm<sup>-1</sup> for 2, 2-*cis*- [Rh<sub>2</sub>(NPhCOCH<sub>3</sub>)<sub>4</sub>]·NC({2-CH<sub>3</sub>}C<sub>6</sub>H<sub>4</sub>) complex. This is indicative that σ-bonding is predominant over π-back-bonding

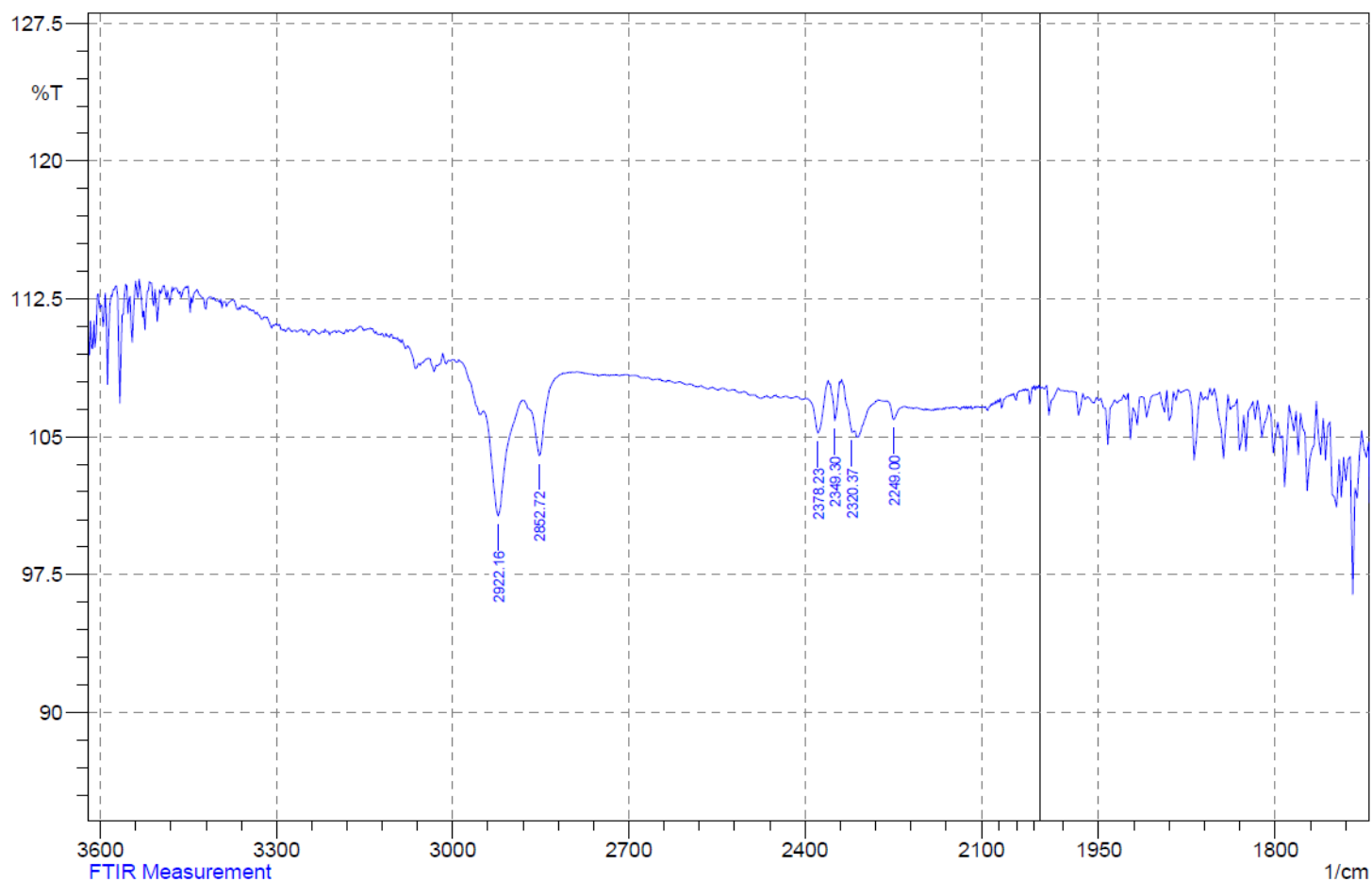
because there is an increase in the stretching frequency of 2, 2-*cis*-[Rh<sub>2</sub>(NPhCOCH<sub>3</sub>)<sub>4</sub>]·NC({2-CH<sub>3</sub>)C<sub>6</sub>H<sub>4</sub>) complex compared to the uncomplexed nitrile.

The IR for the complex was taken as a solid while that of the uncomplexed nitrile was taken as a liquid. The reason for taking complex as a solid is because it was in crushed up crystalline form whereas the uncomplexed nitrile is liquid at room temperature.



	Peak	Intensity	Corr. Intensity	Base (H)	Base (L)	Area	Corr. Area
1	2227.78	71.17	33.31	2262.5	2187.28	0.34	1.76
2	2924.09	103.1	1.39	2941.44	2900.94	-0.68	0.09
3	3035.96	103.85	1.02	3059.1	3016.67	-0.8	0.08

**Figure 3.3:** IR of uncomplexed *o*-tolunitrile (NC({2-CH<sub>3</sub>)C<sub>6</sub>H<sub>4</sub>)



	Peak	Intensity	Corr. Intensity	Base (H)	Base (L)	Area	Corr. Area
1	2249	105.93	0.85	2260.57	2237.43	-0.63	0.03
2	2320.37	105.25	0.76	2337.72	2314.58	-0.62	0.03
3	2349.3	105.86	2.08	2357.01	2341.58	-0.45	0.07
4	2378.23	105.2	2.37	2395.59	2360.87	-0.94	0.16
5	2852.72	103.98	3.63	2881.65	2812.21	-1.95	0.3
6	2922.16	100.69	5.94	2947.23	2881.65	-1.2	0.65

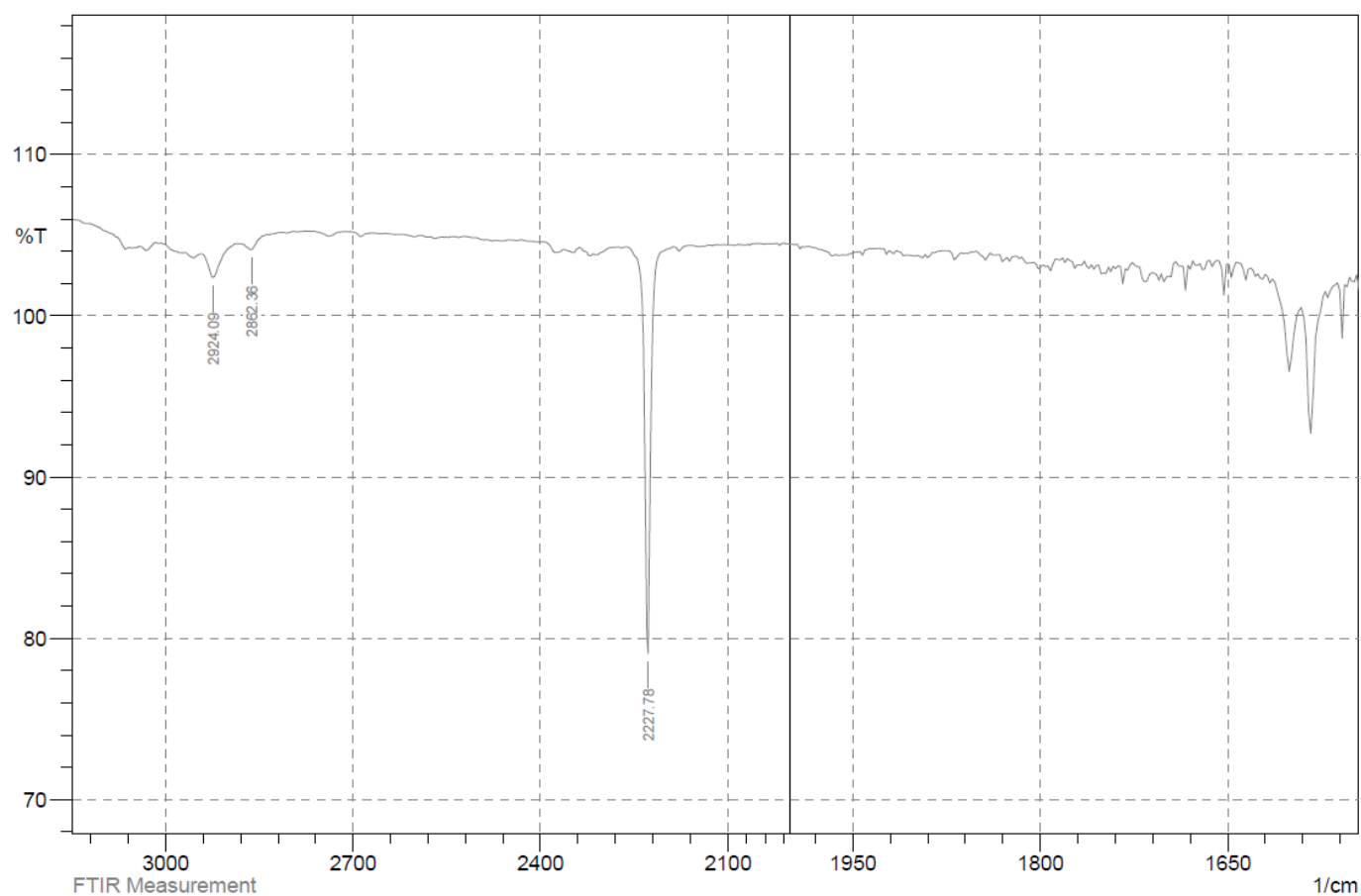
**Figure 3.4:** IR of 2, 2-*cis*-[Rh<sub>2</sub>(NPhCOCH<sub>3</sub>)<sub>4</sub>]·NC({2-CH<sub>3</sub>}C<sub>6</sub>H<sub>4</sub>) complex

Figures 3.5 and 3.6 below are showing the IR (Infrared) spectrum of uncomplexed *m*-tolunitrile(NC{3-CH<sub>3</sub>}C<sub>6</sub>H<sub>4</sub>) and 2, 2-*cis*-[Rh<sub>2</sub>(NPhCOCH<sub>3</sub>)<sub>4</sub>]·NC({3-CH<sub>3</sub>}C<sub>6</sub>H<sub>4</sub>) complex respectively. The stretching frequency for the C≡N group is located at 2227.28cm<sup>-1</sup> for the uncomplexed (NC{3-CH<sub>3</sub>}C<sub>6</sub>H<sub>4</sub>) and 2337.72cm<sup>-1</sup> for 2, 2-*cis*- [Rh<sub>2</sub>(NPhCOCH<sub>3</sub>)<sub>4</sub>]·NC({3-



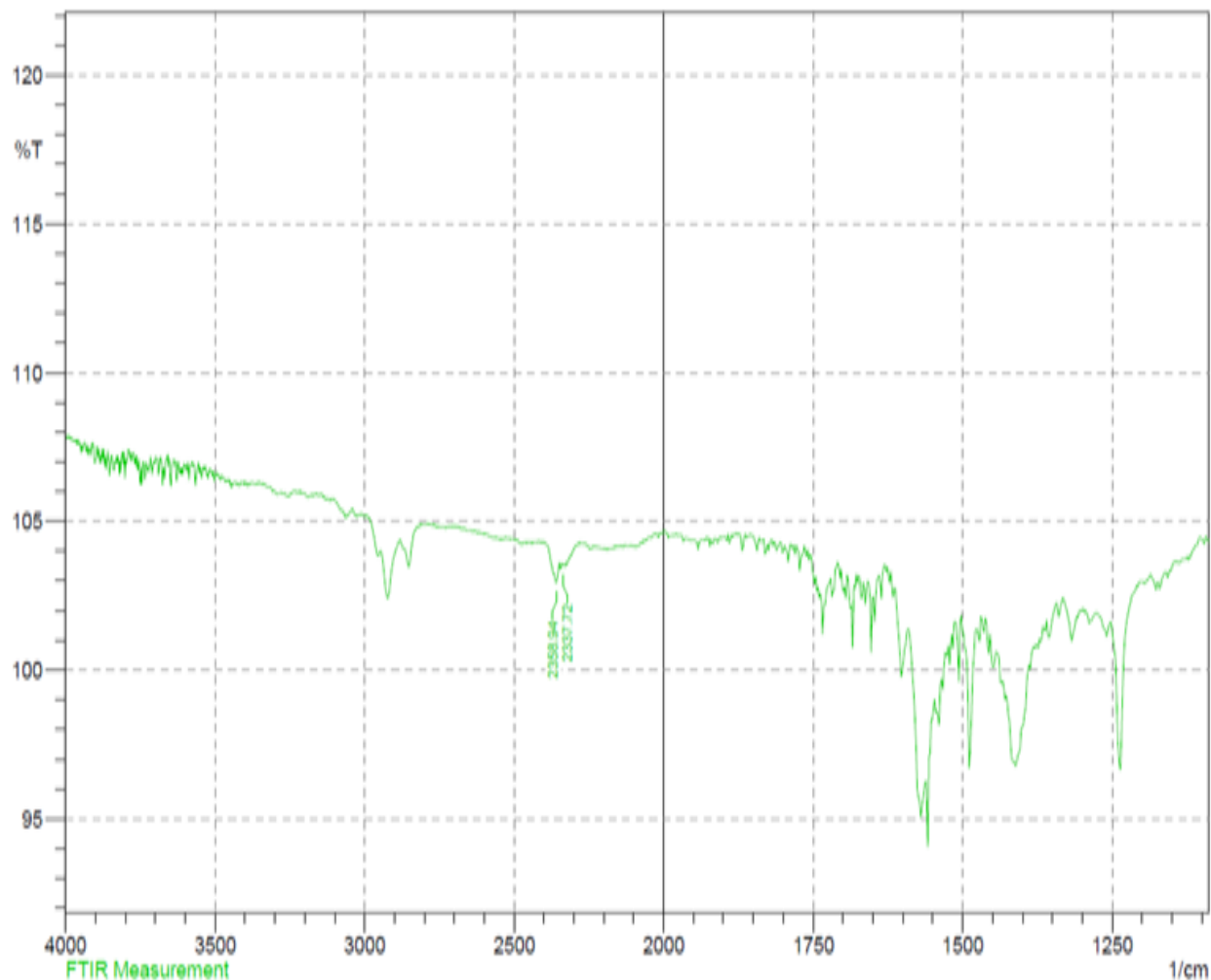
CH<sub>3</sub>}C<sub>6</sub>H<sub>4</sub>) complex. This is indicative that  $\sigma$ -bonding is predominant over  $\pi$ -back-bonding since there is an increase in the stretching frequency of 2, 2-*cis*-[Rh<sub>2</sub>(NPhCOCH<sub>3</sub>)<sub>4</sub>]·NC({3-CH<sub>3</sub>}C<sub>6</sub>H<sub>4</sub>) complex compared to the uncomplexed nitrile.

The IR for the complex was taken as a solid while that of the uncomplexed nitrile was taken as a liquid. The reason for taking complex as a solid is because it was in crushed up crystalline form, whereas the uncomplexed nitrile is liquid at room temperature.



	Peak	Intensity	Corr. Intensity	Base (H)	Base (L)	Area	Corr. Area
1	2227.78	79.06	25.23	2264.43	2187.28	-0.12	1.29
2	2862.36	104.11	0.62	2881.65	2837.29	-0.85	0.04
3	2924.09	102.38	1.65	2941.44	2881.65	-0.92	0.14

**Figure 3. 5:** IR of uncomplexed *m*-tolunitrile (NC{3-CH<sub>3</sub>}C<sub>6</sub>H<sub>4</sub>)



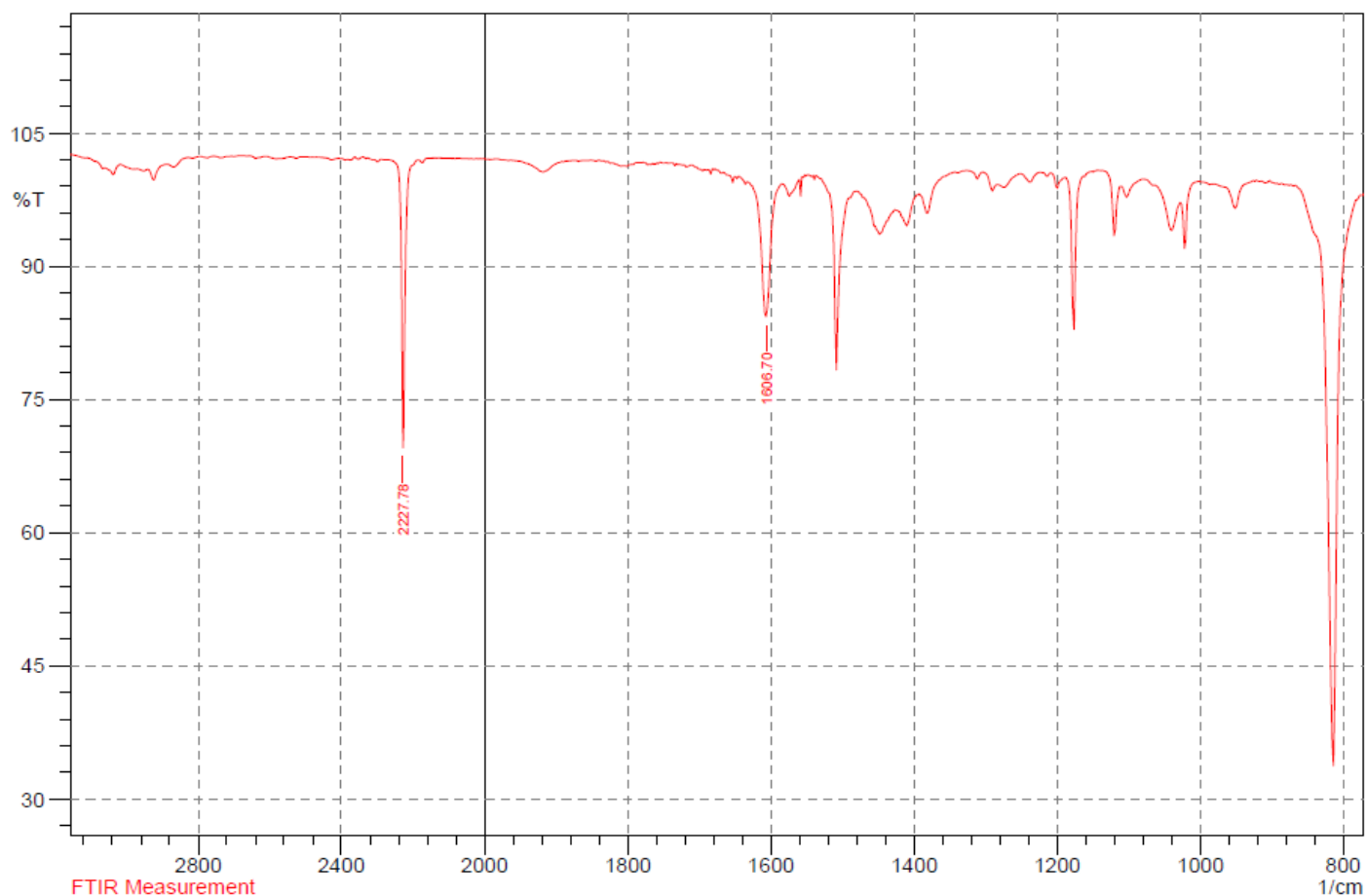
No.	Peak	Intensity	Corr. Intensity	Base (H)	Base (L)	Area	Corr. Area
1	2337.72	103.53	0.04	2339.65	2333.87	-0.09	0
2	2358.94	102.96	0.44	2366.66	2349.3	-0.23	0.02

**Figure 3.6:** IR of 2, 2-*cis*-[Rh<sub>2</sub>(NPhCOCH<sub>3</sub>)<sub>4</sub>]·NC({3-CH<sub>3</sub>}C<sub>6</sub>H<sub>4</sub>) complex

Figures 3.7 and 3.8 below are showing the IR (Infrared) spectrum of uncomplexed *p*-tolunitrile (NC{4-CH<sub>3</sub>}C<sub>6</sub>H<sub>4</sub>) and 2, 2-*cis*-[Rh<sub>2</sub>(NPhCOCH<sub>3</sub>)<sub>4</sub>]·NC({4-CH<sub>3</sub>}C<sub>6</sub>H<sub>4</sub>) complex. The stretching frequency for the C≡N group is located at 2227.28cm<sup>-1</sup> for the uncomplexed (NC{4-CH<sub>3</sub>}C<sub>6</sub>H<sub>4</sub>) and 2231.64cm<sup>-1</sup> for 2, 2-*cis*-[Rh<sub>2</sub>(NPhCOCH<sub>3</sub>)<sub>4</sub>]·NC({4-CH<sub>3</sub>}C<sub>6</sub>H<sub>4</sub>) complex. This is indicative that σ-bonding is predominant over π-back-bonding since there is an increase in the

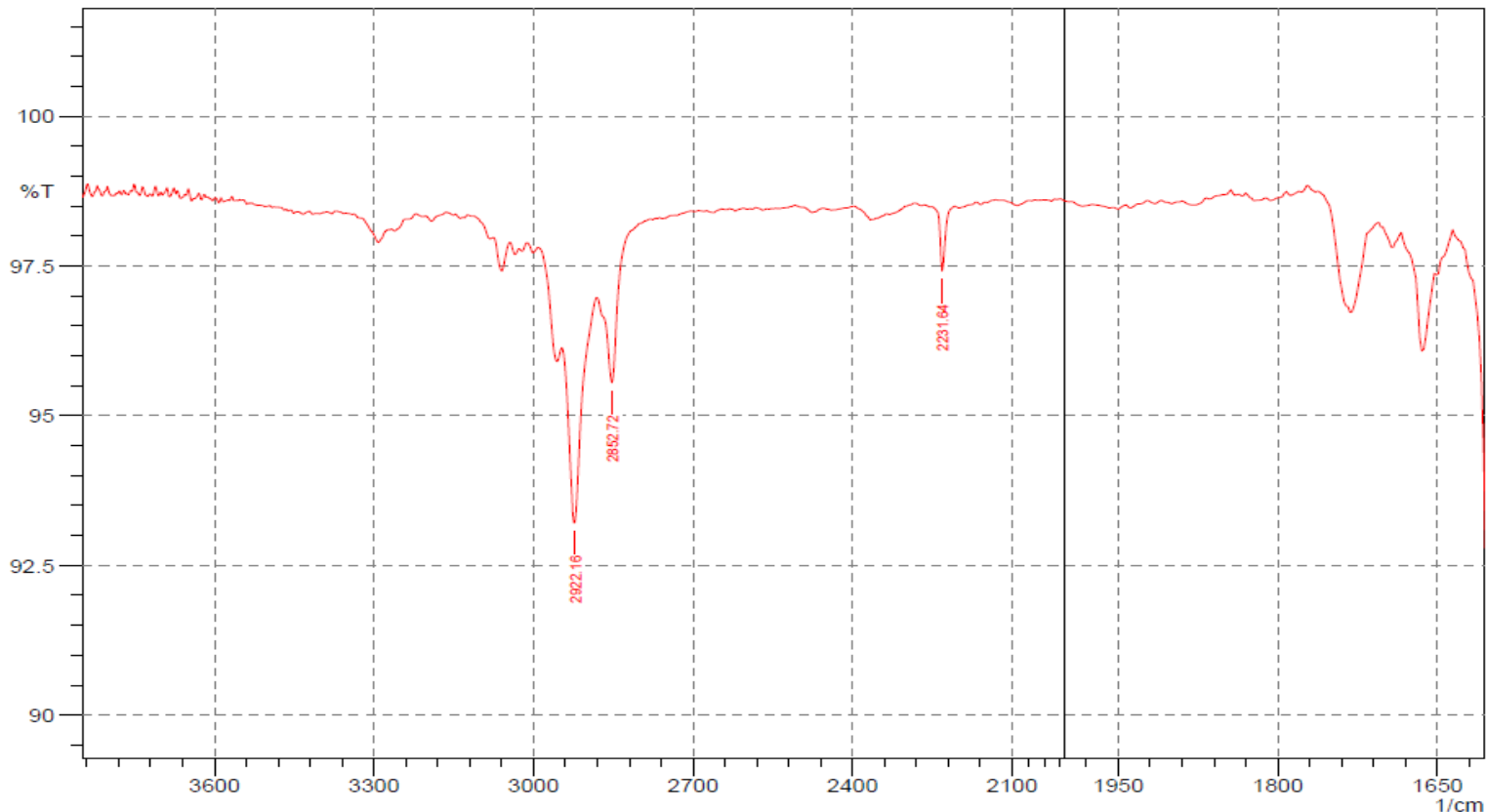
stretching frequency of 2, 2-*cis*- [Rh<sub>2</sub>(NPhCOCH<sub>3</sub>)<sub>4</sub>]·NC({4-CH<sub>3</sub>)C<sub>6</sub>H<sub>4</sub>) complex compared to the uncomplexed nitrile.

The IR for the complex was taken as a solid, while that of the uncomplexed nitrile was taken as a liquid. The reason for taking complex as a solid is because it was in crushed up crystalline form, whereas the uncomplexed nitrile is liquid at room temperature.



No.	Peak	Intensity	Corr. Intensity	Base (H)	Base (L)	Area	Corr. Area
1	1606.7	84	15	1633.71	1583.56	1	1
2	2227.78	70	32	2270.22	2185.35	1	2

**Figure 3.7:** IR of uncomplexed *p*-tolunitrile (NC({4-CH<sub>3</sub>)C<sub>6</sub>H<sub>4</sub>)



	Peak	Intensity	Corr. Intensity	Base (H)	Base (L)	Area	Corr. Area
1	2231.64	97.42	1.08	2250.93	2208.49	0.33	0.05
2	2852.72	95.55	1.86	2881.65	2800.64	1.02	0.16
3	2922.16	93.21	3.25	2947.23	2881.65	1.38	0.38

**Figure 3. 8:** IR of 2, 2-*cis*-[Rh<sub>2</sub>(NPhCOCH<sub>3</sub>)<sub>4</sub>]·NC ({4-CH<sub>3</sub>}C<sub>6</sub>H<sub>4</sub>) complex

Figure 3.9 below shows the IR (Infrared) spectrum of [Rh<sub>2</sub>(O<sub>2</sub>CCH<sub>3</sub>)(NPhCOCF<sub>3</sub>)<sub>3</sub>]·2NCC<sub>6</sub>H<sub>5</sub> complex. The stretching frequency for the C-N group is located at 2227.28 cm<sup>-1</sup> for the uncomplexed NCC<sub>6</sub>H<sub>5</sub> shown in Figure 3.2 above and 2322.29 cm<sup>-1</sup> for [Rh<sub>2</sub>(O<sub>2</sub>CCH<sub>3</sub>)(NPhCOCF<sub>3</sub>)<sub>3</sub>]·2NCC<sub>6</sub>H<sub>5</sub> complex shown below. This is indicative that σ-bonding is predominant over π-back-bonding because there is an increase in the stretching frequency of [Rh<sub>2</sub>(O<sub>2</sub>CCH<sub>3</sub>)(NPhCOCF<sub>3</sub>)<sub>3</sub>]·2NCC<sub>6</sub>H<sub>5</sub> complex compared to the uncomplexed nitrile.

The IR for the complex was taken as a solid while that of the uncomplexed nitrile was taken as a liquid. The reason for taking complex as a solid is because it was in crushed up crystalline form, whereas the uncomplexed nitrile is liquid at room temperature.

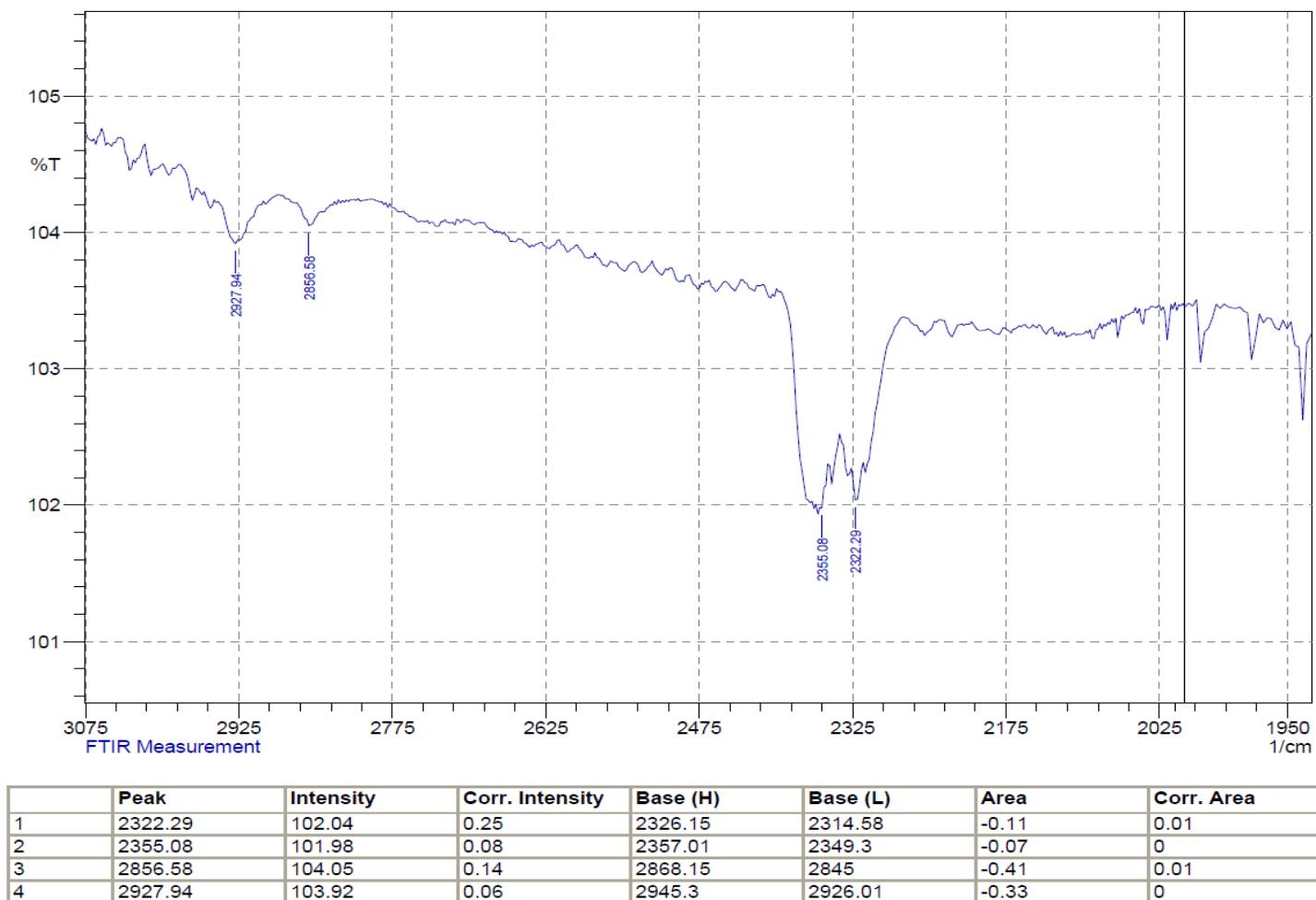


**Figure 3.9:** IR of  $[\text{Rh}_2 (\text{O}_2\text{CCH}_3)(\text{NPhCOCF}_3)_3] \cdot 2\text{NCC}_6\text{H}_5$  complex

While the same stretching frequency is observed for all the uncomplexed nitriles, it is observed that each complexed nitrile had different stretching frequencies. This is indicative of a different amount of interaction between the nitriles and the rhodium complex; in this case, different degrees of  $\sigma$ -bonding interactions.

## <sup>1</sup>H NMR Data

A proton NMR spectrum was obtained for each of the following compounds:

1. 2, 2-*cis*-[Rh<sub>2</sub>(NPhCOCH<sub>3</sub>)<sub>4</sub>]·2NCC<sub>6</sub>H<sub>5</sub>
2. 2, 2-*cis*-[Rh<sub>2</sub>(NPhCOCH<sub>3</sub>)<sub>4</sub>]·NC({2-CH<sub>3</sub>}C<sub>6</sub>H<sub>4</sub>)
3. 2, 2-*cis*-[Rh<sub>2</sub>(NPhCOCH<sub>3</sub>)<sub>4</sub>]·NC({3-CH<sub>3</sub>}C<sub>6</sub>H<sub>4</sub>)
4. 2, 2-*cis*-[Rh<sub>2</sub>(NPhCOCH<sub>3</sub>)<sub>4</sub>]·NC({4-CH<sub>3</sub>}C<sub>6</sub>H<sub>4</sub>)
5. Uncomplexed nitriles: benzonitrile, meta-tolunitrile, ortho-tolunitrile, and para-tolunitrile
6. 2,2,2-trifluoro-N-phenylacetamide (NPhCOCF<sub>3</sub>)
7. [Rh<sub>2</sub>(O<sub>2</sub>CCH<sub>3</sub>)(NPhCOCF<sub>3</sub>)<sub>3</sub>]·2NCC<sub>6</sub>H<sub>5</sub>

The chemical shifts of the protons were compared in order to gain an understanding of the effect of bonding the nitriles to the dirhodium phenyl acetamide complex. Protons farther to the right side of the spectrum are considered to be shielded and upfield. Shielding refers to the electrons in a molecule shielding the nucleus. Protons on the left side of the spectrum are considered to be deshielded and downfield.

Figure 3.10 shows the proton labels of the uncomplexed benzonitrile. Due to the resonance effect of the phenyl ring, the protons in the ortho and meta positions (H<sub>3</sub> and H<sub>2</sub> respectively) to the C≡N functional group in the benzonitrile are deshielded. The C in the C≡N functional group is electron deficient, thus deshields the proton closest to it (H<sub>3</sub>). The H<sub>3</sub> protons in the ortho position are the most deshielded by the electron donated by the nitrogen atom, as such appearing more downfield. The H<sub>3</sub> protons are split by H<sub>2</sub> protons and appear as a doublet.

The H<sub>1</sub> protons however are split by both H<sub>2</sub> and H<sub>3</sub>, thus, appearing as a triplet. The H<sub>2</sub> protons are also split by H<sub>1</sub> and H<sub>3</sub> and thus, appear as a triplet. Because there are twice as many

H<sub>2</sub> and H<sub>3</sub>, these peaks are longer than the H<sub>1</sub> peaks. The peaks at (1.9644, 2.1302 and 2.1678) ppm are solvent impurities from CDCl<sub>3</sub>. The 7.2891 ppm peak is the proton from the CHCl<sub>3</sub> in the CDCl<sub>3</sub> solvent (see Figure 3.11)

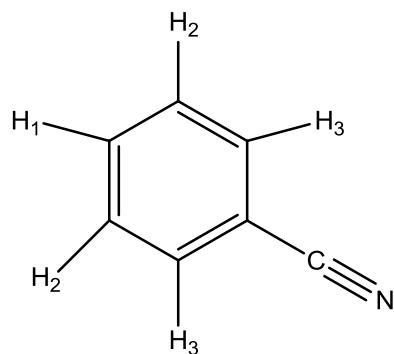


**Figure 3.10:** <sup>1</sup>H labels of uncomplexed Benzonitrile

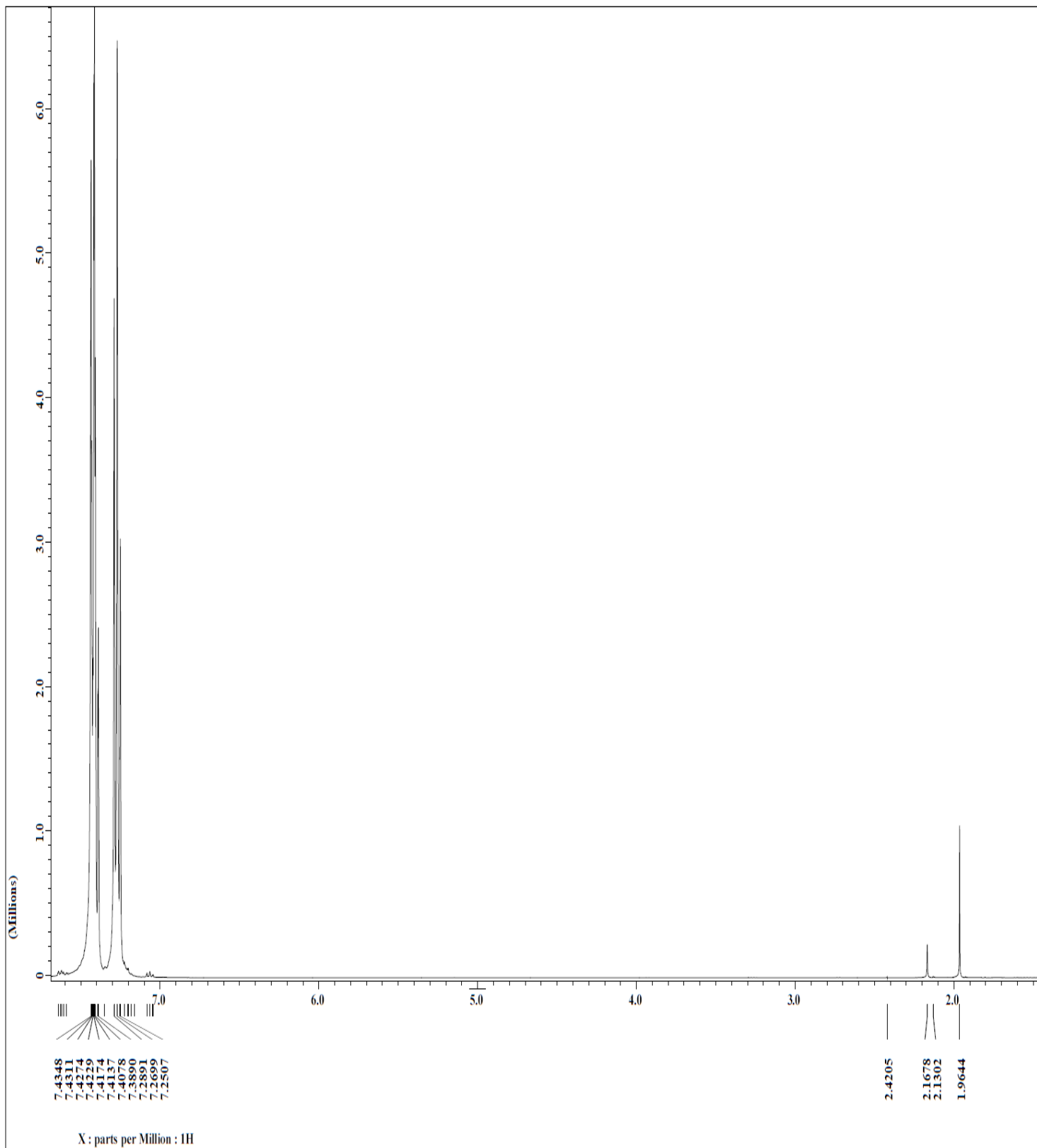
The phenyl peak positions and protons of the uncomplexed benzonitrile are shown in Table 3.1 below.



**Table 3.1:** Phenyl peak positions and protons for uncomplexed benzonitrile.

Phenyl Peaks (ppm)	Phenyl Protons
7.4348	H <sub>3</sub>
7.4311	H <sub>3</sub>
7.4274	H <sub>3</sub>
7.4299	H <sub>3</sub>
7.4174	H <sub>3</sub> ,H <sub>2</sub>
7.4137	H <sub>3</sub> ,H <sub>2</sub>
7.4078	H <sub>3</sub> ,H <sub>2</sub>
7.3890	H <sub>3</sub> ,H <sub>2</sub>
7.2891	H <sub>1</sub> ,CHCl <sub>3</sub>
7.2699	H <sub>1</sub>
7.2507	H <sub>1</sub>

Figure 3.11 below shows the <sup>1</sup>H NMR of uncomplexed benzonitrile.



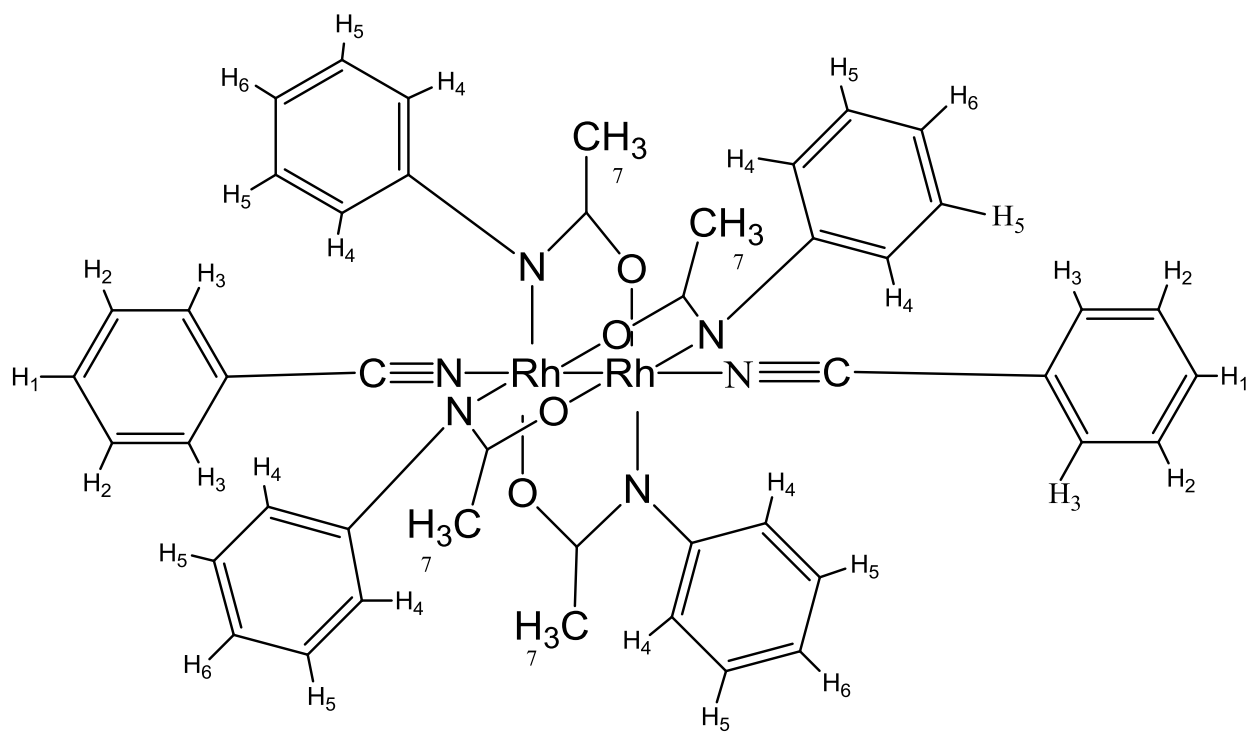
**Figure 3.11:**  $^1\text{H}$  NMR spectrum of uncomplexed benzonitrile ( $\text{NCC}_6\text{H}_5$ )

Figure 3.12 shows the proton labels for 2, 2-*cis*-[Rh<sub>2</sub>(NPhCOCH<sub>3</sub>)<sub>4</sub>] $\cdot$ 2NCC<sub>6</sub>H<sub>5</sub> complex. The rhodium atom, being a metal bound to the C $\equiv$ N functional group, manipulates the C $\equiv$ N functional group's properties from acting as an electron withdrawing group to acting similar to an electron donating group.

Protons on the phenyl ring of the benzonitrile are deshielded by the C $\equiv$ N functional group, but the protons in the ortho position are more deshielded than the protons in the para position.

The H<sub>3</sub> protons are more deshielded through inductive effect than the H<sub>2</sub> or H<sub>1</sub> protons because they are the closest to the C $\equiv$ N. The H<sub>3</sub> protons appear as a doublet because they are split by H<sub>2</sub> protons. By the same inductive effect, the H<sub>2</sub> protons are also deshielded by the C $\equiv$ N functional group, thus since the H<sub>2</sub> protons are not as close to the C $\equiv$ N functional group as the H<sub>3</sub> protons, the H<sub>2</sub> protons appear slightly more upfield to the H<sub>3</sub> protons. The H<sub>2</sub> protons appear as a triplet because they are split by the H<sub>1</sub> and H<sub>3</sub> protons. The H<sub>1</sub> protons also appear as a triplet because they are split by the H<sub>2</sub> and H<sub>3</sub> protons. The peak that appears at 7.1944 ppm is the CHCl<sub>3</sub> in the CDCl<sub>3</sub> solvent peak .

The phenyl protons (H<sub>4</sub>, H<sub>5</sub>, and H<sub>6</sub>) are attached to the electron withdrawing nitrogen atom (from the *N*-phenylacetamide). The protons ortho and para to the electron withdrawing group would be shielded because the electrons are delocalized by the N-C-O group of the 2, 2-*cis*-[Rh<sub>2</sub>(NPhCOCH<sub>3</sub>)<sub>4</sub>] $\cdot$ 2NCC<sub>6</sub>H<sub>5</sub> complex.



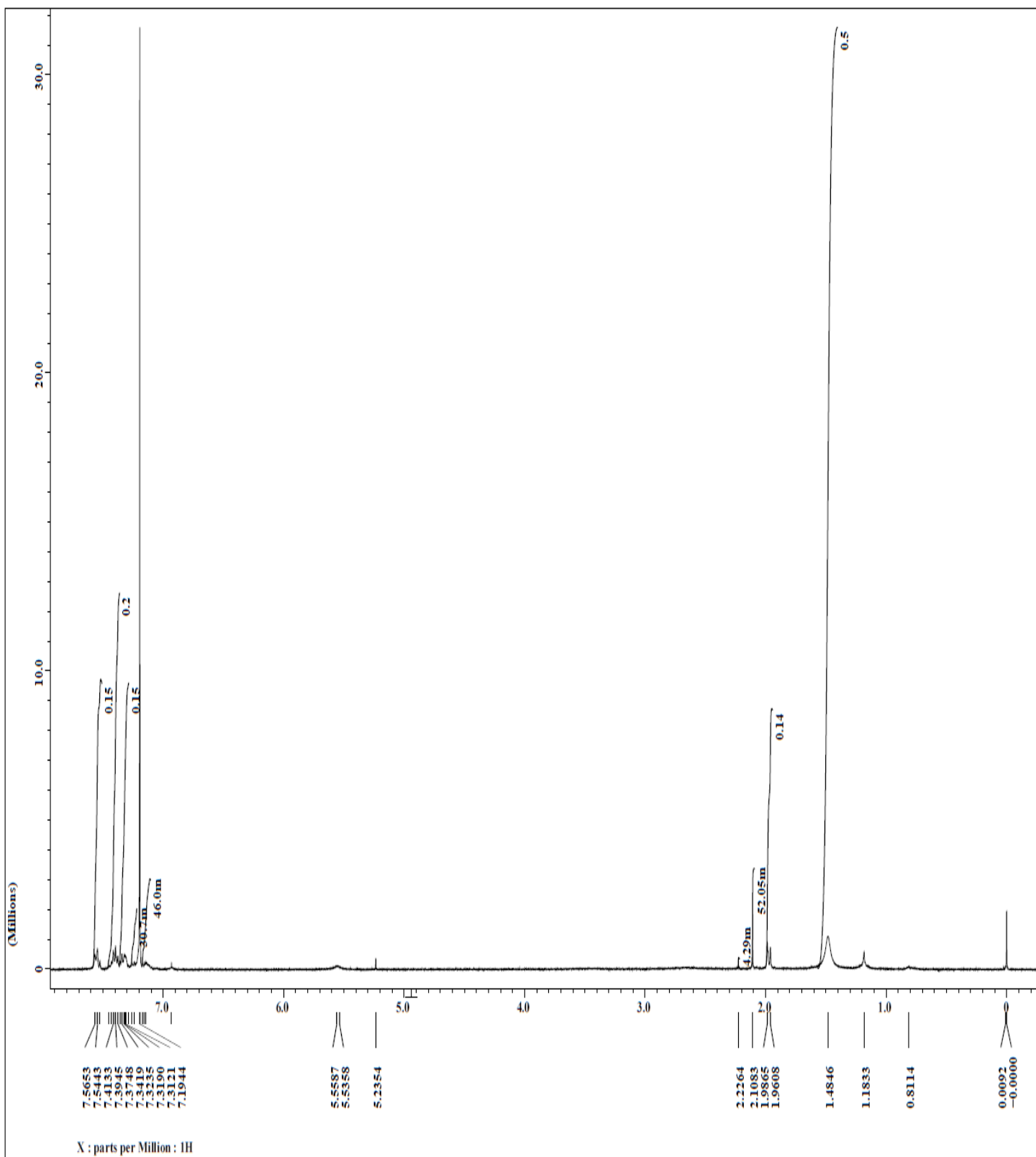
**Figure 3.12:**  $^1\text{H}$  labels of 2, 2-*cis*- $[\text{Rh}_2(\text{NPhCOCH}_3)_4] \cdot 2\text{NCC}_6\text{H}_5$  complex

The phenyl peak positions and protons of 2, 2-*cis*- $[\text{Rh}_2(\text{NPhCOCH}_3)_4] \cdot 2\text{NCC}_6\text{H}_5$  complex are shown in Table 3.2 below.

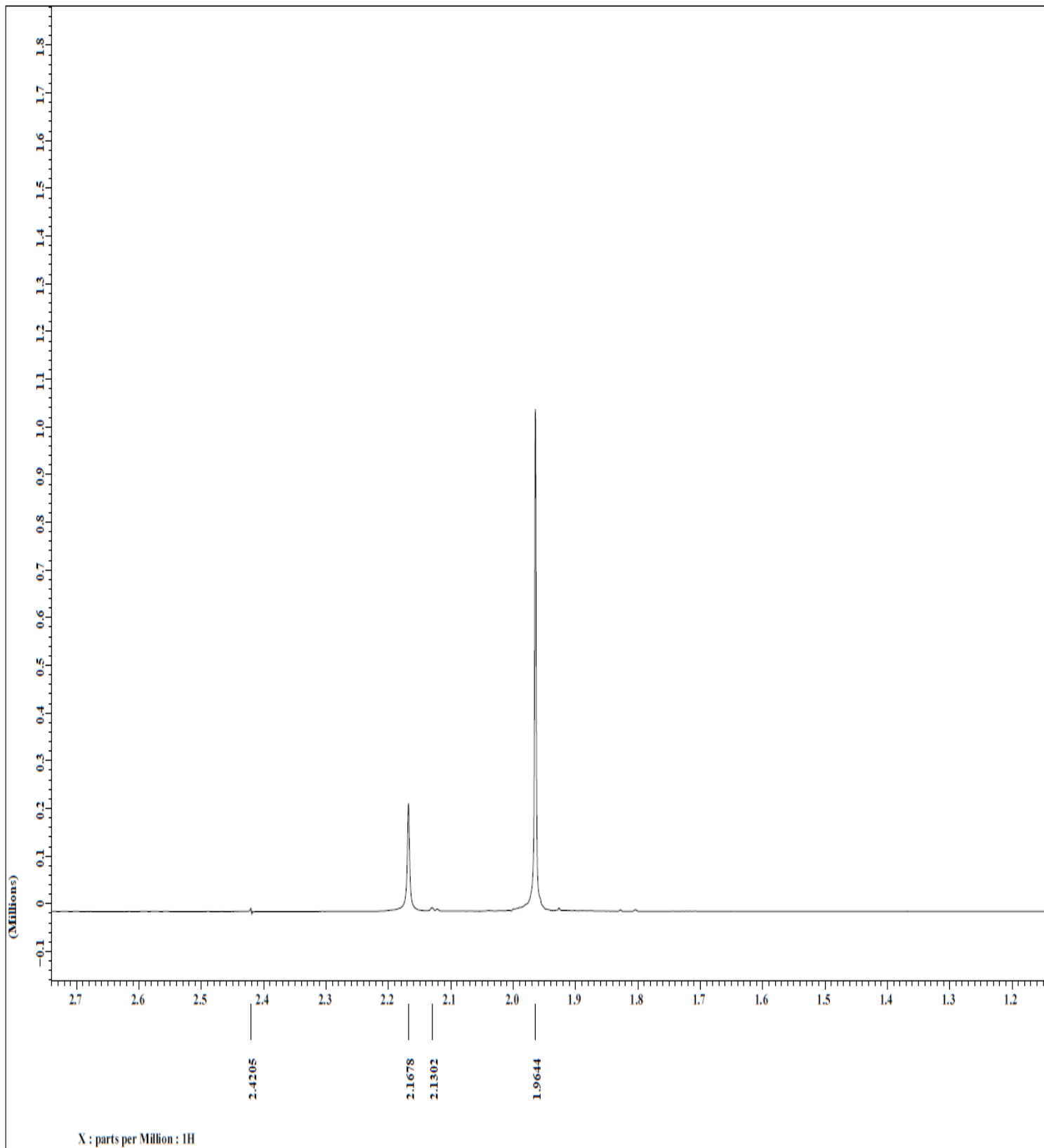
**Table 3.2:** Phenyl peak positions and protons for 2, 2-*cis*-[Rh<sub>2</sub>(NPhCOCH<sub>3</sub>)<sub>4</sub>]·2NCC<sub>6</sub>H<sub>5</sub> complex

Phenyl Peaks (ppm)	Phenyl Protons
7.5653	H <sub>3</sub>
7.5443	H <sub>3</sub>
7.4133	H <sub>2</sub>
7.3945	H <sub>2</sub>
7.3748	H <sub>2</sub>
7.3419	H <sub>2</sub>
7.3235	H <sub>1</sub>
7.3190	H <sub>1</sub>
7.3121	H <sub>1</sub>
7.1944	CHCl <sub>3</sub>

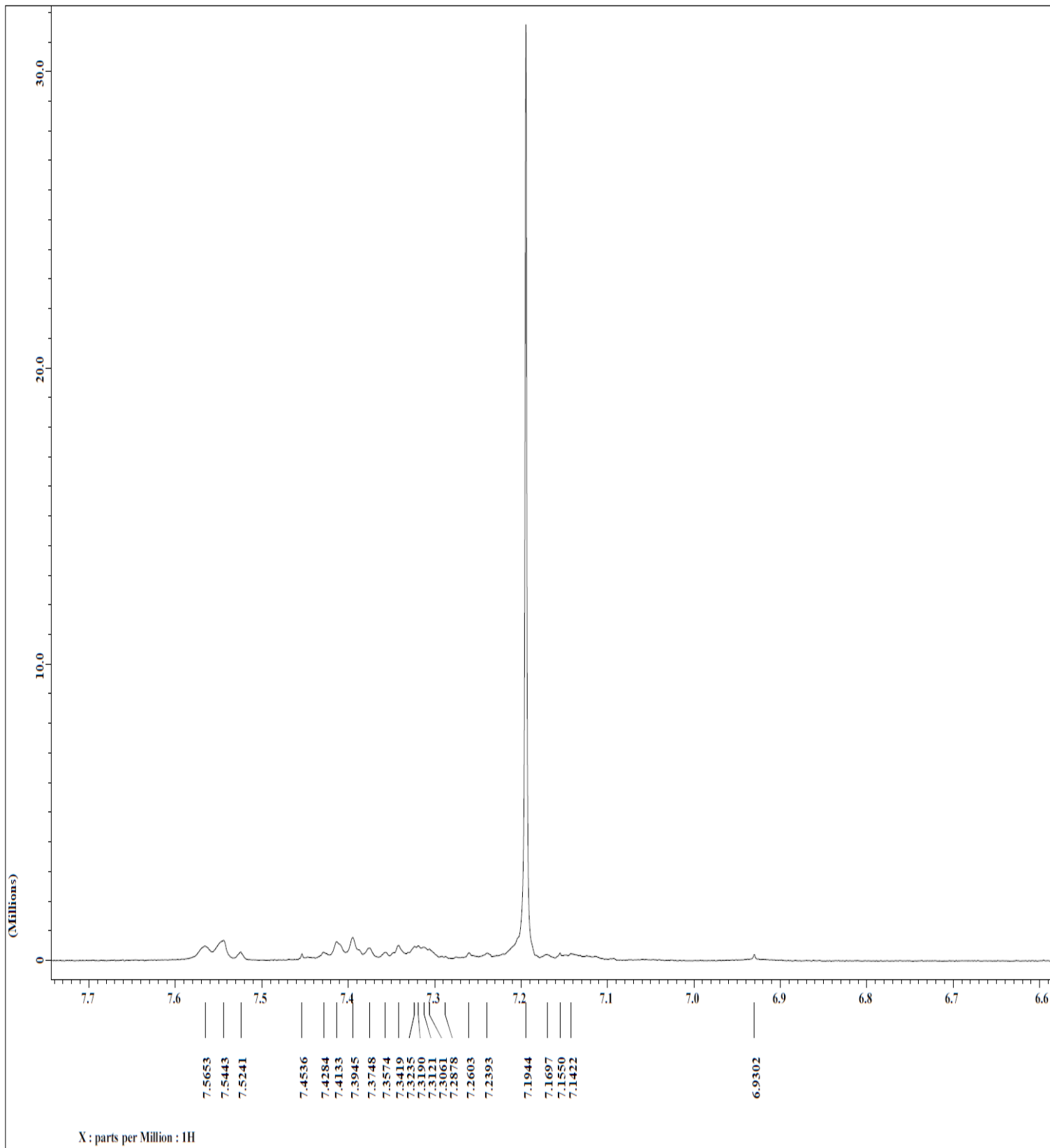
Figure 3.13 is the <sup>1</sup>H NMR spectrum of 2, 2-*cis*-[Rh<sub>2</sub>(NPhCOCH<sub>3</sub>)<sub>4</sub>]·2NCC<sub>6</sub>H<sub>5</sub> complex, Figures 3.14 and 3.15, however, are the <sup>1</sup>H NMR spectrum of 2, 2-*cis*- [Rh<sub>2</sub>(NPhCOCH<sub>3</sub>)<sub>4</sub>]·2NCC<sub>6</sub>H<sub>5</sub> complex expanded in the regions (1.2 – 2.7) ppm and (6.6-7.7) ppm respectively.



**Figure 3.13:**  $^1\text{H}$  NMR spectrum of 2, 2-*cis*- $[\text{Rh}_2(\text{NPhCOCH}_3)_4] \cdot 2\text{NCC}_6\text{H}_5$  complex



**Figure 3.14:**  $^1\text{H}$  NMR spectrum of  $2, 2\text{-cis-}[\text{Rh}_2(\text{NPhCOCH}_3)_4] \cdot 2\text{NCC}_6\text{H}_5$  complex (expanded 1.2-2.7 ppm)



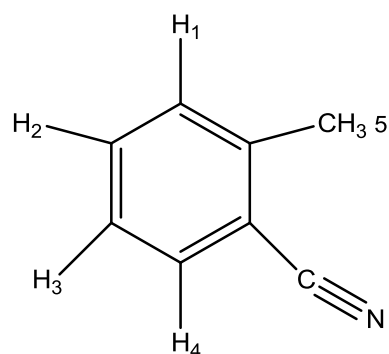
**Figure 3.15:**  $^1\text{H}$  NMR spectrum of 2, 2-*cis*- $[\text{Rh}_2(\text{NPhCOCH}_3)_4] \cdot 2\text{NCC}_6\text{H}_5$  complex (expanded 6.6-7.7ppm)



Figure 3.16 shows the proton labels of the uncomplexed *o*-tolunitrile. Due to the resonance effect of the phenyl ring, the protons in the ortho and meta positions ( $H_3$  and  $H_4$  respectively) to the  $C\equiv N$  functional group in the ortho-tolunitrile appear downfield because they are deshielded by the  $C\equiv N$  functional group. The C in the  $C\equiv N$  functional group is electron deficient, thus deshields the proton closest to it ( $H_4$ ). The  $H_2$  protons in the para position to the  $C\equiv N$  functional group also appear downfield but a bit upfield than  $H_3$  and  $H_4$  because they are deshielded by the  $C\equiv N$  functional group very slightly. The  $H_4$  protons are split by  $H_3$  protons and appear as a doublet.

The  $H_2$  protons, however, are split by both  $H_1$  and  $H_3$ , thus, appearing as a triplet. The  $H_3$  protons are also split by  $H_2$  and  $H_3$  and thus, appear as a triplet.

The 7.2576 ppm peak is an overlap of the proton from the  $CHCl_3$  in the  $CDCl_3$  solvent (see Figure 3.17). The peak that appears at 2.5323 ppm however is  $H_5$  protons from the methyl group on the *o*-tolunitrile ligand.



**Figure 3.16:**  $^1H$  labels of uncomplexed *o*-tolunitrile

The phenyl peak positions and protons of the uncomplexed *o*-tolunitrile are shown in Table 3.3 below.

**Table 3.3:** Phenyl peak positions and protons for uncomplexed *o*-tolunitrile

Phenyl Peaks (ppm)	Phenyl Protons
7.5369	H <sub>4</sub>
7.5346	H <sub>4</sub>
7.5177	H <sub>4</sub>
7.5149	H <sub>4</sub>
7.4380	H <sub>3</sub> ,H <sub>1</sub>
7.4348	H <sub>3</sub> ,H <sub>1</sub>
7.2772	H <sub>3</sub> ,H <sub>1</sub>
7.2576	H <sub>3</sub> , CHCl <sub>3</sub>
7.2214	H <sub>2</sub>
7.2021	H <sub>2</sub>

Figures 3.17-3.20 below show the <sup>1</sup>H NMR of uncomplexed *o*-tolunitrile.

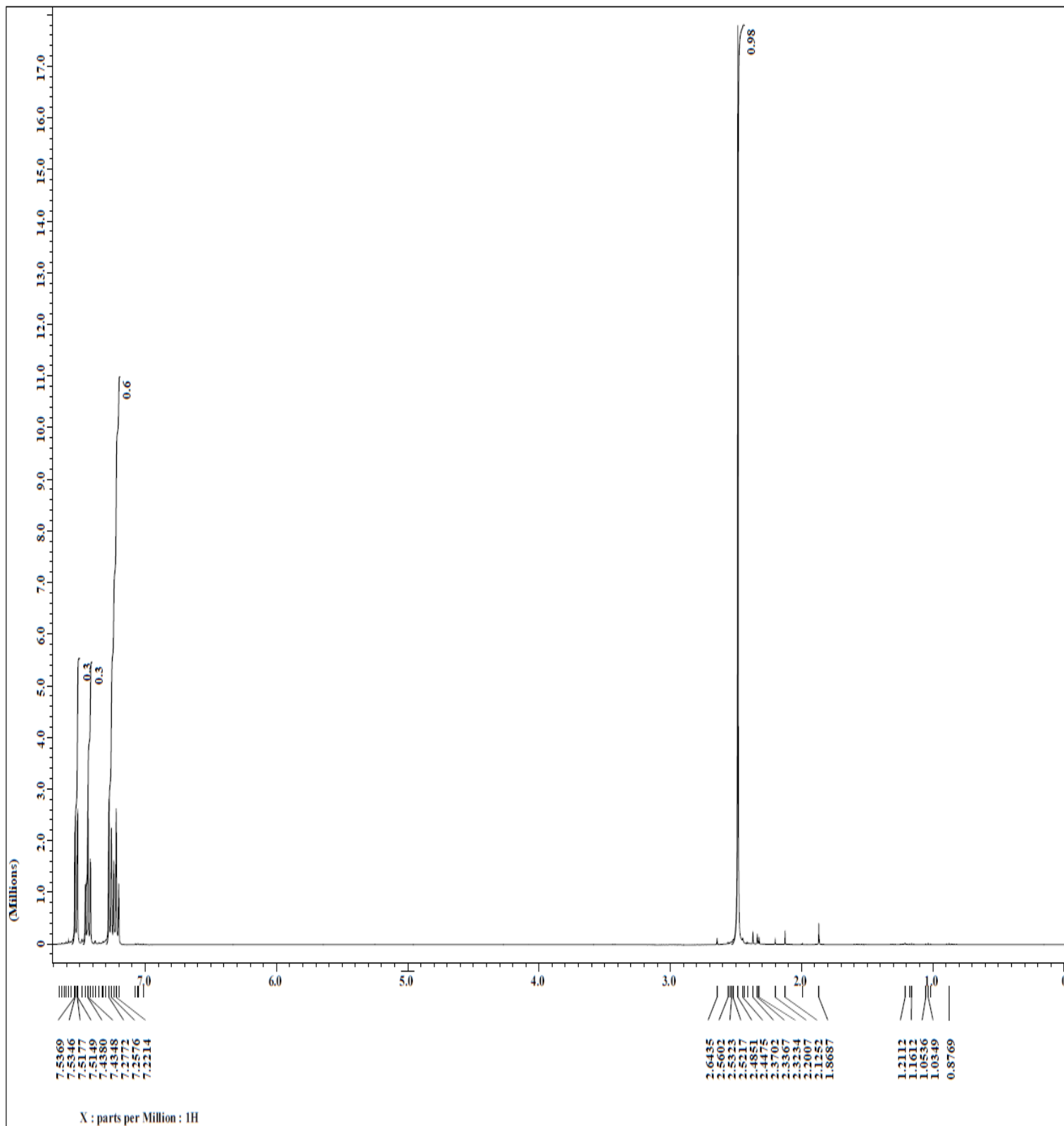
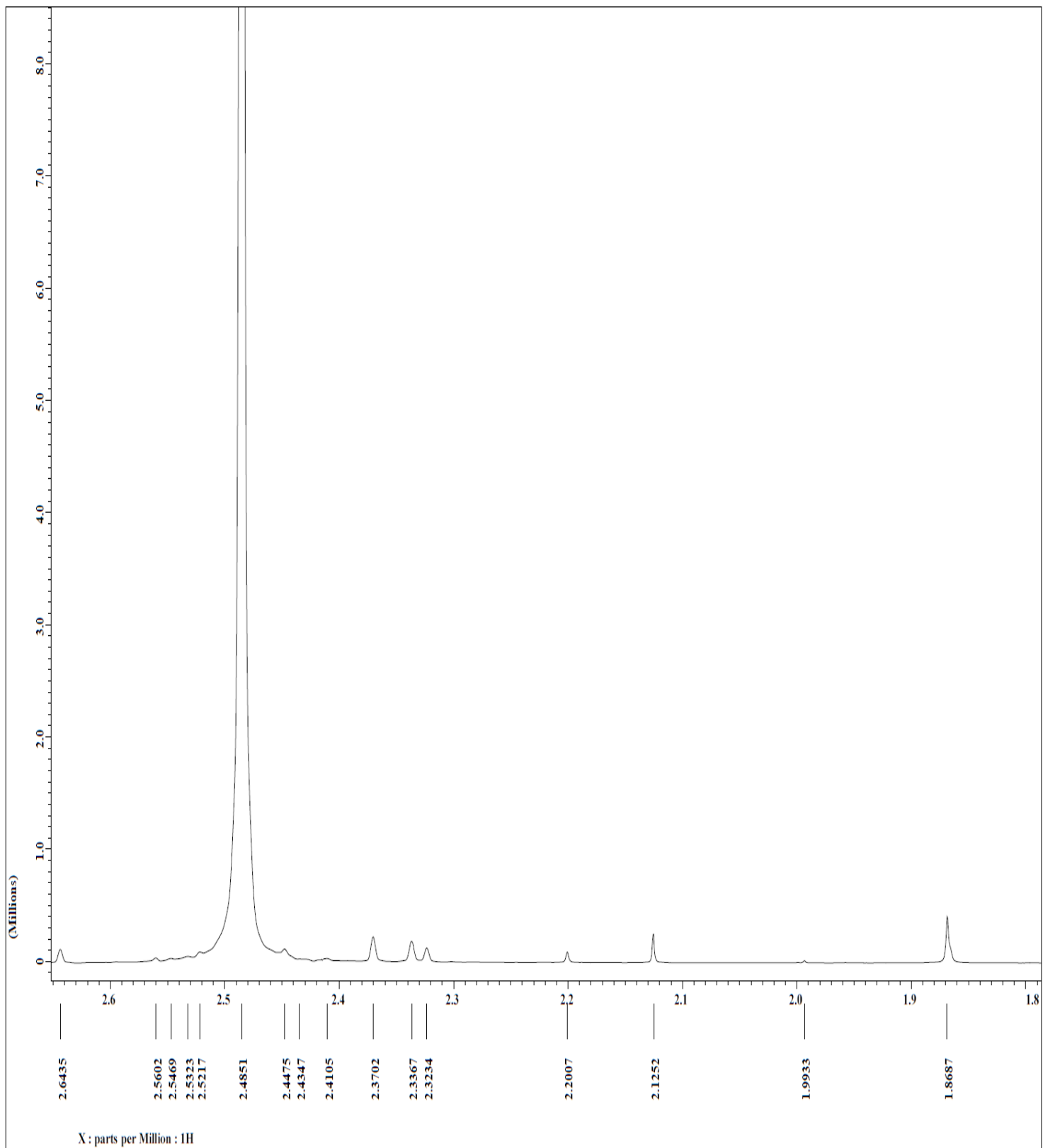
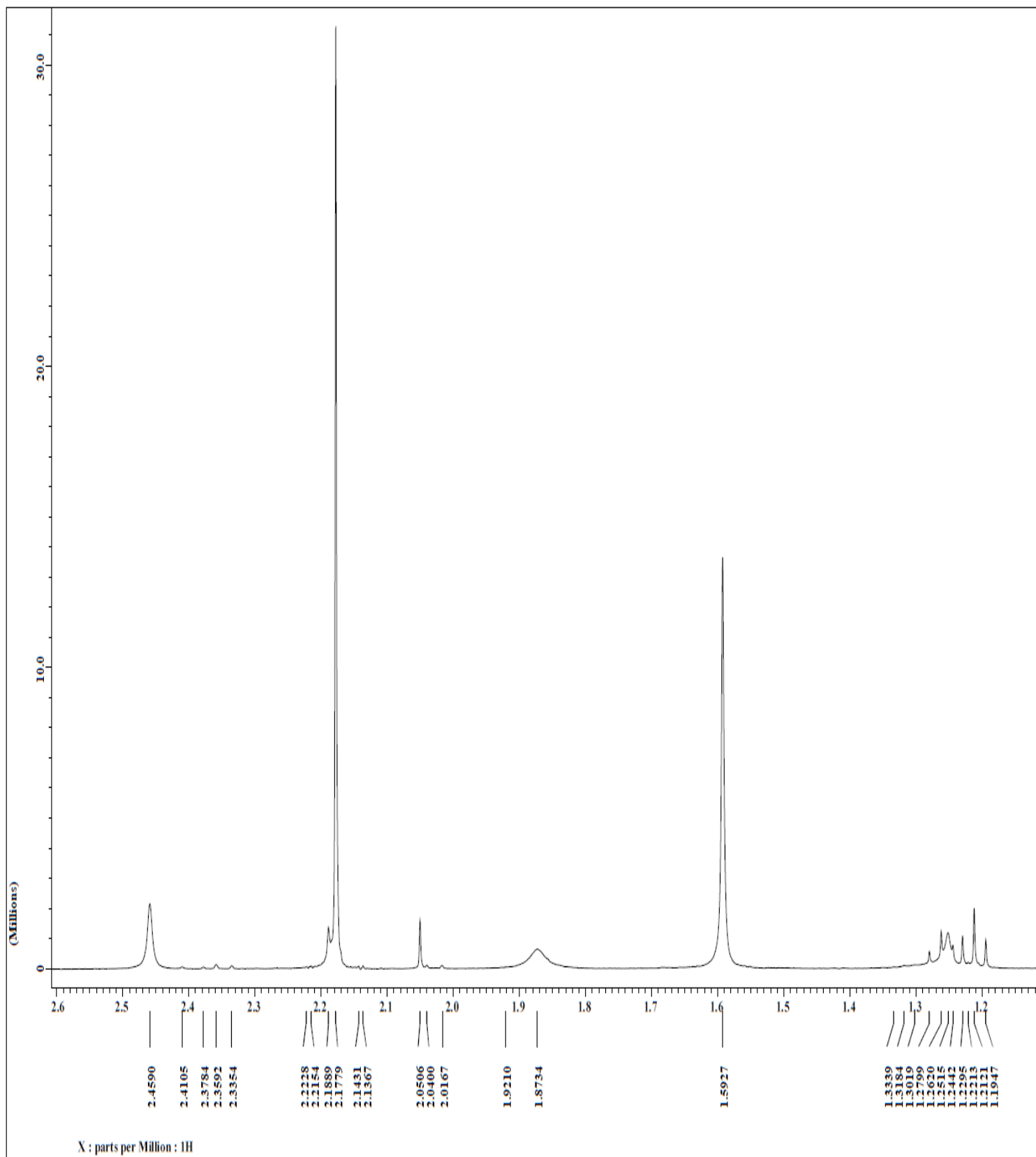


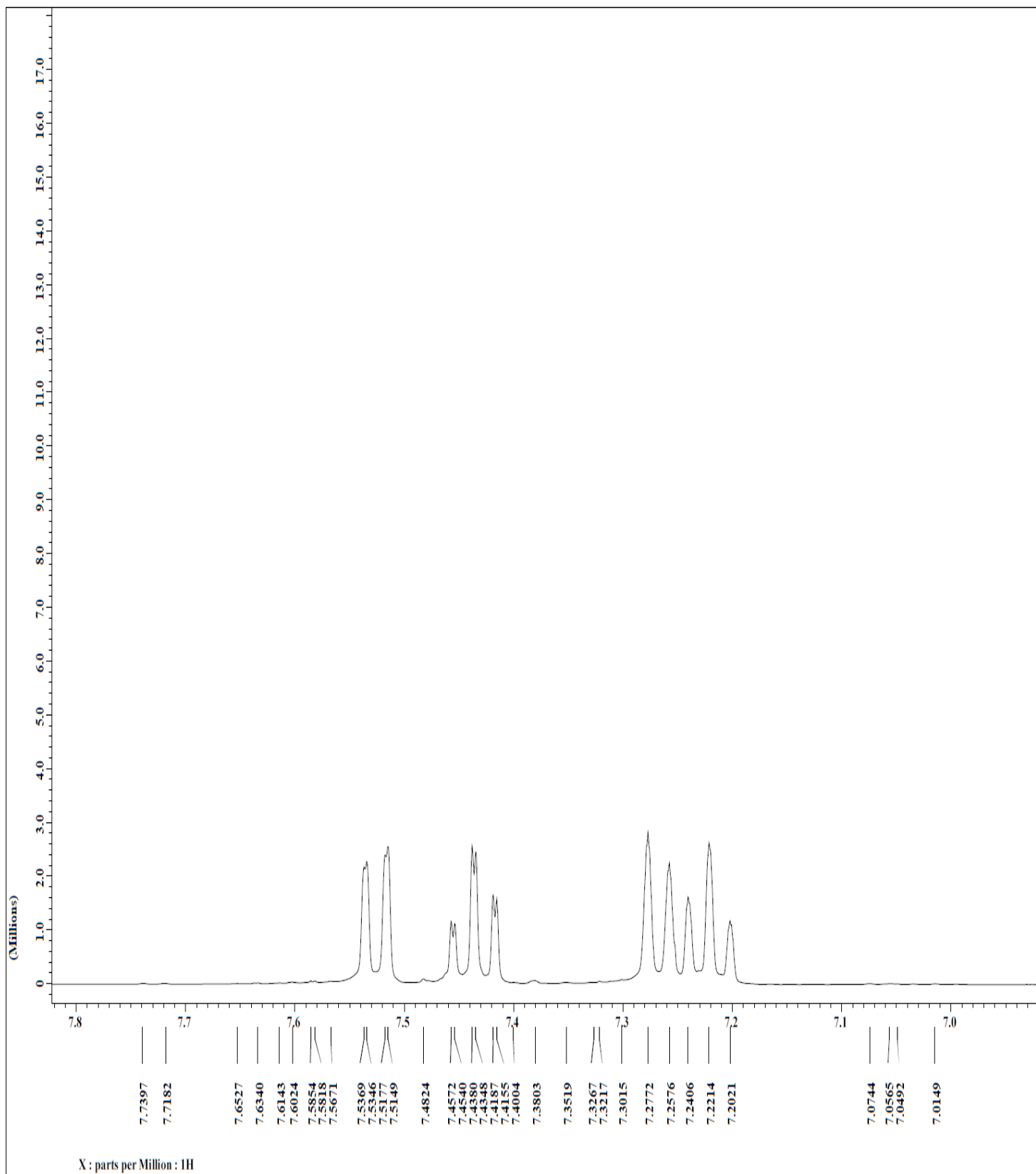
Figure 3.17:  $^1\text{H}$  NMR of uncomplexed *o*-tolunitrile



**Figure 3.18:**  $^1\text{H}$  NMR of uncomplexed *o*-tolunitrile (expanded 1.8-2.6 ppm)



**Figure 3.19:**  $^1\text{H}$  NMR of uncomplexed *o*-tolunitrile (expanded 1.2-2.6 ppm)



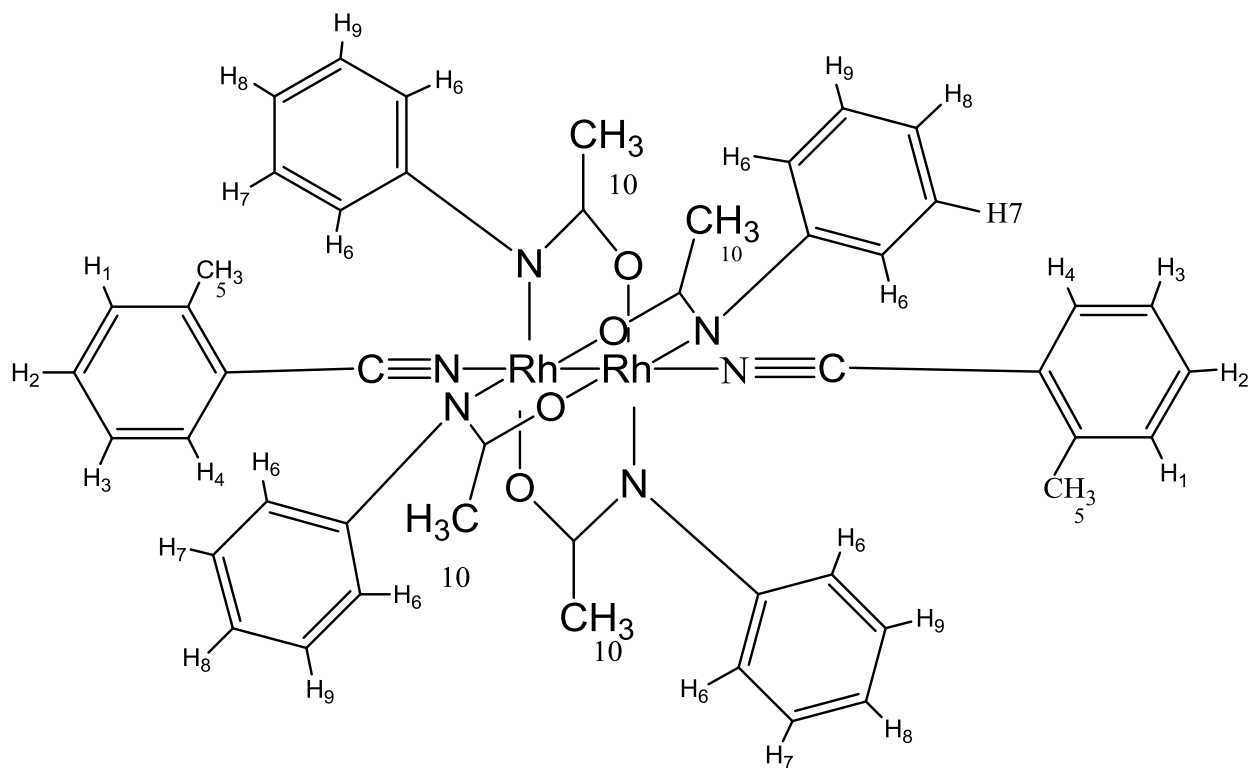
**Figure 3.20:**  $^1\text{H}$  NMR of uncomplexed *o*-tolunitrile (expanded 7.0-7.8 ppm)

Figure 3.21 shows the proton labels for 2, 2-*cis*- [Rh<sub>2</sub>(NPhCOCH<sub>3</sub>)<sub>4</sub>]·NC({2-CH<sub>3</sub>}C<sub>6</sub>H<sub>4</sub>) complex. The rhodium atom, being a metal bound to the C≡N functional group, manipulates the C≡N functional group's properties from acting as an electron withdrawing group to acting similar to an electron donating group.

Protons on the phenyl ring of the ortho-tolunitrile are deshielded by the C≡N functional group, but the protons in the ortho position (H<sub>4</sub>) are most deshielded because they are closest to the C≡N functional group, thus appears more downfield. The H<sub>4</sub> protons also appear as a doublet because it is split by H<sub>2</sub>. The H<sub>3</sub> and H<sub>2</sub> protons, meta and para to the C≡N functional group respectively are also deshielded by the C≡N functional group. The H<sub>2</sub> protons appear as a triplet because they are split by the H<sub>1</sub> and H<sub>3</sub> protons. The H<sub>2</sub> protons appear more upfield because it is poorly deshielded by the C≡N functional group. Because H<sub>1</sub> protons are split by H<sub>2</sub> it also appears as a doublet. The peak that appears at 7.2645 ppm is the CHCl<sub>3</sub> solvent peak which also masks the H<sub>3</sub> peak.

The methyl group in the ortho position of the phenyl ring is an electron donating group. The H<sub>5</sub> protons from the methyl group of the ortho-tolunitrile ligand appear at 2.4590 ppm while H<sub>10</sub> protons (methyl group on rhodium adduct) appears at 1.5927 ppm. H<sub>10</sub> appears to be more intense than H<sub>5</sub> because there is a 12:6 ratio of H<sub>10</sub>:H<sub>5</sub>.

The phenyl protons (H<sub>6</sub>, H<sub>7</sub>, and H<sub>8</sub>) are attached to the electron withdrawing nitrogen atom (from the *N*-phenylacetamide). The protons ortho and para to the electron withdrawing group would be shielded because the electrons are delocalized by the N-C-O group of the 2, 2-*cis*- [Rh<sub>2</sub>(NPhCOCH<sub>3</sub>)<sub>4</sub>]·NC({2-CH<sub>3</sub>}C<sub>6</sub>H<sub>4</sub>) complex.



**Figure 3.21:**  $^1\text{H}$  labels for 2, 2-*cis*- $[\text{Rh}_2(\text{NPhCOCH}_3)_4] \cdot \text{NC}(\{2\text{-CH}_3\}\text{C}_6\text{H}_4)$  complex

The phenyl peak positions and protons of 2, 2-*cis*- $[\text{Rh}_2(\text{NPhCOCH}_3)_4] \cdot \text{NC}(\{2\text{-CH}_3\}\text{C}_6\text{H}_4)$  complex are shown in Table 3.4 below;



**Table 3.4:** Phenyl peak positions and protons of 2, 2-*cis*-[Rh<sub>2</sub>(NPhCOCH<sub>3</sub>)<sub>4</sub>]·NC({2-CH<sub>3</sub>}C<sub>6</sub>H<sub>4</sub>) complex

Phenyl Peaks (ppm)	Phenyl Protons
7.5072	H <sub>4</sub>
7.4866	H <sub>4</sub>
7.4673	H <sub>3</sub> and H <sub>1</sub>
7.2956	H <sub>3</sub> and H <sub>1</sub>
7.2750	H <sub>3</sub> and H <sub>1</sub>
7.2645	CHCl <sub>3</sub>
7.2429	H <sub>2</sub>
7.1747	H <sub>2</sub>

Figures 3.22-3.24 below show the <sup>1</sup>H NMR of 2, 2-*cis*-[Rh<sub>2</sub>(NPhCOCH<sub>3</sub>)<sub>4</sub>]·NC({2-CH<sub>3</sub>}C<sub>6</sub>H<sub>4</sub>) complex

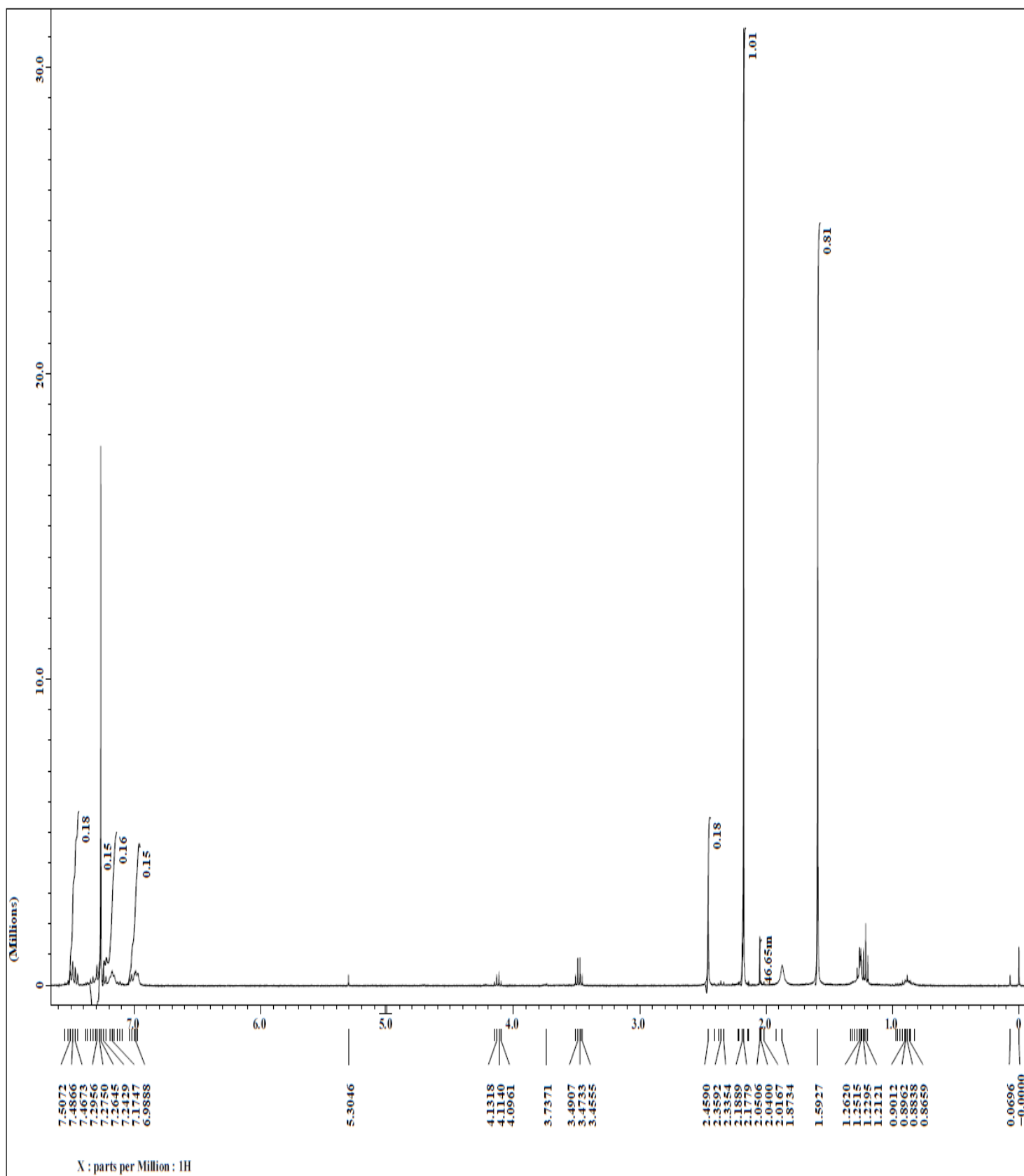


**Figure 3.22:**  $^1\text{H}$  NMR spectrum of 2, 2-*cis*- $[\text{Rh}_2(\text{NPhCOCH}_3)_4] \cdot \text{NC}(\{2\text{-CH}_3\}\text{C}_6\text{H}_4)$  complex

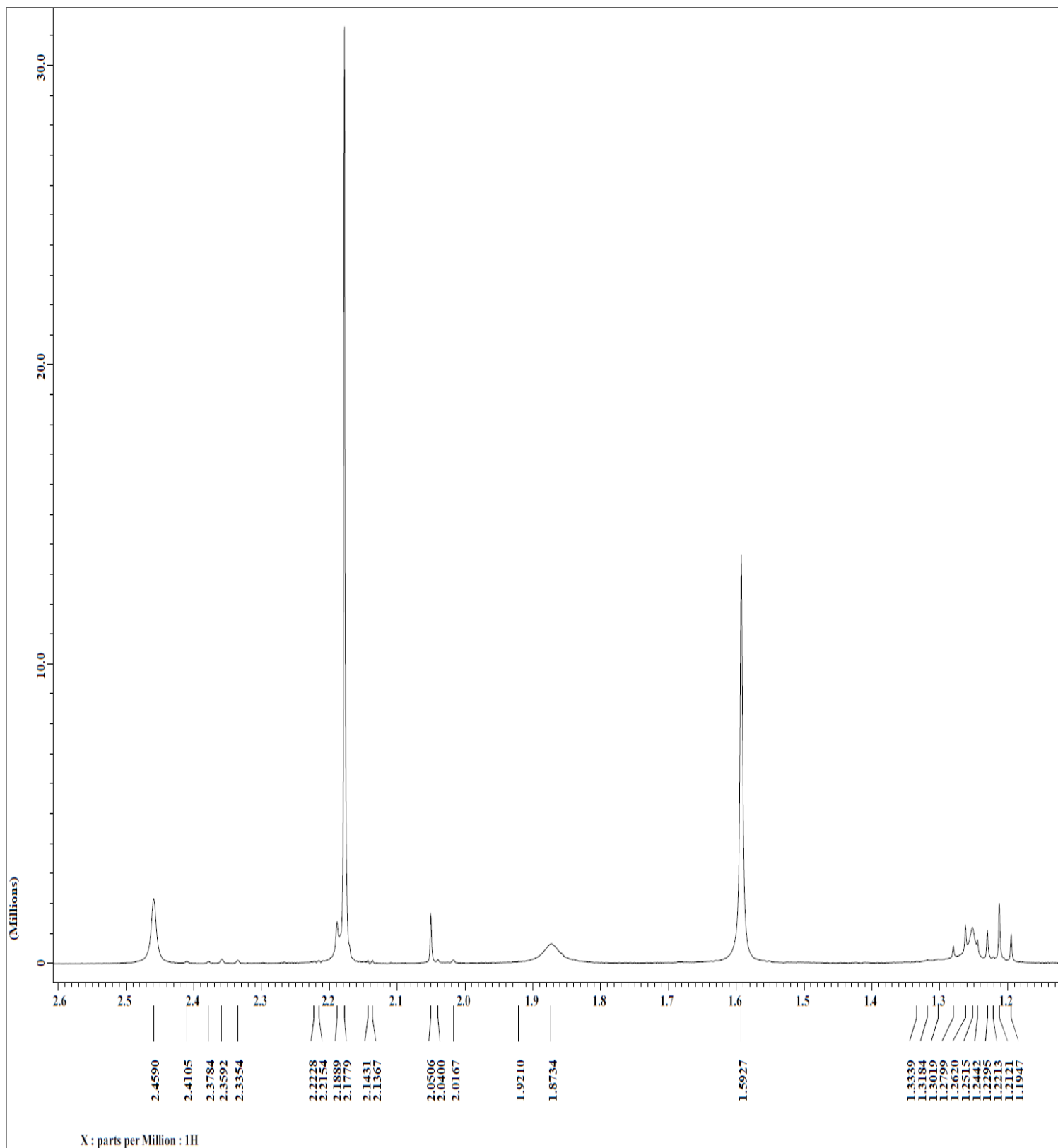


**Figure 3.23:**  $^1\text{H}$  NMR spectrum of 2, 2-*cis*- $[\text{Rh}_2(\text{NPhCOCH}_3)_4] \cdot \text{NC}(\{2\text{-CH}_3\}\text{C}_6\text{H}_4)$  complex (expanded 1.2 ppm-2.6 ppm)

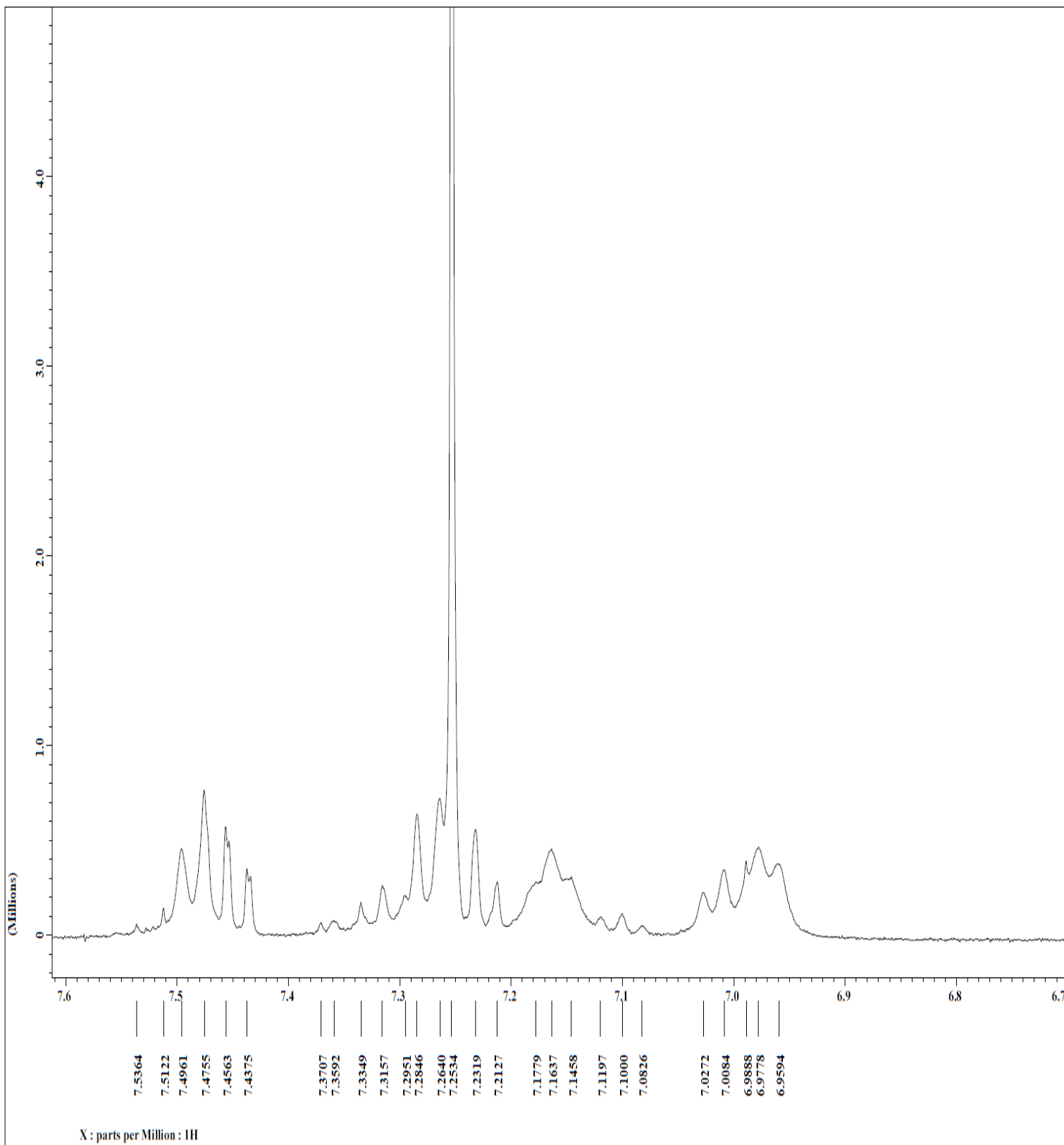


**Figure 3.24:**  $^1\text{H}$  NMR spectrum of 2, 2-*cis*- $[\text{Rh}_2(\text{NPhCOCH}_3)_4]\cdot\text{NC}(\{2\text{-CH}_3\}\text{C}_6\text{H}_4)$  complex (expanded 6.7 ppm-7.6 ppm)

Figure 3.25 shows the proton labels of the uncomplexed meta-tolunitrile. Protons ortho and meta to the  $C\equiv N$  functional group of the meta-tolunitrile ligand,  $H_2$  and  $H_4$  appear the most downfield since these protons are most deshielded by the  $C\equiv N$  functional group through inductive effect.  $H_3$  protons and  $H_4$  protons show peaks that overlap. The peaks appear as a triplet but have smaller doublet peaks amongst the triplet peaks. The  $H_1$  peaks are split by  $H_3$ , thus, should appear as a doublet.  $H_3$  protons are split by both  $H_1$  and  $H_4$  and as such appear as a triplet. The  $H_4$  protons are also split by  $H_3$  protons and appear as a doublet. The  $H_2$  protons, however, are not split, thus, appearing as a singlet.

The 7.2704 ppm peak is an overlap of the proton from the  $CHCl_3$  in the  $CDCl_3$  solvent (see Figure 3.26). The peak that appears at 2.3926 ppm is  $H_5$  protons from the methyl group on the meta-tolunitrile ligand.

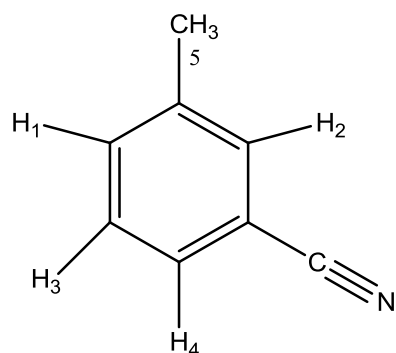


**Figure 3.25:**  $^1H$  labels of uncomplexed *m*-tolunitrile

The phenyl peaks and protons are shown in Table 3.5 below;

**Table 3.5:** Phenyl peak positions and protons of uncomplexed *m*-tolunitrile

Phenyl Peaks (ppm)	Phenyl Protons
7.4220	H <sub>1</sub>
7.4211	H <sub>1</sub>
7.4023	H <sub>1</sub>
7.4009	H <sub>1</sub>
7.3730	H <sub>3</sub> and H <sub>4</sub>
7.3634	H <sub>3</sub> and H <sub>4</sub>
7.3533	H <sub>3</sub> and H <sub>4</sub>
7.3432	H <sub>3</sub> and H <sub>4</sub>
7.3336	H <sub>2</sub>
7.2704	CHCl <sub>3</sub>

Figures 3.26-3.28 below show the <sup>1</sup>H NMR of uncomplexed *m*-tolunitrile

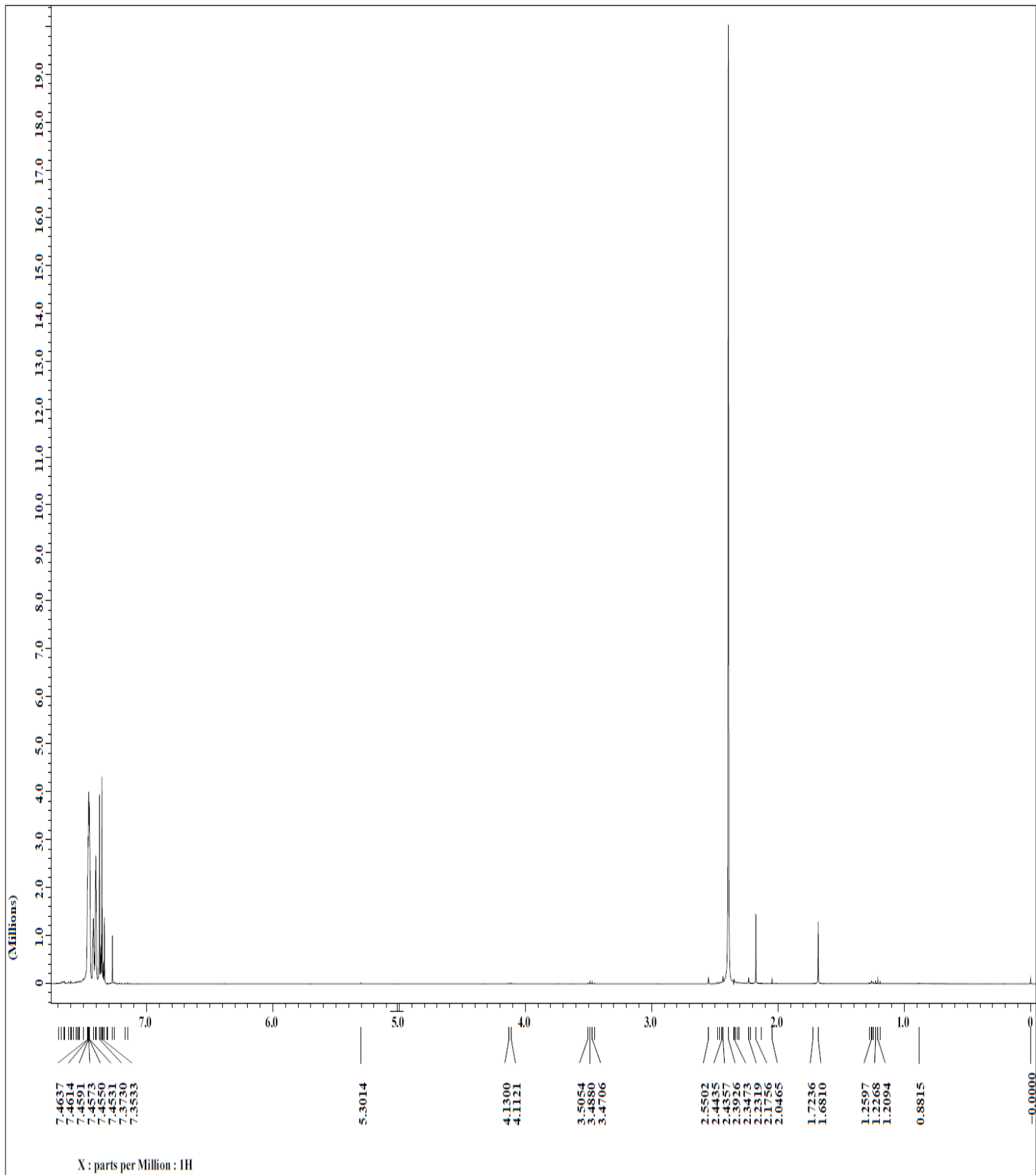
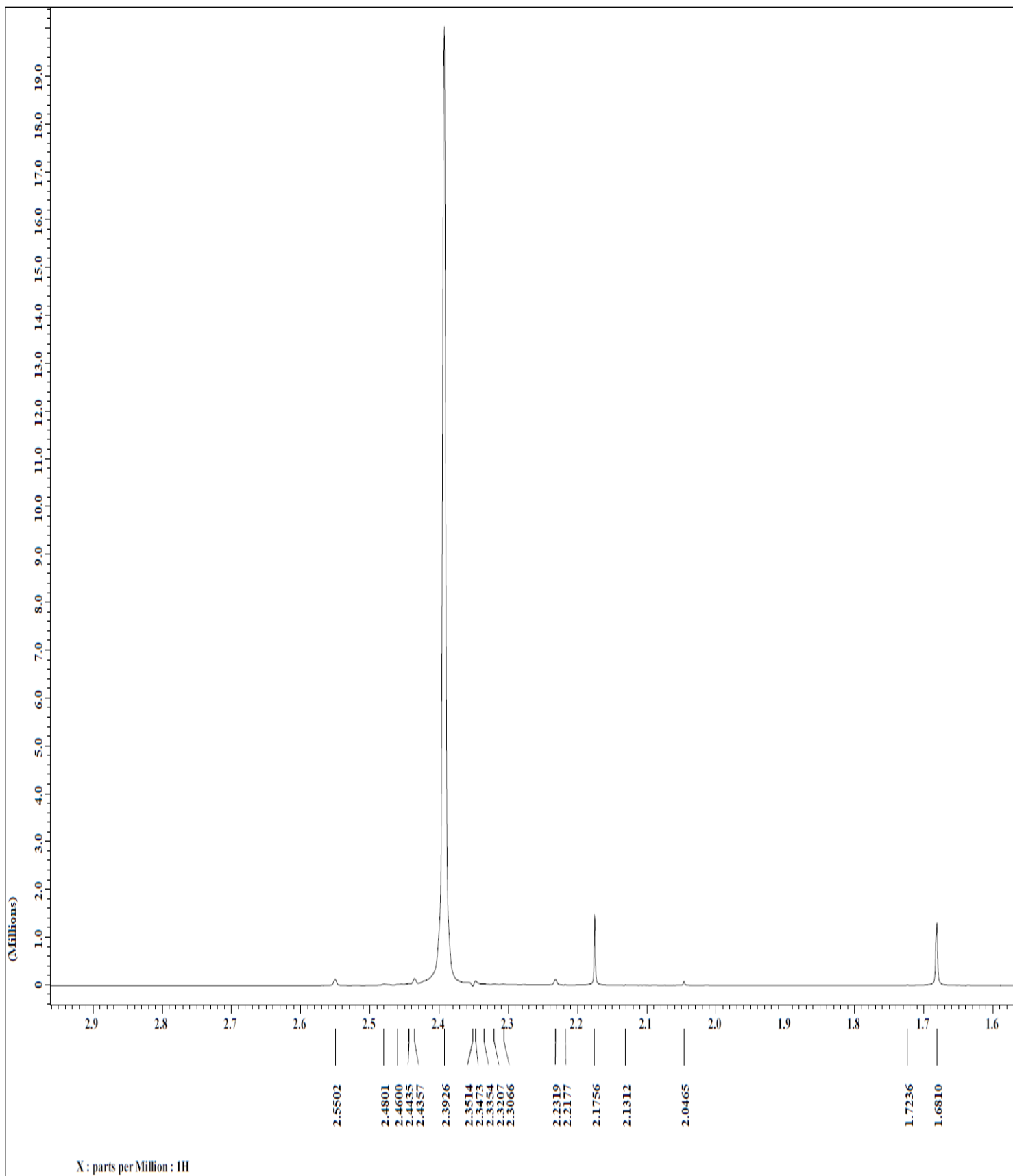
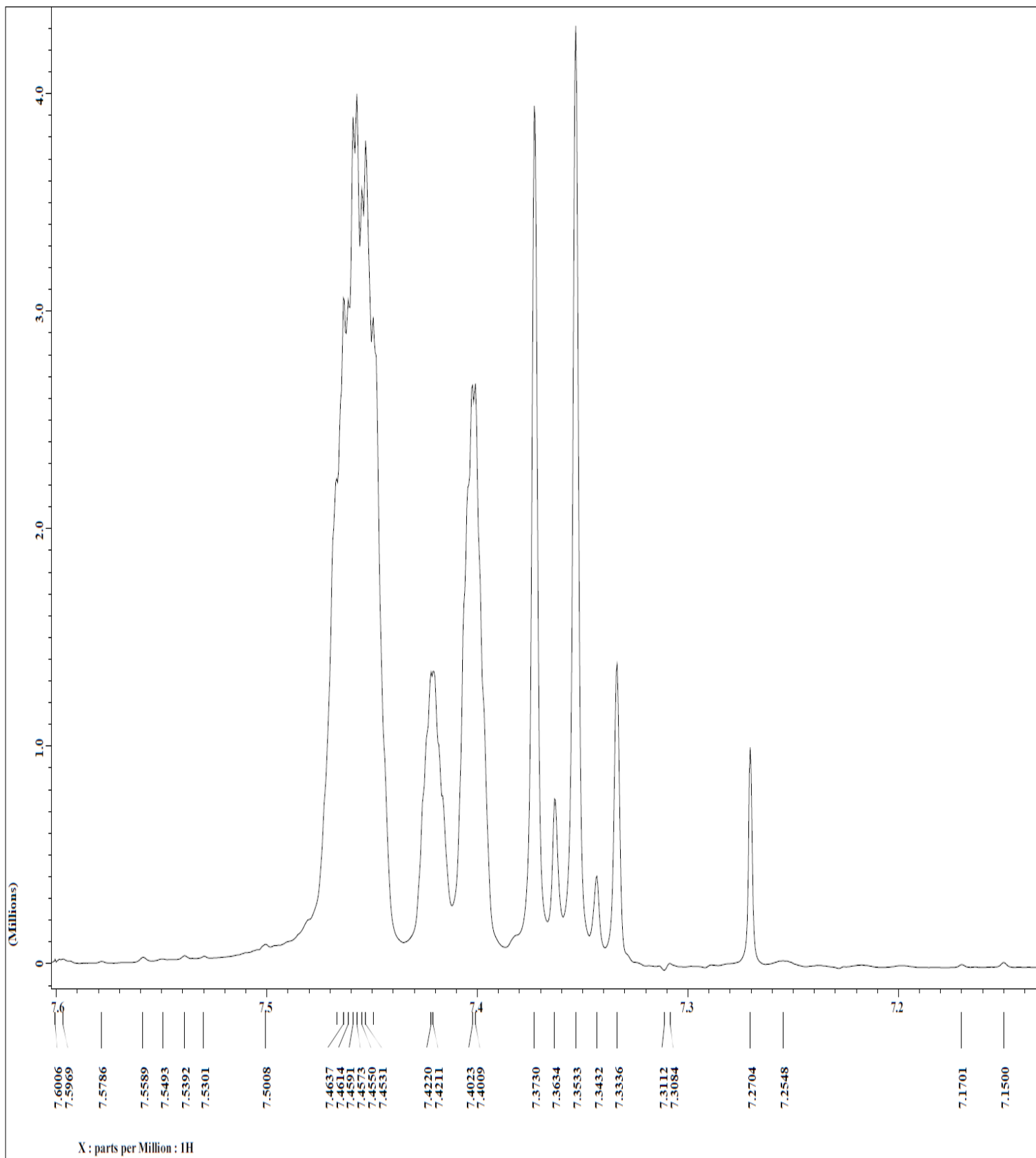


Figure 3.26:  $^1\text{H}$  NMR spectrum of *m*-tolunitrile



**Figure 3.27:**  $^1\text{H}$  NMR spectrum of uncomplexed *m*-tolunitrile (expanded 1.6 ppm-2.9 ppm)





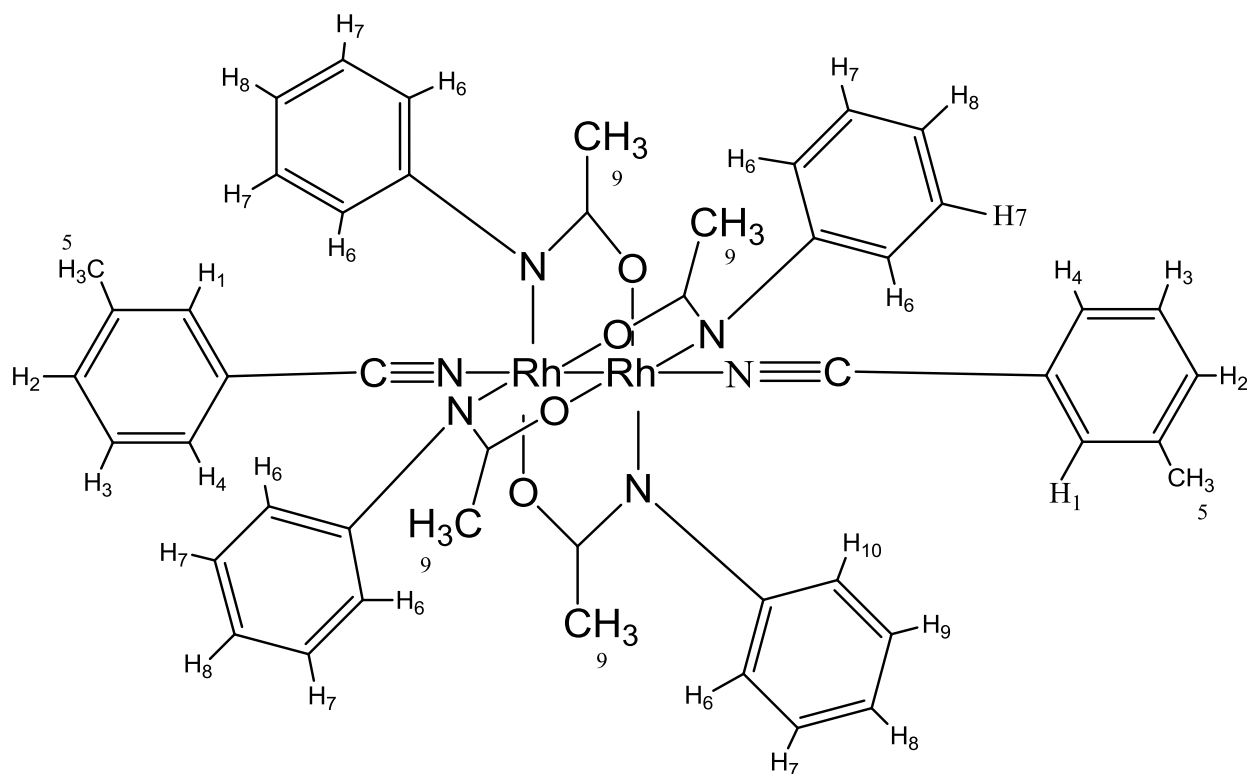
**Figure 3.28:**  $^1\text{H}$  NMR spectrum of uncomplexed *m*-tolunitrile (expanded 7.2 ppm-7.6 ppm)

Figure 3.29 shows the proton labels for 2, 2-*cis*-[Rh<sub>2</sub>(NPhCOCH<sub>3</sub>)<sub>4</sub>]·NC({3-CH<sub>3</sub>}C<sub>6</sub>H<sub>4</sub>) complex. Similarly, rhodium atom, being a metal bound to the C≡N functional group, manipulates the C≡N functional group's properties from acting as an electron withdrawing group to acting similar to an electron donating group.

Protons on the phenyl ring of the meta-tolunitrile are deshielded by the C≡N functional group, but the protons in the ortho position H<sub>1</sub> and H<sub>4</sub> are most deshielded. The H<sub>3</sub> peaks are split by H<sub>2</sub> and H<sub>4</sub>, thus, resulting in a triplet peak. The H<sub>3</sub> protons are also deshielded through inductive effect since H<sub>3</sub> protons are the next closest to the C≡N functional group.

The H<sub>3</sub> protons and H<sub>4</sub> protons shows peaks that overlap. The peaks appear as a triplet but have smaller doublet peaks amongst the triplet peaks. The peak that appears at 7.2530 ppm is the CHCl<sub>3</sub> solvent peak. The H<sub>1</sub> protons appear as a singlet because it is not split by any neighboring protons. The methyl group in the meta position of the phenyl ring is an electron donating group. The H<sub>5</sub> protons from the methyl group of the meta-tolunitrile ligand appear at 1.8637ppm while H<sub>10</sub> protons (methyl group on rhodium adduct) appears at 2.3848 ppm. H<sub>10</sub> appears to be more intense than H<sub>5</sub> because there is a 12:6 ratio of H<sub>10</sub>:H<sub>5</sub>.

The phenyl protons (H<sub>6</sub>, H<sub>7</sub>, and H<sub>8</sub>) are attached to the electron withdrawing nitrogen atom (from the *N*-phenylacetamide). The protons ortho and para to the electron withdrawing group would be shielded because the electrons are delocalized by the N-C-O group of the 2, 2-*cis*-[Rh<sub>2</sub>(NPhCOCH<sub>3</sub>)<sub>4</sub>]·NC({3-CH<sub>3</sub>}C<sub>6</sub>H<sub>4</sub>) complex.



**Figure 3.29:**  $^1\text{H}$  labels for 2, 2-*cis*- $[\text{Rh}_2(\text{NPhCOCH}_3)_4] \cdot \text{NC}(\{3\text{-CH}_3\}\text{C}_6\text{H}_4)$  complex

The phenyl peak positions and protons of 2, 2-*cis*- $[\text{Rh}_2(\text{NPhCOCH}_3)_4] \cdot \text{NC}(\{3\text{-CH}_3\}\text{C}_6\text{H}_4)$  complex are shown in Table 3.6 below;

**Table 3.6:** Phenyl peak positions and protons of 2, 2-*cis*-[Rh<sub>2</sub>(NPhCOCH<sub>3</sub>)<sub>4</sub>]·NC({3-CH<sub>3</sub>}C<sub>6</sub>H<sub>4</sub>) complex

Phenyl Peaks (ppm)	Phenyl Protons
7.4393	H <sub>1</sub> and H <sub>4</sub>
7.4334	H <sub>1</sub> and H <sub>4</sub>
7.4293	H <sub>1</sub> and H <sub>4</sub>
7.3583	H <sub>3</sub>
7.3491	H <sub>3</sub>
7.3386	H <sub>3</sub>
7.3290	H <sub>2</sub>
7.3194	H <sub>2</sub>
7.2530	CHCl <sub>3</sub>

Figures 3.30-3.33 below show the <sup>1</sup>H NMR of 2, 2-*cis*-[Rh<sub>2</sub>(NPhCOCH<sub>3</sub>)<sub>4</sub>]·NC({3-CH<sub>3</sub>}C<sub>6</sub>H<sub>4</sub>) complex

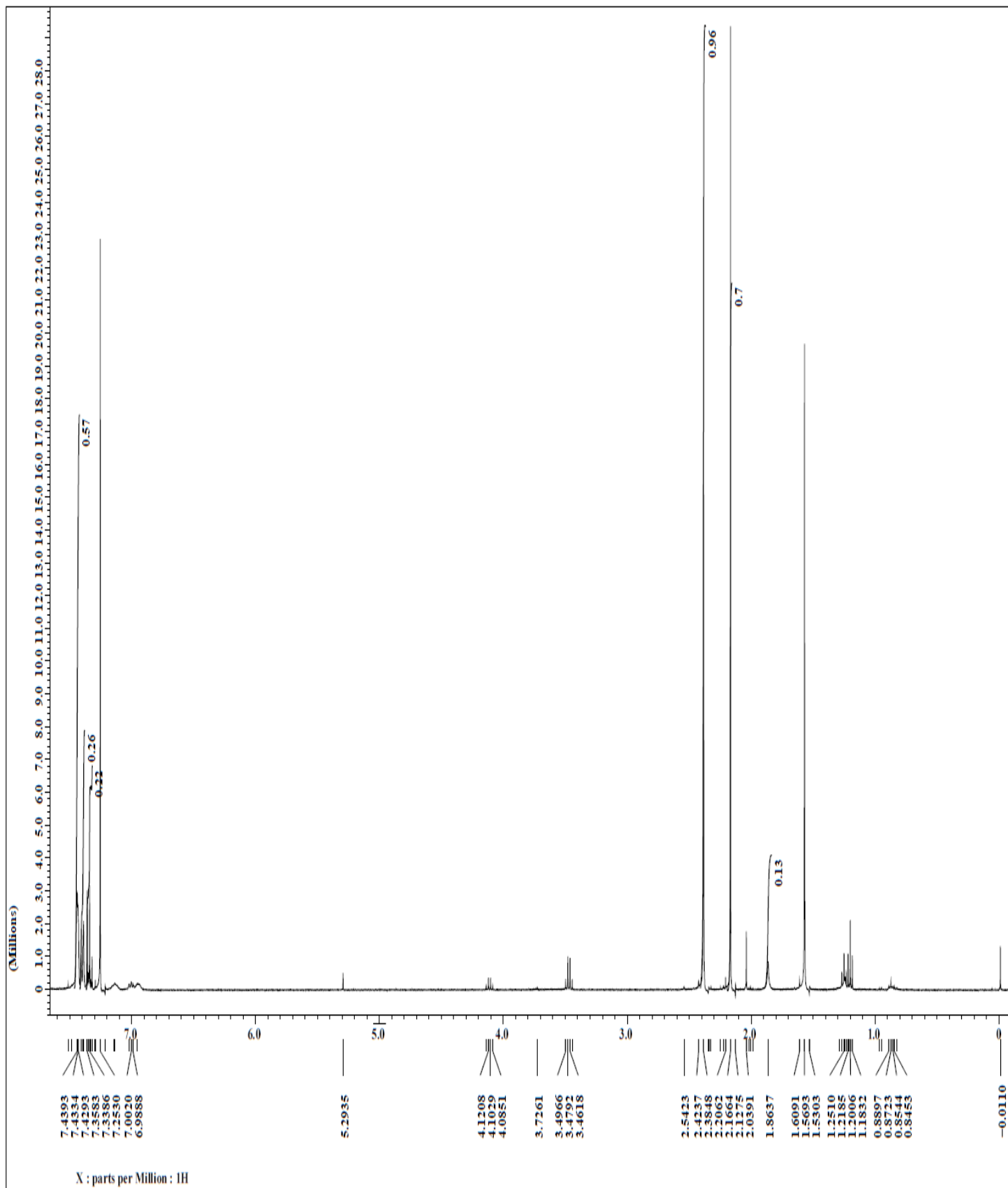


**Figure 3.30:**  $^1\text{H}$  NMR spectrum of  $2, 2\text{-cis-}[\text{Rh}_2(\text{NPhCOCH}_3)_4] \cdot \text{NC}(\{3\text{-CH}_3\}\text{C}_6\text{H}_4)$  complex

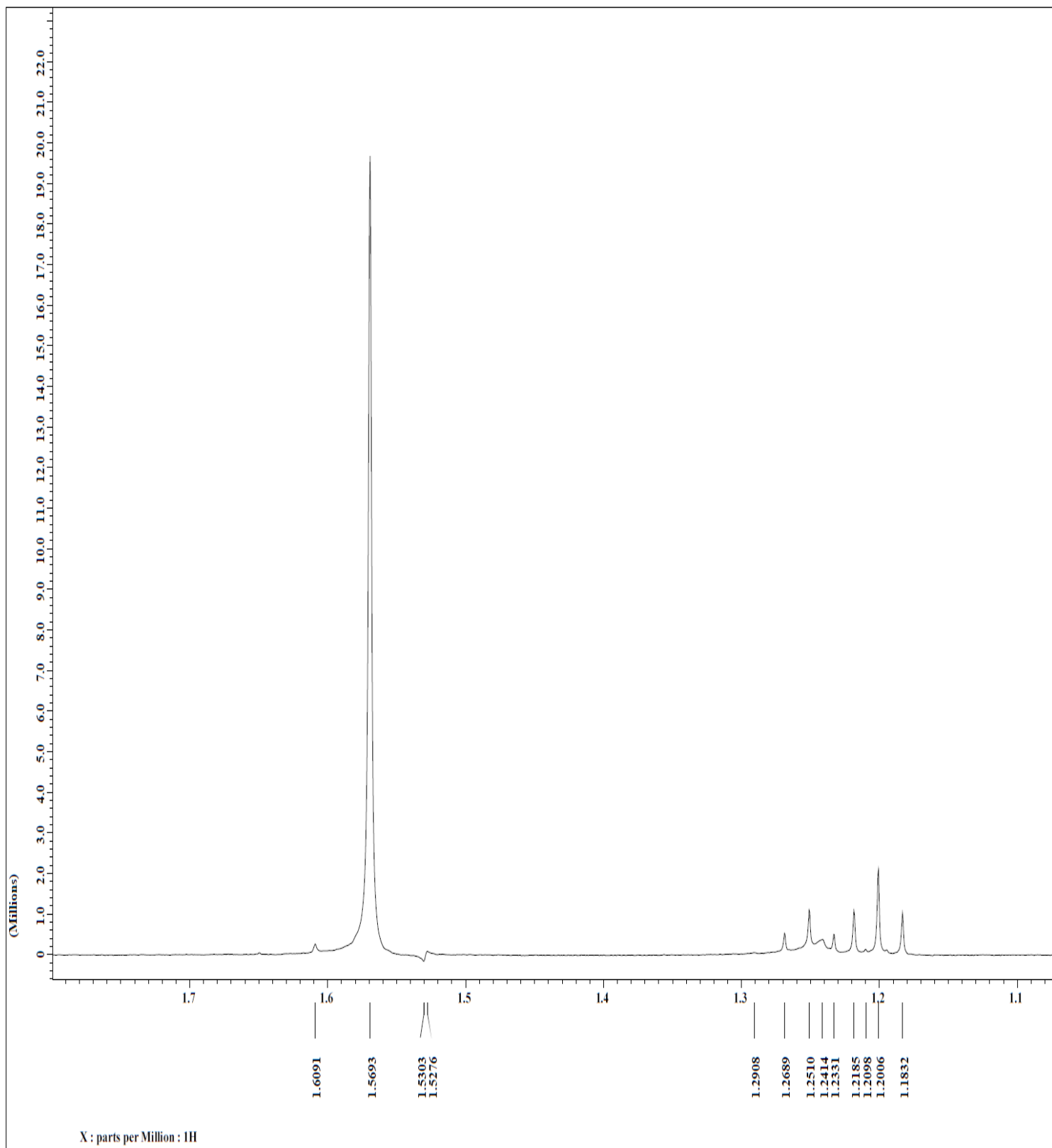


**Figure 3.31:**  $^1\text{H}$  NMR spectrum of 2, 2-*cis*- $[\text{Rh}_2(\text{NPhCOCH}_3)_4] \cdot \text{NC}(\{3\text{-CH}_3\}\text{C}_6\text{H}_4)$  complex (expanded 1.1 ppm-1.7 ppm)

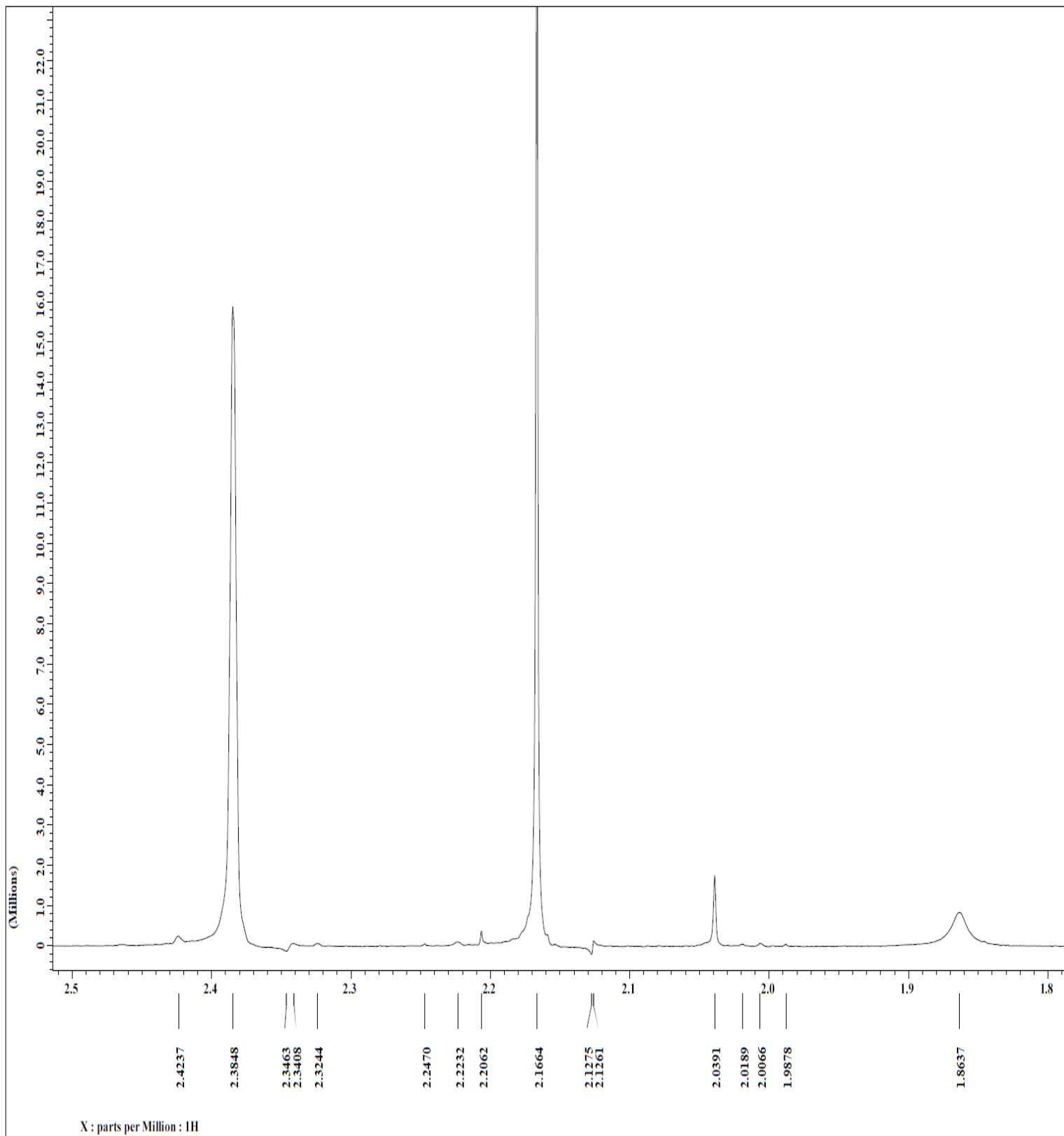


**Figure 3.32:**  $^1\text{H}$  NMR spectrum of 2, 2-*cis*- $[\text{Rh}_2(\text{NPhCOCH}_3)_4] \cdot \text{NC}(\{3\text{-CH}_3\}\text{C}_6\text{H}_4)$  complex (expanded 1.8 ppm-2.5 ppm)

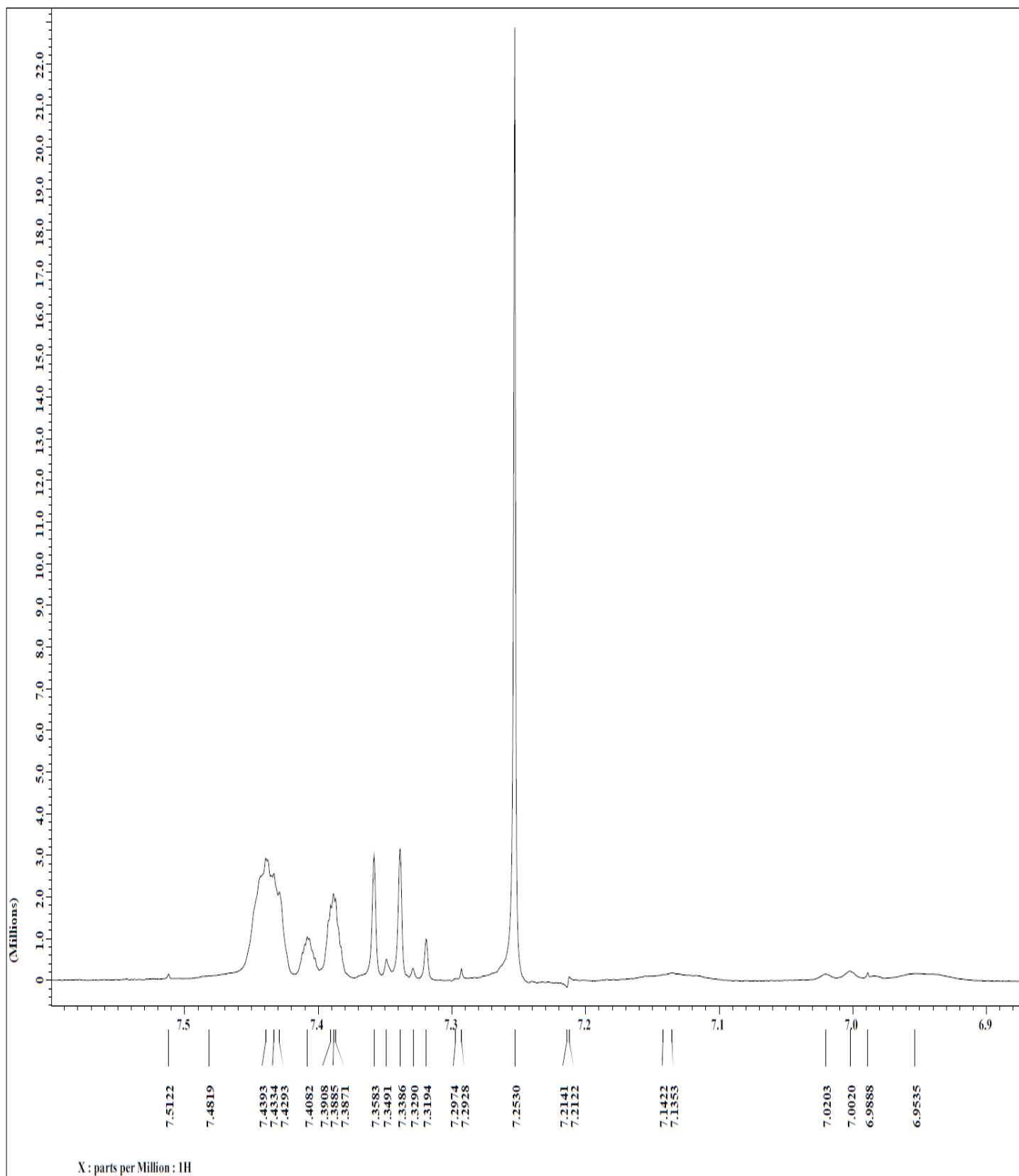


**Figure 3.33:**  $^1\text{H}$  NMR spectrum of  $2,2\text{-cis-}[\text{Rh}_2(\text{NPhCOCH}_3)_4] \cdot \text{NC}(\{3\text{-CH}_3\}\text{C}_6\text{H}_4)$  complex (expanded 6.9 ppm-7.5 ppm)



Figure 3.34 shows the proton labels of the uncomplexed para-tolunitrile. Protons ortho to the  $C\equiv N$  functional group,  $H_2$  protons of the para-tolunitrile ligand, appear more downfield since these protons are deshielded by  $C\equiv N$  functional group. The  $H_1$  protons meta to the  $C\equiv N$  functional group in the para-tolunitrile ligand also appear downfield because they are deshielded by the  $C\equiv N$  functional group.  $H_1$  and  $H_2$  protons all appear as doublet peaks because they are all split by neighboring protons.

The 7.2653 ppm peak is an overlap of the proton from the  $CHCl_3$  in the  $CDCl_3$  solvent (see Figure 3.35). The peak that appears at 2.4068 ppm is  $H_5$  protons from the methyl group on the para-tolunitrile ligand.

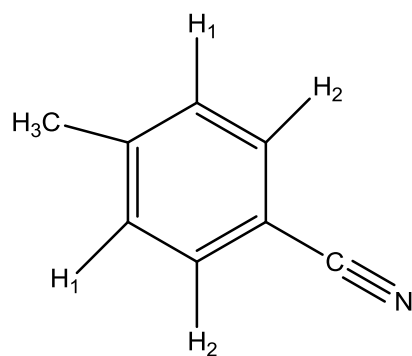


**Figure 3.34:**  $^1H$  labels of uncomplexed *p*-tolunitrile

The phenyl peaks and protons are shown in Table 3.7 below;

**Table 3.7:** Phenyl peak positions and protons of uncomplexed *p*-tolunitrile

Phenyl Peaks (ppm)	Phenyl Protons
7.5387	H <sub>2</sub>
7.5181	H <sub>2</sub>
7.4957	H <sub>2</sub>
7.2653	CHCl <sub>3</sub>
7.2530	H <sub>1</sub>
7.2454	H <sub>1</sub>

Figures 3.35-3.37 below show the <sup>1</sup>H NMR of uncomplexed *p*-tolunitrile

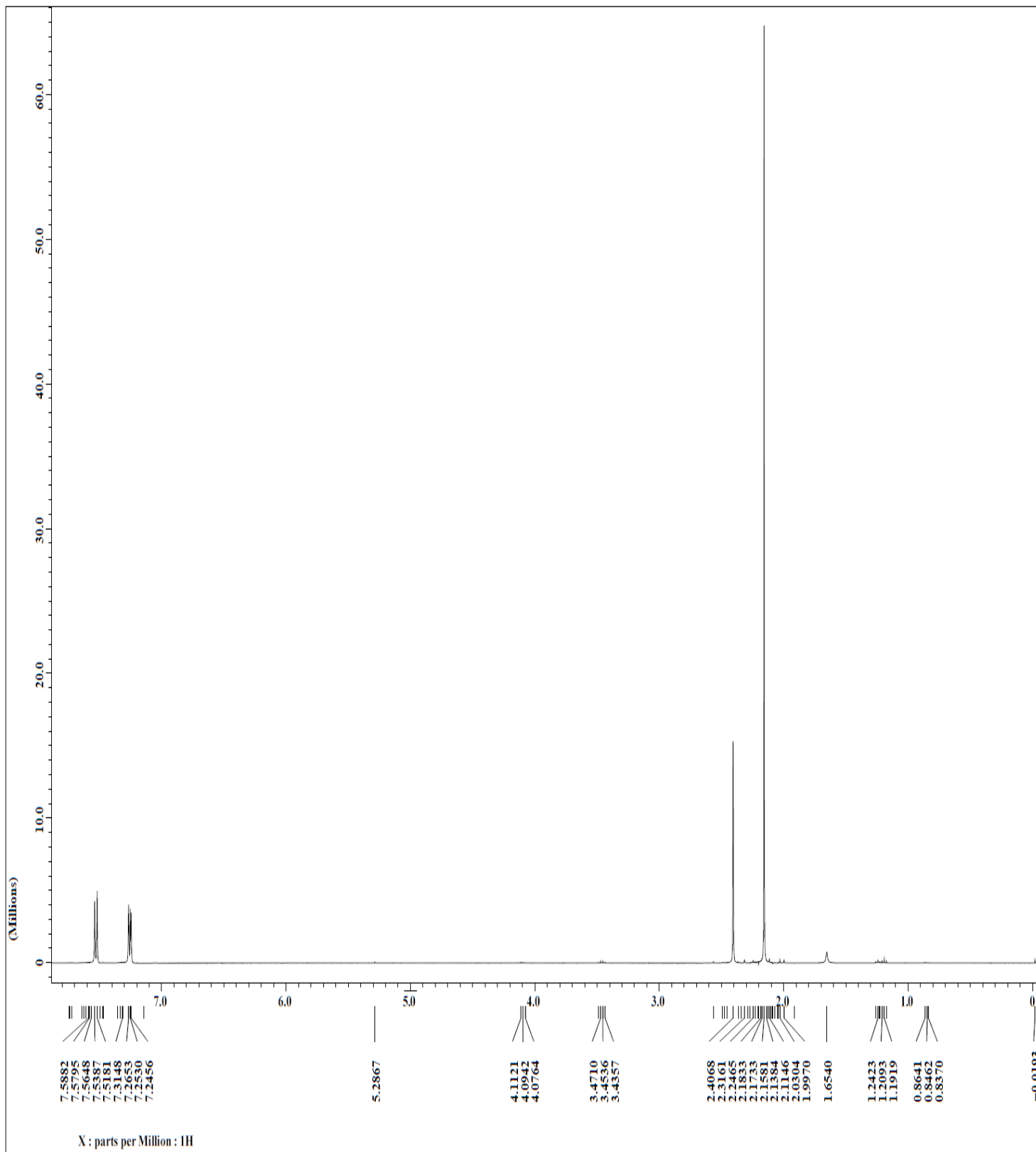
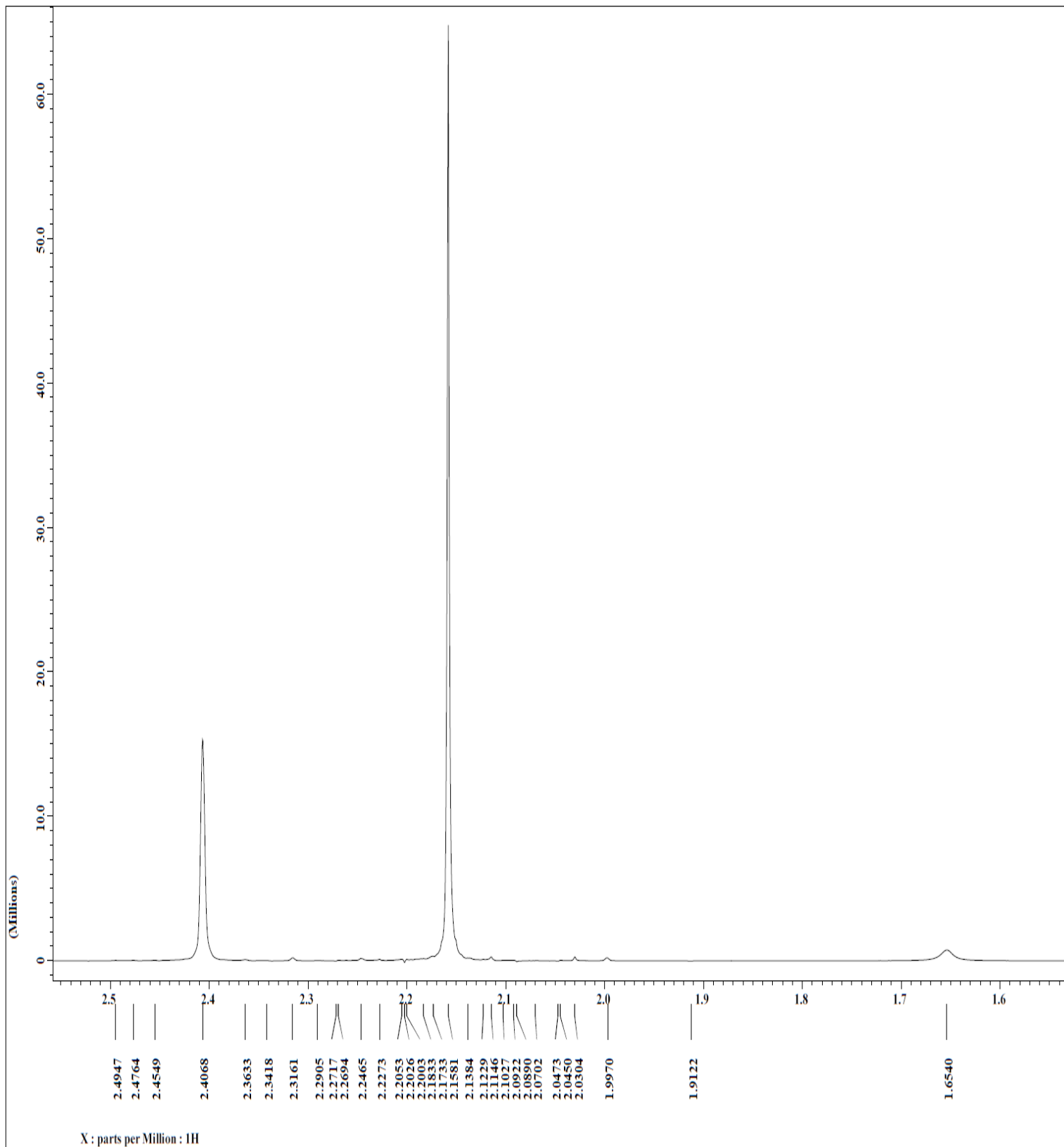
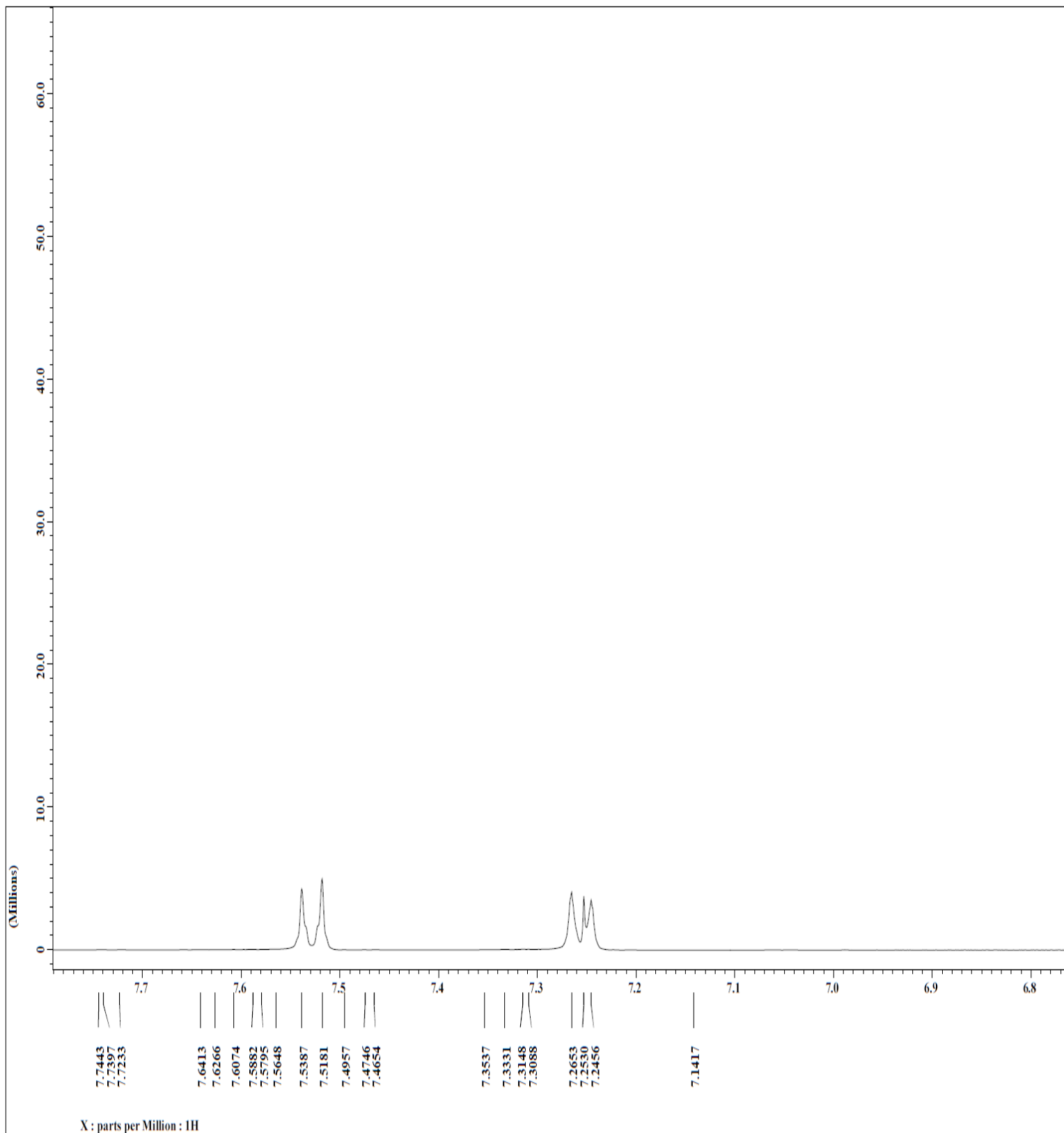


Figure 3.35:  $^1\text{H}$  NMR spectrum of uncomplexed *p*-tolunitrile



**Figure 3.36:**  $^1\text{H}$  NMR spectrum of uncomplexed *p*-tolunitrile (expanded 1.6 ppm-2.5 ppm)



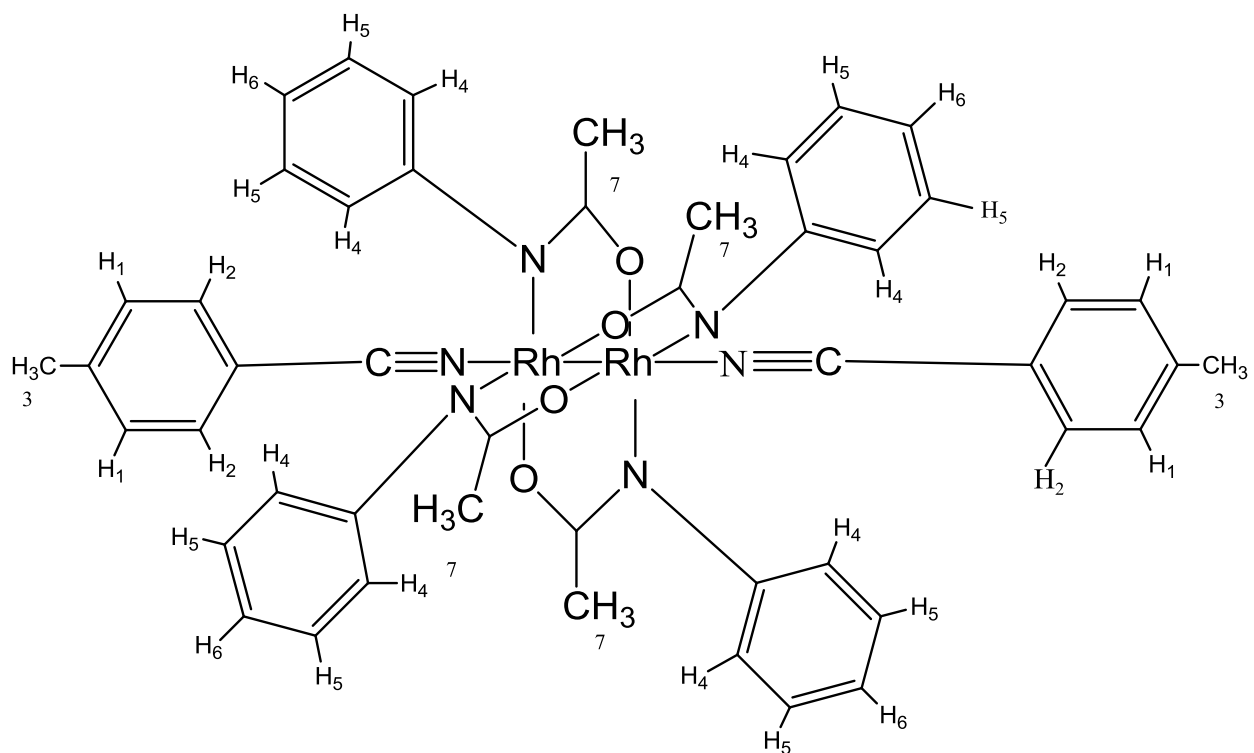
**Figure 3.37:**  $^1\text{H}$  NMR spectrum of uncomplexed *p*-tolunitrile (expanded 6.8 ppm-7.7 ppm)

Figure 3.38 shows the proton labels for 2, 2-*cis*-[Rh<sub>2</sub>(NPhCOCH<sub>3</sub>)<sub>4</sub>]·NC({4-CH<sub>3</sub>}C<sub>6</sub>H<sub>4</sub>) complex. Similar to the complexes above, rhodium atom, being a metal bound to the C≡N functional group, manipulates the C≡N functional group's properties from acting as an electron withdrawing group to acting similar to an electron donating group.

Protons on the phenyl ring of the para-tolunitrile are shielded by the C≡N functional group, but the protons in the ortho position to the C≡N functional group, H<sub>2</sub>, appear more downfield since these protons are deshielded by C≡N functional group through inductive effect. H<sub>1</sub> and H<sub>2</sub> protons all appear as doublet peaks since they are all split by neighboring protons.

The peaks that appear at 7.2535 ppm represent the CHCl<sub>3</sub> solvent peak. The methyl group in the para position of the phenyl ring is an electron donating group. The H<sub>3</sub> protons from the methyl group of the para-tolunitrile ligand appear at 2.3143 ppm while H<sub>7</sub> protons (methyl group on rhodium adduct) appears at 1.5176 ppm. H<sub>7</sub> appears to be more intense than H<sub>3</sub> because there is a 12:6 ratio of H<sub>7</sub>:H<sub>3</sub>.

The phenyl protons (H<sub>6</sub>, H<sub>7</sub>, and H<sub>8</sub>) are attached to the electron withdrawing nitrogen atom (from the *N*-phenylacetamide). The protons ortho and para to the electron withdrawing group would be shielded because the electrons are delocalized by the N-C-O group of the 2, 2-*cis*-[Rh<sub>2</sub>(NPhCOCH<sub>3</sub>)<sub>4</sub>]·NC({4-CH<sub>3</sub>}C<sub>6</sub>H<sub>4</sub>) complex.



**Figure 3.38:**  $^1\text{H}$  labels for  $2,2\text{-cis-}[\text{Rh}_2(\text{NPhCOCH}_3)_4]\cdot\text{NC}(\{4\text{-CH}_3\}\text{C}_6\text{H}_4)$  complex

The phenyl peak positions and protons of  $2,2\text{-cis-}[\text{Rh}_2(\text{NPhCOCH}_3)_4]\cdot\text{NC}(\{4\text{-CH}_3\}\text{C}_6\text{H}_4)$  complex are shown in Table 3.8 below;

**Table 3.8:** Phenyl peak positions protons of 2,2-*cis*- [Rh<sub>2</sub>(NPhCOCH<sub>3</sub>)<sub>4</sub>].NC({4-CH<sub>3</sub>}C<sub>6</sub>H<sub>4</sub>) complex

Phenyl Peaks (ppm)	Phenyl Protons
7.5209	H <sub>2</sub>
7.4824	H <sub>2</sub>
7.4623	H <sub>2</sub>
7.4064	H <sub>2</sub>
7.2535	CHCl <sub>3</sub>
7.2113	H <sub>1</sub>
7.1939	H <sub>1</sub>
7.1546	H <sub>1</sub>

Figures 3.39-3.41 below show the <sup>1</sup>H NMR of 2,2-*cis*-[Rh<sub>2</sub>(NPhCOCH<sub>3</sub>)<sub>4</sub>].NC({4-CH<sub>3</sub>}C<sub>6</sub>H<sub>4</sub>) complex



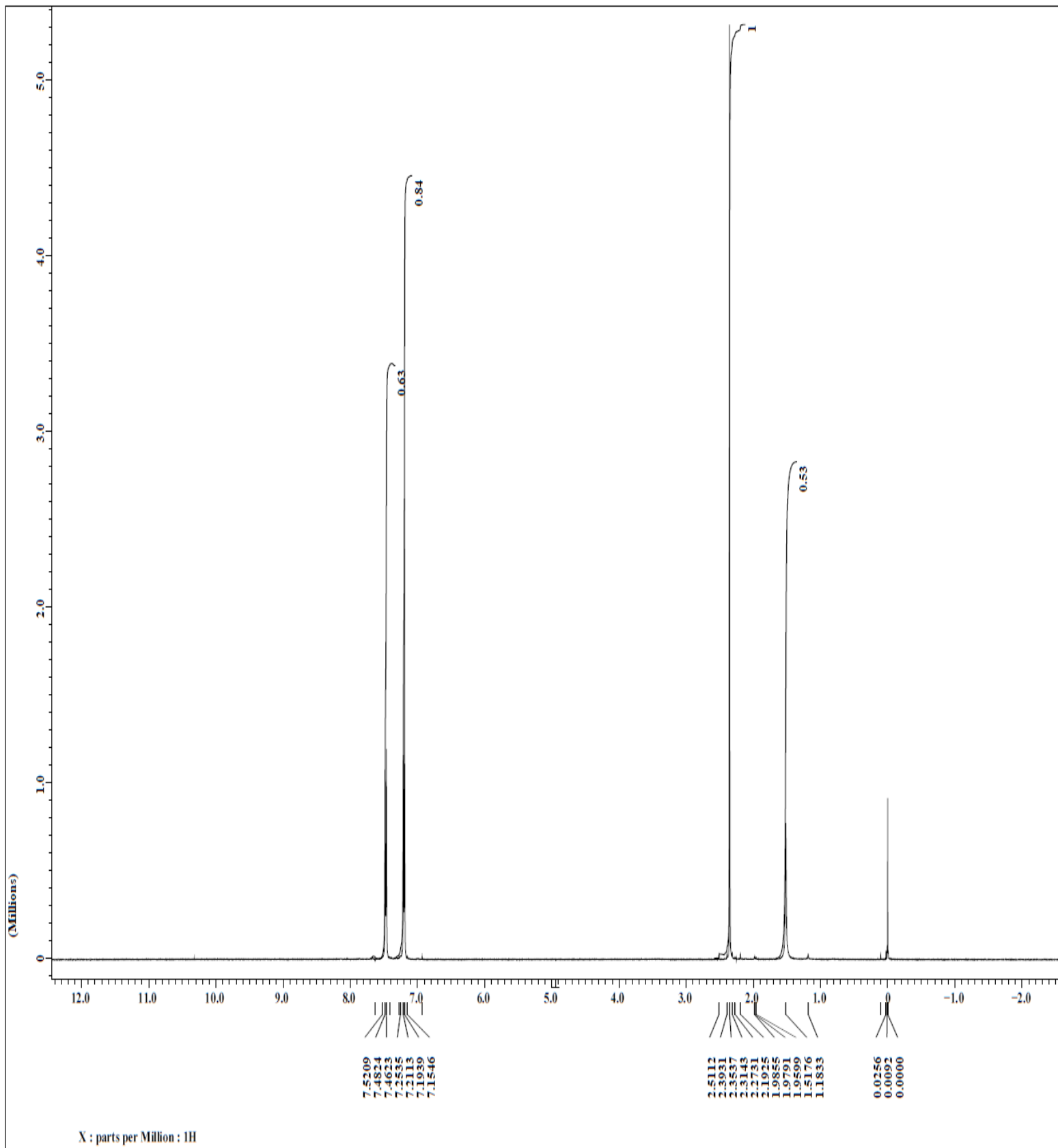


**Figure 3.39:**  $^1\text{H}$  NMR spectrum of 2,2-*cis*-[ $\text{Rh}_2(\text{NPhCOCH}_3)_4$ ]·NC({4- $\text{CH}_3$ ) $\text{C}_6\text{H}_4$ ) complex

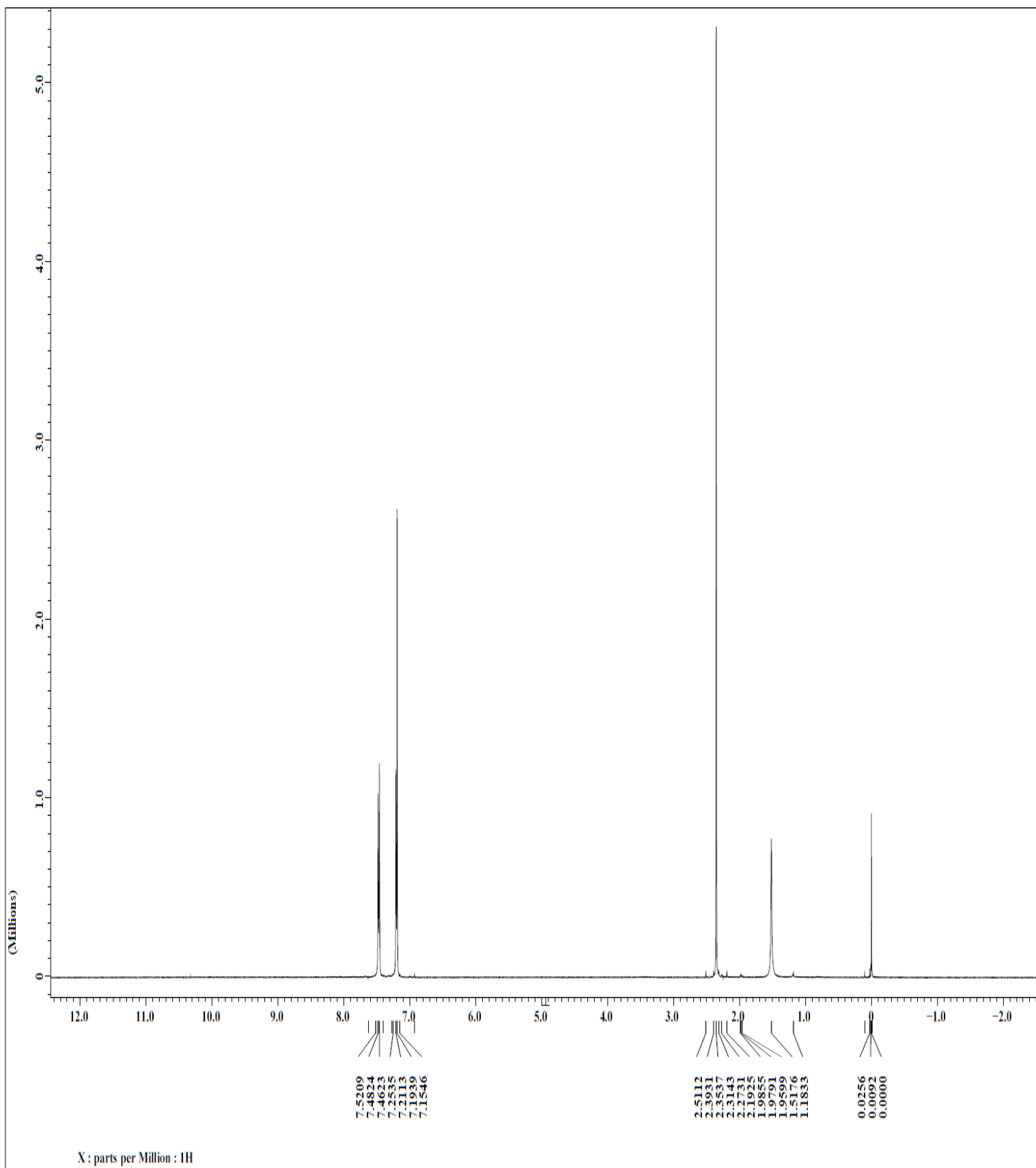


**Figure 3.40:**  $^1\text{H}$  NMR spectrum of 2,2-*cis*-[ $\text{Rh}_2(\text{NPhCOCH}_3)_4$ ]·NC({4- $\text{CH}_3$ ) $\text{C}_6\text{H}_4$ ) complex

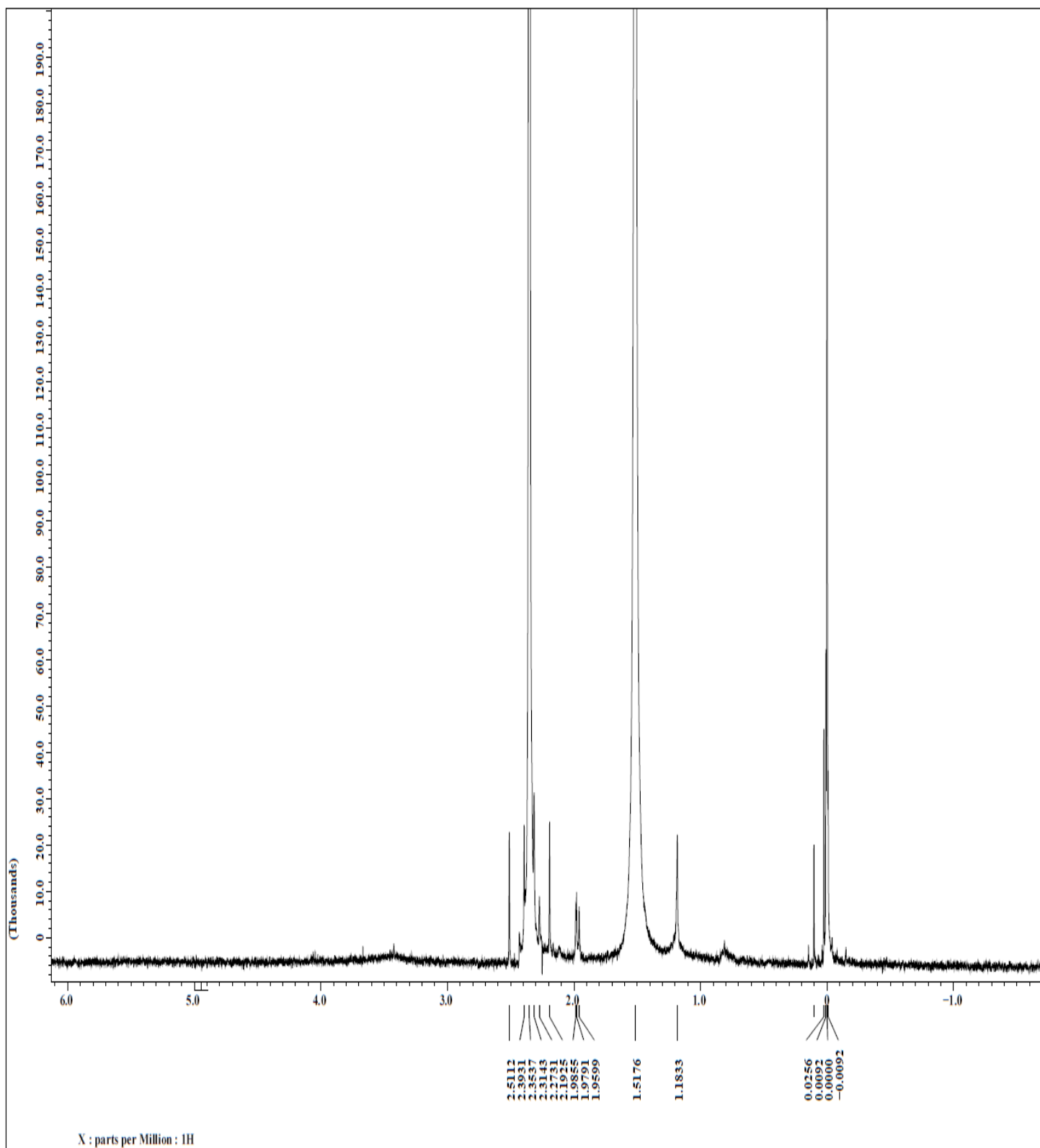


**Figure 3.41:**  $^1\text{H}$  NMR spectrum of  $2,2\text{-cis-}[\text{Rh}_2(\text{NPhCOCH}_3)_4] \cdot \text{NC}(\{4\text{-CH}_3\}\text{C}_6\text{H}_4)$  complex (expanded region from -1.0 ppm-6.0 ppm)

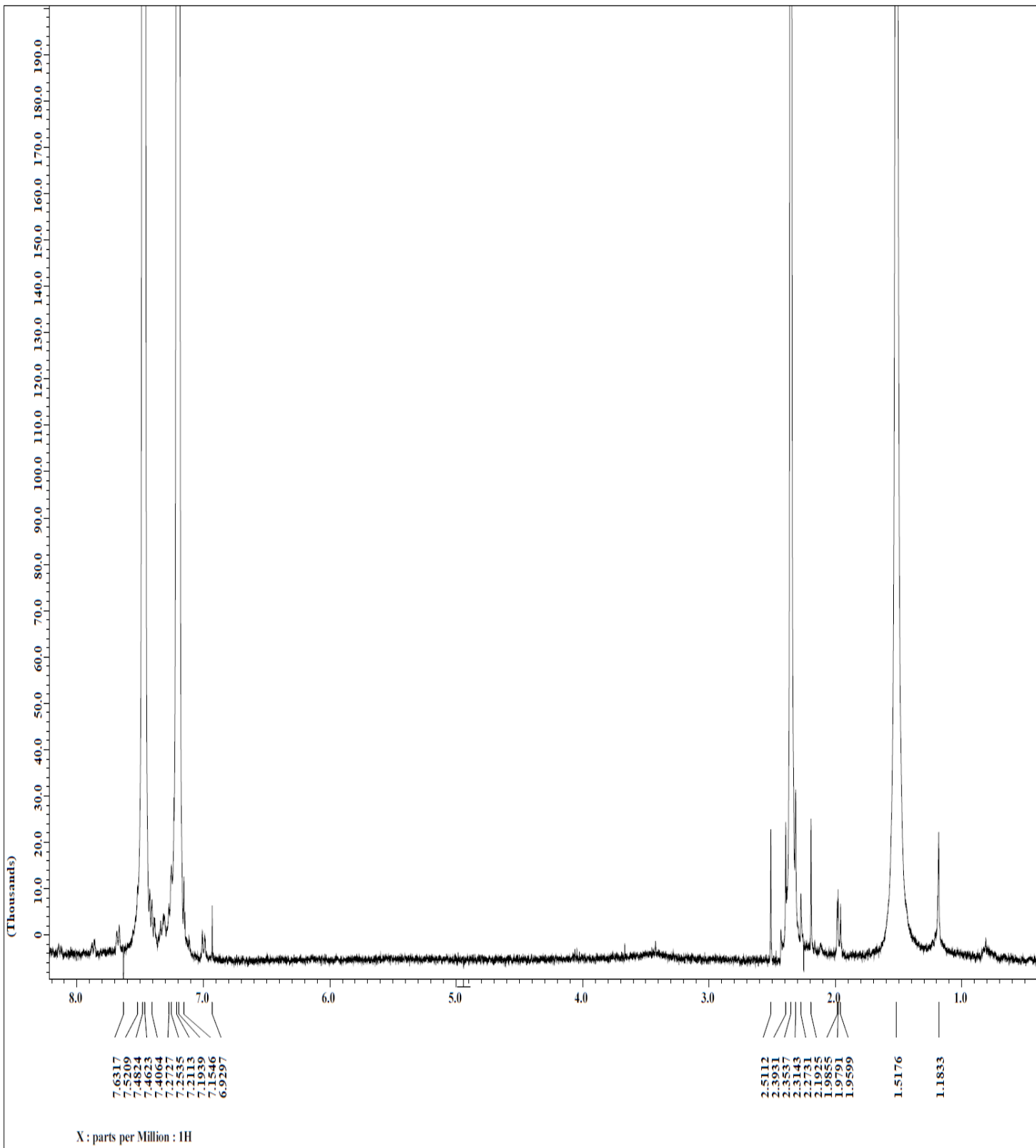


**Figure 3.42:**  $^1\text{H}$  NMR spectrum of  $2,2\text{-cis-}[\text{Rh}_2(\text{NPhCOCH}_3)_4] \cdot \text{NC}(\{4\text{-CH}_3\}\text{C}_6\text{H}_4)$  complex (expanded region from 1.0 ppm-8.0 ppm)

Figure 3.43 shows the proton labels of the 2,2,2-trifluoro-N-phenylacetamide (NPhCOCF<sub>3</sub>) nitrile. H<sub>1</sub> protons appear as doublet peaks because they are split by H<sub>2</sub> protons. H<sub>2</sub> protons appear as triplet because it is split by H<sub>1</sub> and H<sub>3</sub>. H<sub>3</sub> protons also appear as a triplet since it is split by two H<sub>2</sub> protons.

H<sub>1</sub> protons appear most downfield because they are the most deshielded by N-H group. H<sub>2</sub> protons are also deshielded by N-H functional group through inductive effect and as a result also appear downfield. H<sub>3</sub> protons do not have a lot of effect from the N-H functional group and as such appear more upfield.

The 7.2539 ppm peak is an overlap of the proton from the CHCl<sub>3</sub> in the CDCl<sub>3</sub> solvent (see Figure 3.44).

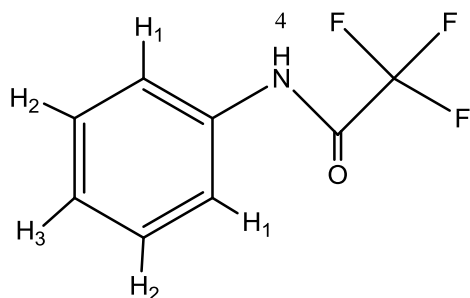


**Figure 3.43:** <sup>1</sup>H labels for 2,2,2-trifluoro-N-phenylacetamide (NPhCOCF<sub>3</sub>)

The phenyl peak positions and protons of 2,2,2-trifluoro-N-phenylacetamide (NPhCOCF<sub>3</sub>) nitrile are shown in Table 3.9 below:

**Table 3.9:** Phenyl peak positions and protons of 2,2,2-trifluoro-N-phenylacetamide (NPhCOCF<sub>3</sub>)

Phenyl Peaks (ppm)	Phenyl Protons
7.5827	H <sub>1</sub>
7.5795	H <sub>1</sub>
7.5607	H <sub>1</sub>
7.5584	H <sub>1</sub>
7.4160	H <sub>2</sub>
7.4114	H <sub>2</sub>
7.3926	H <sub>2</sub>
7.3716	H <sub>2</sub>
7.2539	CHCl <sub>3</sub>
7.2430	H <sub>3</sub>
7.2383	H <sub>3</sub>
7.2200	H <sub>3</sub>
7.2173	H <sub>3</sub>

Figures 3.44-3.46 below show the <sup>1</sup>HNMR of 2,2,2-trifluoro-N-phenylacetamide (NPhCOCF<sub>3</sub>)

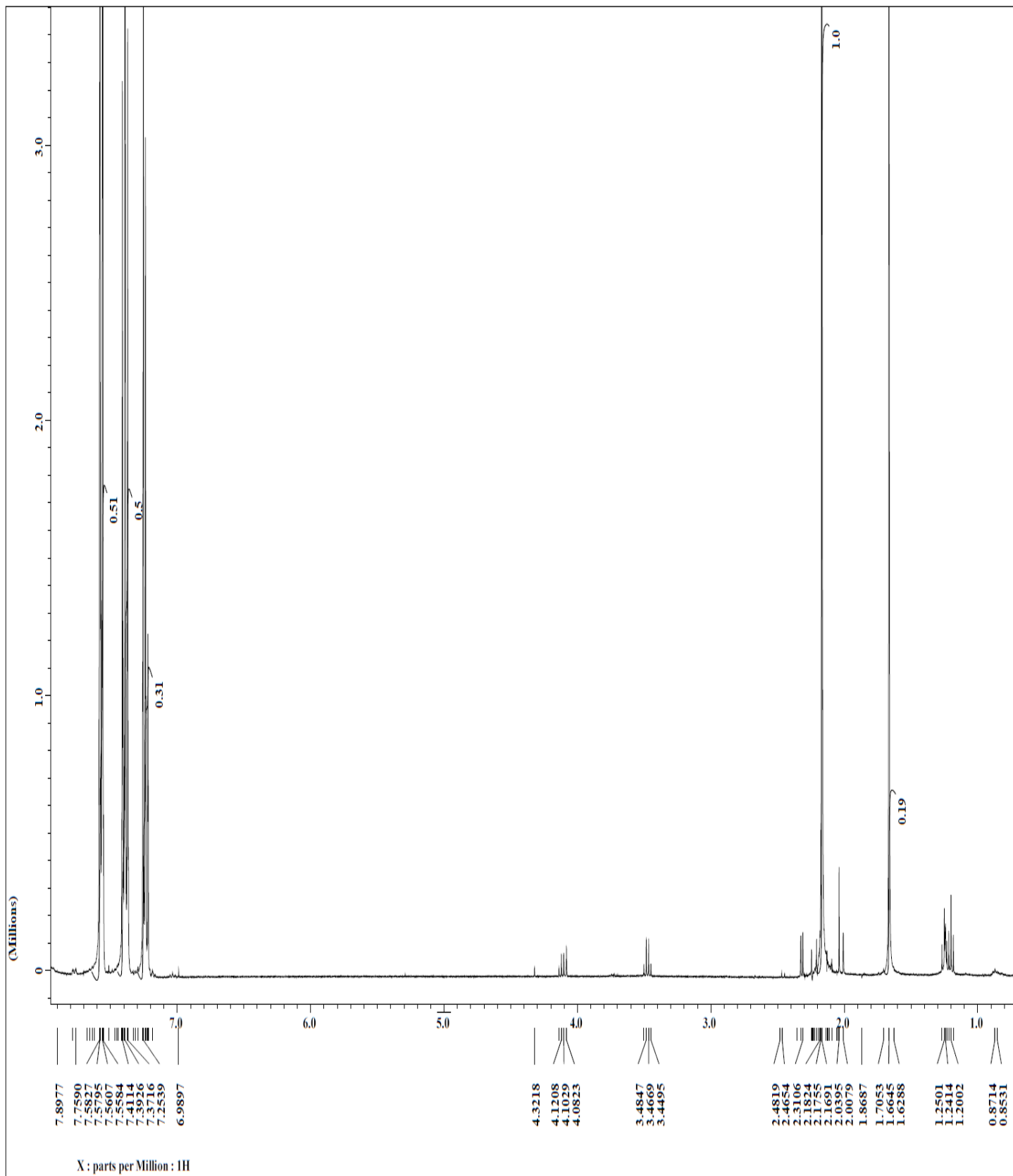


**Figure 3.44:**  $^1\text{H}$  NMR of 2,2,2-trifluoro-N-phenylacetamide ( $\text{NPhCOCF}_3$ )

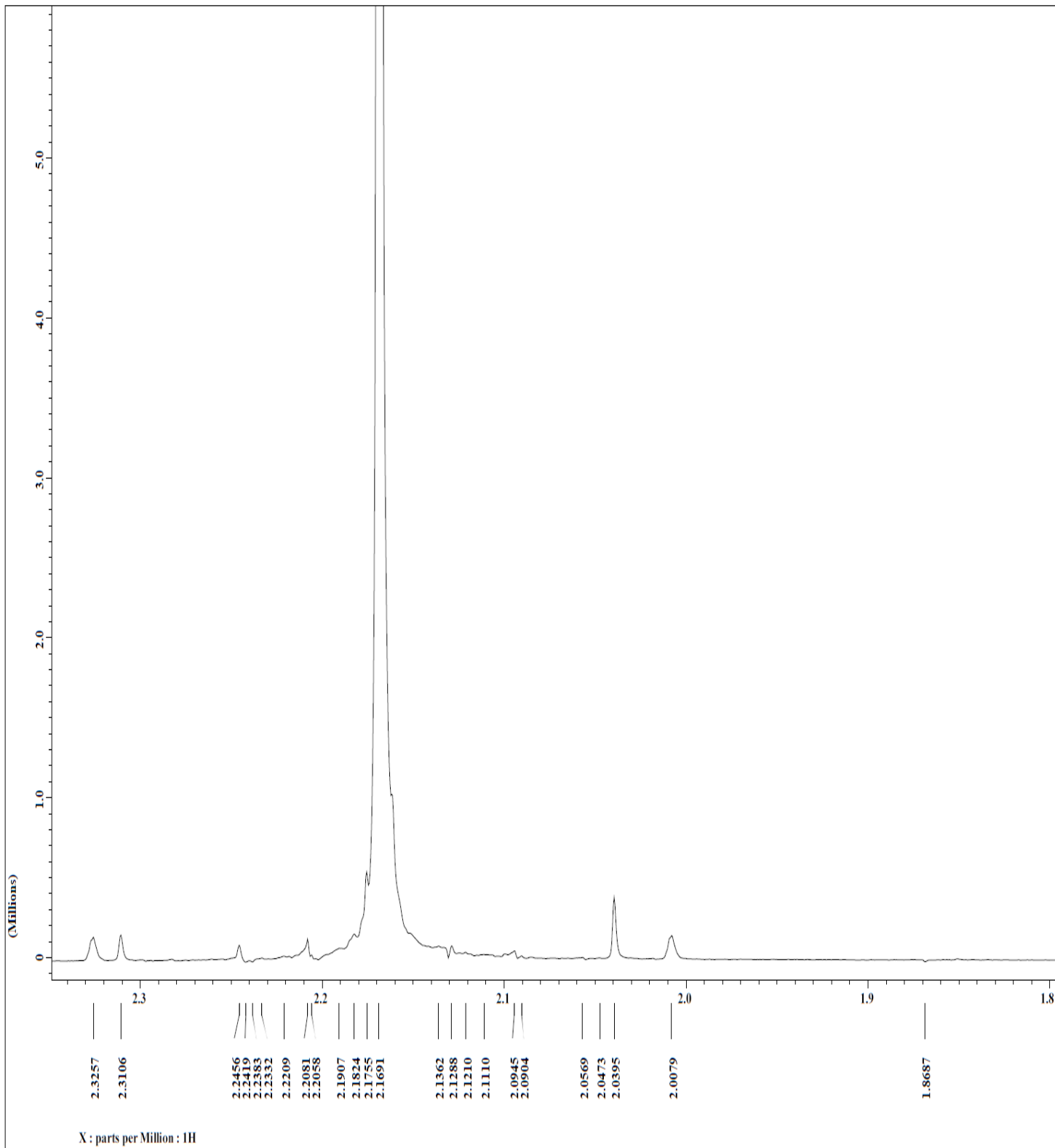


**Figure 3.45:**  $^1\text{H}$  NMR of 2,2,2-trifluoro-N-phenylacetamide( $\text{NPhCOCF}_3$ )(expanded 1.8ppm-2.3ppm)



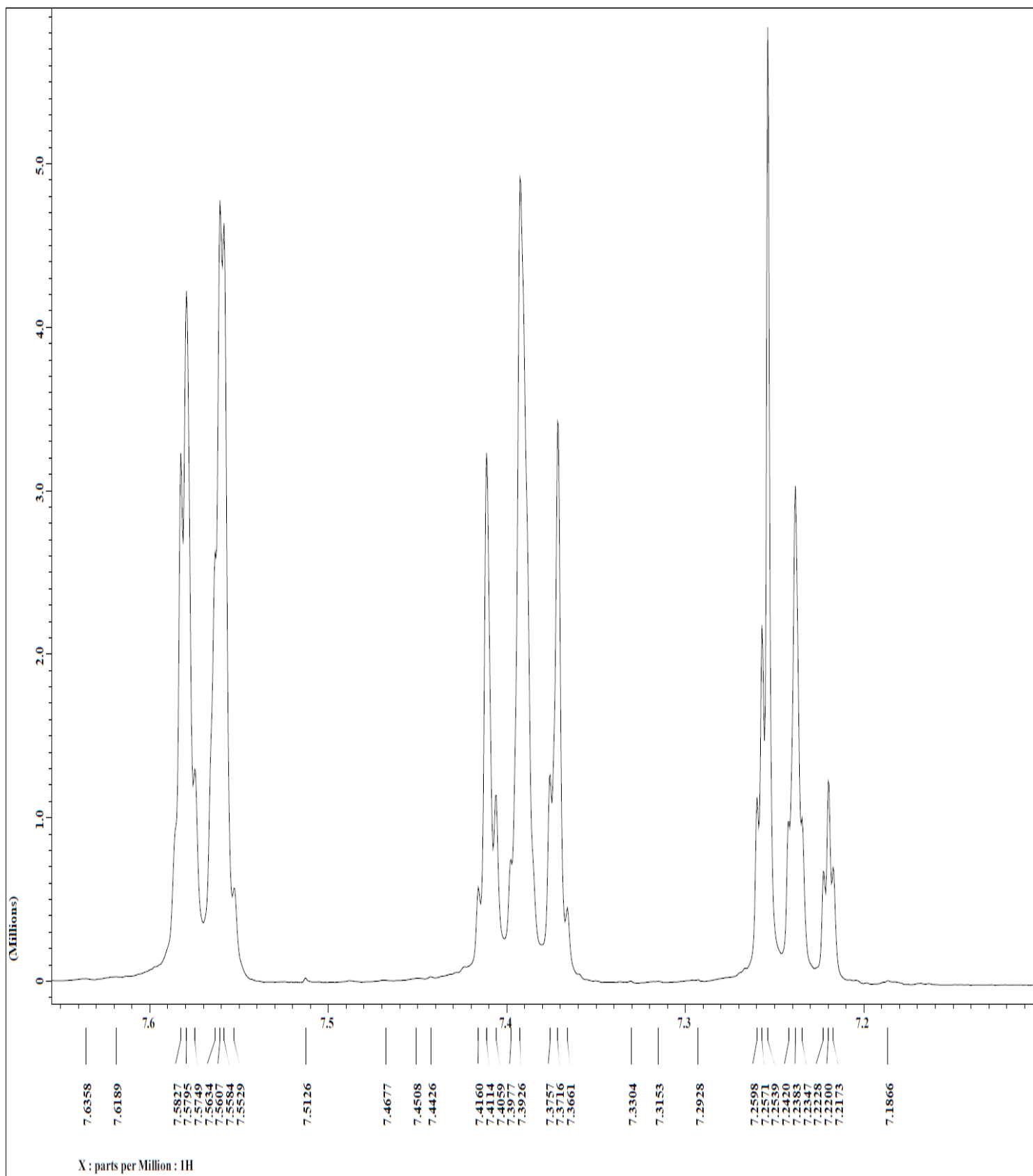


**Figure 3.46:** <sup>1</sup>H NMR of 2,2,2-trifluoro-N-phenylacetamide(NPhCOCF<sub>3</sub>)(expanded 7.2ppm-7.6ppm)

Figure 3.47 shows the proton labels of  $[\text{Rh}_2(\text{O}_2\text{CCH}_3)(\text{NPhCOCF}_3)_3] \cdot 2\text{NCC}_6\text{H}_5$  complex. The rhodium atom, being a metal bound to the  $\text{C}\equiv\text{N}$  functional group, manipulates the  $\text{C}\equiv\text{N}$  functional group's properties from acting as an electron withdrawing group to acting similar to an electron donating group.

Protons on the phenyl ring of the benzonitrile are deshielded by the  $\text{C}\equiv\text{N}$  functional group, but the protons in the ortho position are more deshielded than the protons in the para position.

The  $\text{H}_3$  protons are more deshielded through inductive effect than the  $\text{H}_2$  or  $\text{H}_1$  protons because they are the closest to the  $\text{C}\equiv\text{N}$ . The  $\text{H}_3$  protons appear as a doublet because they are split by  $\text{H}_2$  protons. By the same inductive effect, the  $\text{H}_2$  protons are also deshielded by the  $\text{C}\equiv\text{N}$  functional group, thus because the  $\text{H}_2$  protons are not as close to the  $\text{C}\equiv\text{N}$  functional group as the  $\text{H}_3$  protons, the  $\text{H}_2$  protons appear slightly more upfield to the  $\text{H}_3$  protons. The  $\text{H}_2$  protons appear as a triplet because they are split by the  $\text{H}_1$  and  $\text{H}_3$  protons. The  $\text{H}_1$  protons also appear as a triplet because they are split by the  $\text{H}_2$  and  $\text{H}_3$  protons. The peak that appears at 7.1944 ppm is the  $\text{CHCl}_3$  in the  $\text{CDCl}_3$  solvent peak .

The phenyl protons ( $\text{H}_4$ ,  $\text{H}_5$ , and  $\text{H}_6$ ) are attached to the electron withdrawing nitrogen atom (from the *N*-phenylacetamide). The protons ortho and para to the electron withdrawing group would be shielded because the electrons are delocalized by the  $\text{N-C-O}$  group of the of  $[\text{Rh}_2(\text{O}_2\text{CCH}_3)(\text{NPhCOCF}_3)_3] \cdot 2\text{NCC}_6\text{H}_5$  complex.

$\text{H}_1$  and  $\text{H}_5$  protons appear as doublet peaks since they are split by  $\text{H}_2$  and  $\text{H}_4$  protons respectively.  $\text{H}_4$  protons appear as triplet because it is split by  $\text{H}_3$  and  $\text{H}_5$ ;  $\text{H}_3$  protons are split by  $\text{H}_2$  and  $\text{H}_4$  protons, thus appear as a triplet and  $\text{H}_2$  protons are split by  $\text{H}_1$  and  $\text{H}_3$  protons, thus appearing as a triplet. The  $\text{H}_7$  protons appear at 2.0840ppm.

The 7.2924ppm peak is an overlap of the proton from the  $\text{CHCl}_3$  in the  $\text{CDCl}_3$  solvent (see Figure 3.46).

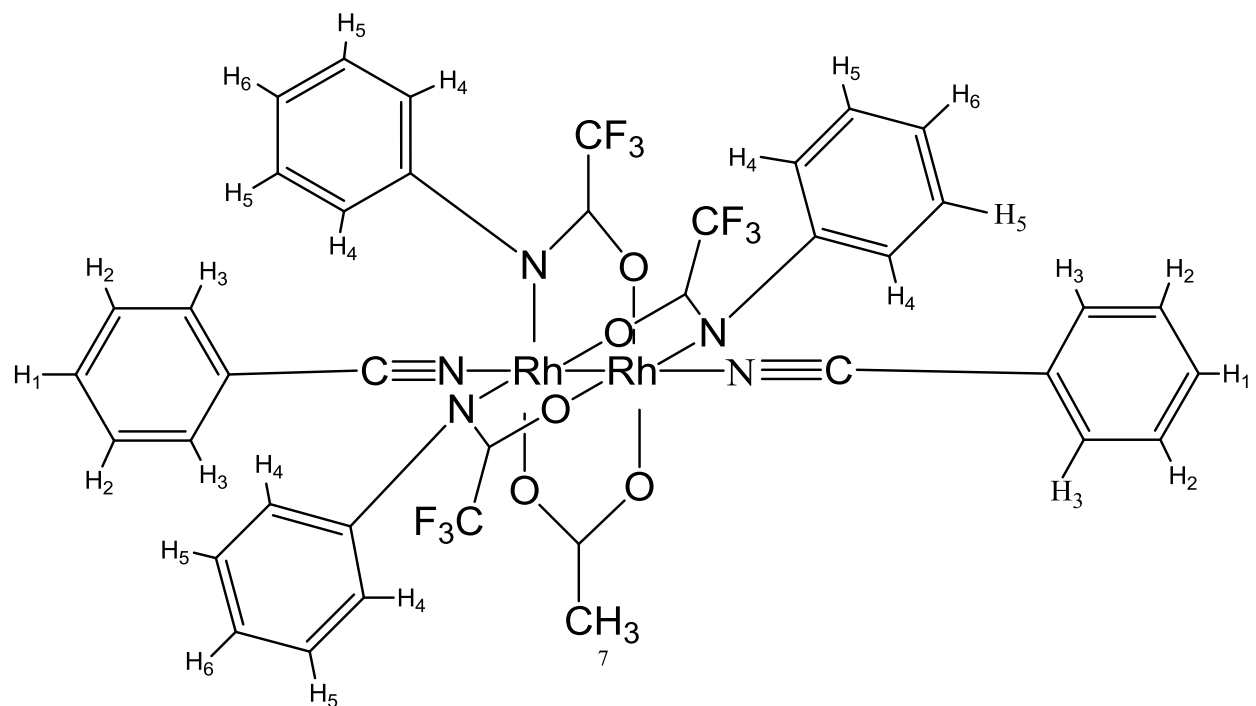


**Figure 3.47:**  $^1\text{H}$  labels for of  $[\text{Rh}_2(\text{O}_2\text{CCH}_3)(\text{NPhCOCF}_3)_3] \cdot 2\text{NCC}_6\text{H}_5$  complex

The phenyl peak positions and protons of  $[\text{Rh}_2(\text{O}_2\text{CCH}_3)(\text{NPhCOCF}_3)_3] \cdot 2\text{NCC}_6\text{H}_5$  complex are shown in Table 3.10 below:

**Table 3.10:** Phenyl peak positions and protons of  $[\text{Rh}_2(\text{O}_2\text{CCH}_3)(\text{NPhCOCF}_3)_3] \cdot 2\text{NCC}_6\text{H}_5$

Phenyl Peaks (ppm)	Phenyl Protons
7.5374	H <sub>3</sub>
7.3785	H <sub>3</sub>
7.3670	H <sub>3</sub>
7.2924	H <sub>2</sub>
7.1939	H <sub>2</sub> , CHCl <sub>3</sub>
7.1582	H <sub>2</sub>
7.1289	H <sub>1</sub>
6.9673	H <sub>1</sub>
6.9467	H <sub>1</sub>
6.9293	H <sub>1</sub>

Figures 3.48-3.50 below show the  $^1\text{H}$  NMR of  $[\text{Rh}_2(\text{O}_2\text{CCH}_3)(\text{NPhCOCF}_3)_3] \cdot 2\text{NCC}_6\text{H}_5$

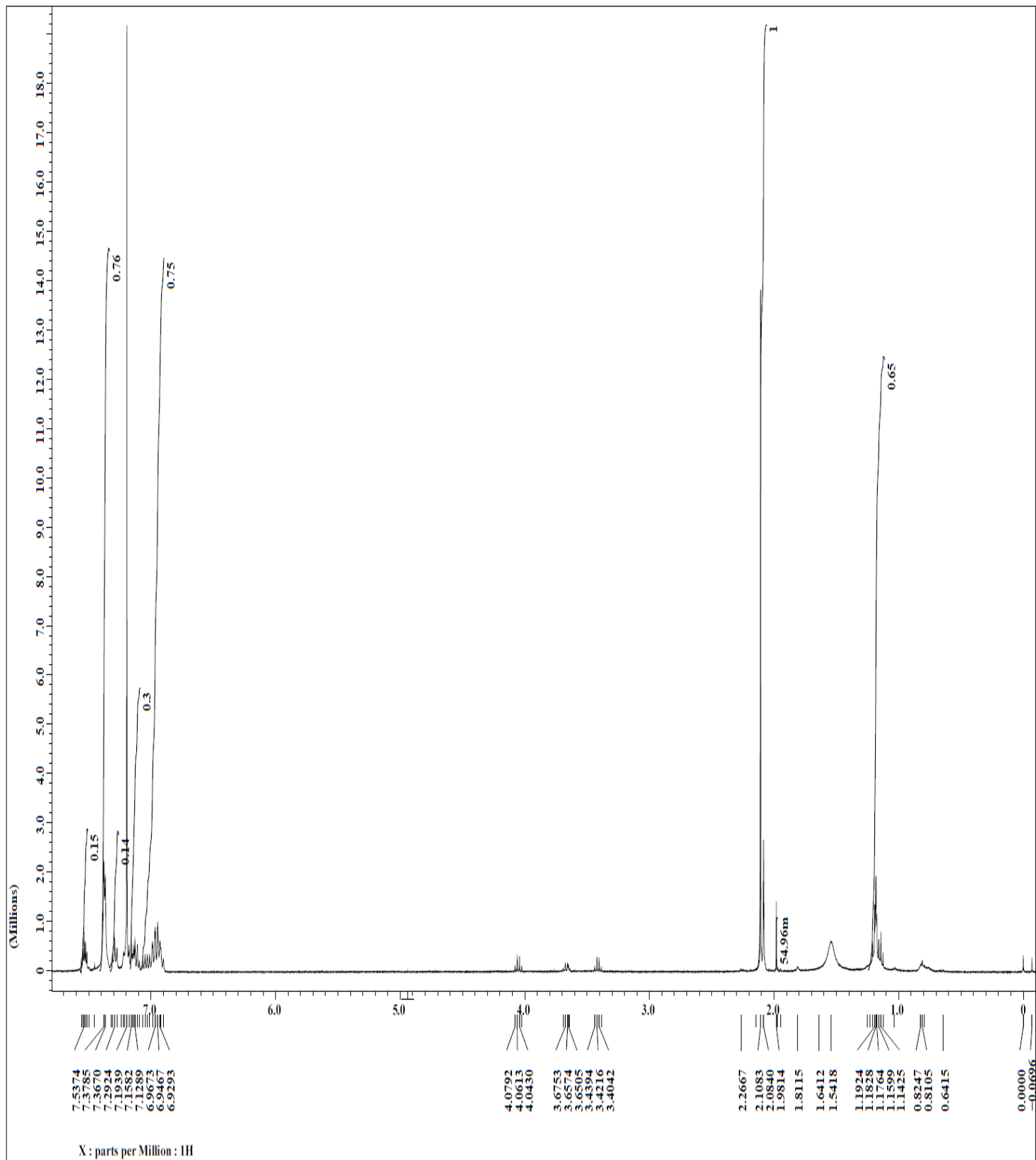


**Figure 3.48:**  $^1\text{H}$  NMR of  $[\text{Rh}_2(\text{O}_2\text{CCH}_3)(\text{NPhCOCF}_3)_3] \cdot 2\text{NCC}_6\text{H}_5$

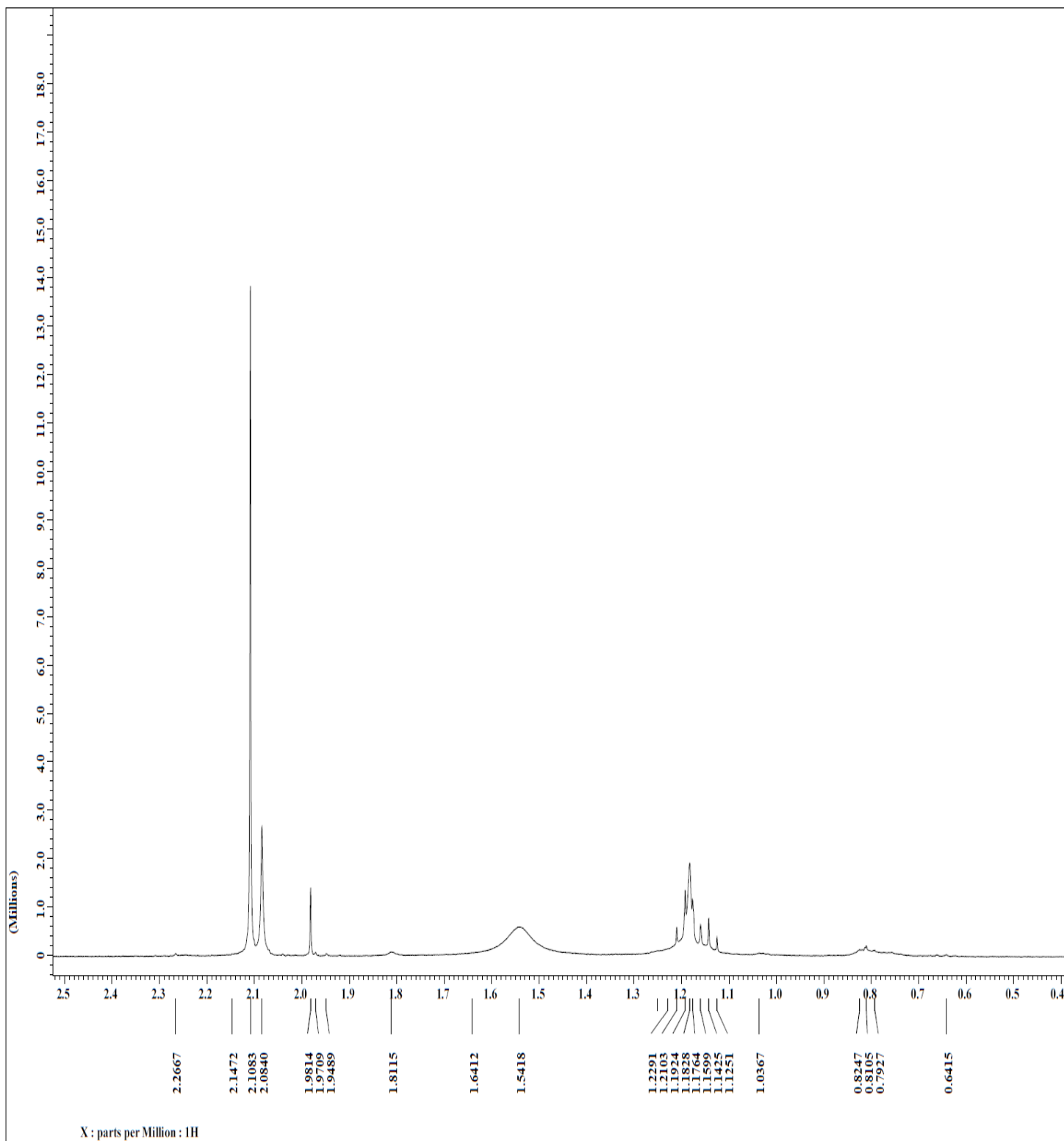


**Figure 3.49:**  $^1\text{H}$  NMR of  $[\text{Rh}_2(\text{O}_2\text{CCH}_3)(\text{NPhCOCF}_3)_3] \cdot 2\text{NCC}_6\text{H}_5$  (expanded 0.4ppm-2.5ppm)

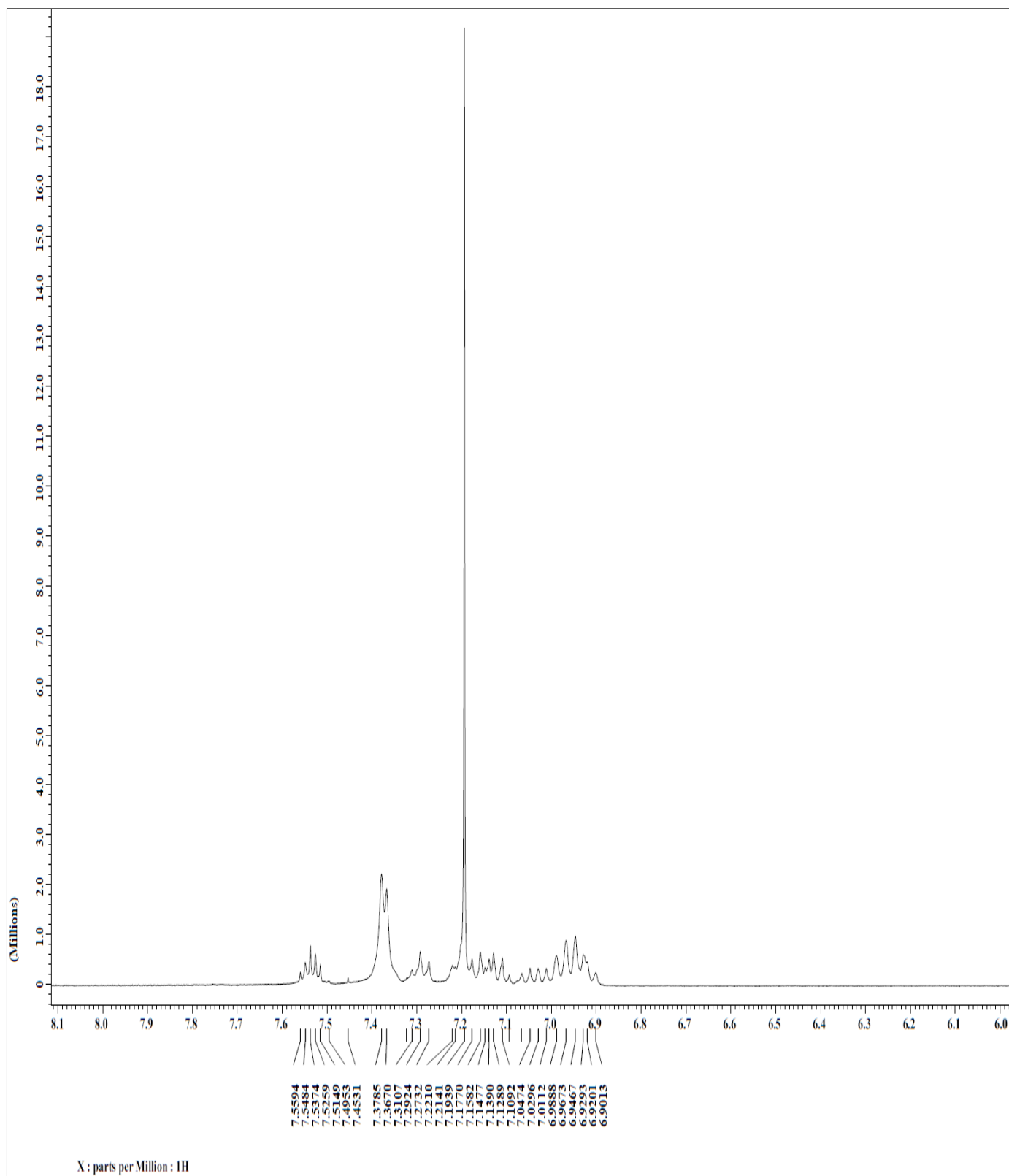


**Figure 3.50:**  $^1\text{H}$  NMR of  $[\text{Rh}_2(\text{O}_2\text{CCH}_3)(\text{NPhCOCF}_3)_3] \cdot 2\text{NCC}_6\text{H}_5$  (expanded 6.0ppm-8.1ppm)

## X-ray Results

Crystals were grown by vapor diffusion techniques where the rhodium compound was dissolved in dichloromethane in an inner vial and a variety of different solvents were used in outer vials to induce crystallization.

All data were collected by use of a Rigaku Mercury 375R/M CCD XtaLAB mini diffractometer (manufactured in May 2011). The X-ray source was Molybdenum  $K\alpha$  radiation,  $\lambda = 0.71075 \text{ \AA}$ . The crystal-to-detector distance was 50.00 mm.

$R_1$  value shows how best the model fits the data and an  $R_1$  value below 7 % shows that the model fits the data very well.

The formulae for computing  $R_1$  is as follows:

$$R_1 = \frac{\sum ||F_o| - |F_c||}{\sum |F_o|}$$

Where  $F_o$  is the observed structure factor and  $F_c$  is calculated structure factor, which is related to the intensity of the reflection.<sup>15</sup> The structure factor  $F_{hkl}$  is a mathematical function that defines the amplitude and phase of a wave diffracted from crystal lattice planes characterized by Miller indices ( $h, k, l$ .)

2, 2-*cis*-[Rh<sub>2</sub>(NPhCOCH<sub>3</sub>)<sub>4</sub>].2NCC<sub>6</sub>H<sub>5</sub>

BENZONITRILE (Two Equivalentents)

A successful structure of 2, 2-*cis*-[Rh<sub>2</sub>(NPhCOCH<sub>3</sub>)<sub>4</sub>].2NCC<sub>6</sub>H<sub>5</sub> was solved on a crystal grown from acetone (solvent in outer sample vial). Among all the other solvents used, acetone was the solvent that grew X-ray quality crystals. Some other solvents grew crystals but none of



those crystals diffracted properly. Hexane grew very tiny blue and red crystals. H<sub>2</sub>O grew many large red crystals, but they were very thin and weakly diffracting. The structure solved with the nitrile attached to both of the axial sites of the rhodium core.

A single crystal was selected from the crystals obtained from acetone. This was done under a microscope of a magnification of 1. This crystal was then mounted on a Mitogen loop by using a mounting pin and securing the crystal unto goniometer in the diffractometer.

The X-ray data for the crystal were collected using Crystal Clear-SM Auto program and the structure was solved using Crystal Structure SM Auto program (SIR2004).<sup>16,17</sup> The data was collected at a temperature of  $-50 \pm 1^\circ\text{C}$  and the crystal exposure time to the X-ray beam was 15 sec/ $^\circ$ . After the initial structure was obtained it was refined using least squares until a goodness of fit of 1.030 and a maximum shift/error of 0.005 was attained.

From Table 3.11 below, the structure solves in a monoclinic crystal system and P2<sub>1</sub>/n space group with the angles  $\alpha = \gamma = 90^\circ$  and  $\beta = 100.971^\circ$  and sides  $a = 10.2115(7) \text{ \AA}$ ,  $b = 9.9667(7) \text{ \AA}$  and  $c = 21.367(2) \text{ \AA}$ .

The  $R_1$  value was 2.41% which shows that the model fits the data very well and the structure is a very good one.

**Table 3.11:** Crystallographic data of 2,2-*cis*-[Rh<sub>2</sub>(N(C<sub>6</sub>H<sub>5</sub>)COCH<sub>3</sub>)<sub>4</sub>] $\cdot$ 2NCC<sub>6</sub>H<sub>5</sub>

Crystal Dimensions	
Crystal System	Monoclinic
Space Group	P2 <sub>1</sub> /n
Unit Cell Parameters	a = 10.2115(7) Å
	b = 9.9667(7) Å
	c = 21.367(2) Å
	$\beta$ = 100.971(7)°
	V = 2134.9(3) Å <sup>3</sup>
Exposure Temperature	-50.0 °C
Exposure Rate	15.0 sec/°
R1	0.0214
R (All reflections)	0.0250
wR2 (All reflections)	0.0542
Goodness of Fit	1.030
Max Shift/Error	0.005

Figures 3.51 and 3.52 below are the ORTEP and packing diagram of 2,2-*cis*-[Rh<sub>2</sub>(N(C<sub>6</sub>H<sub>5</sub>)COCH<sub>3</sub>)<sub>4</sub>] $\cdot$ 2NCC<sub>6</sub>H<sub>5</sub> at 30% probability. Hydrogens are shown as small spheres.

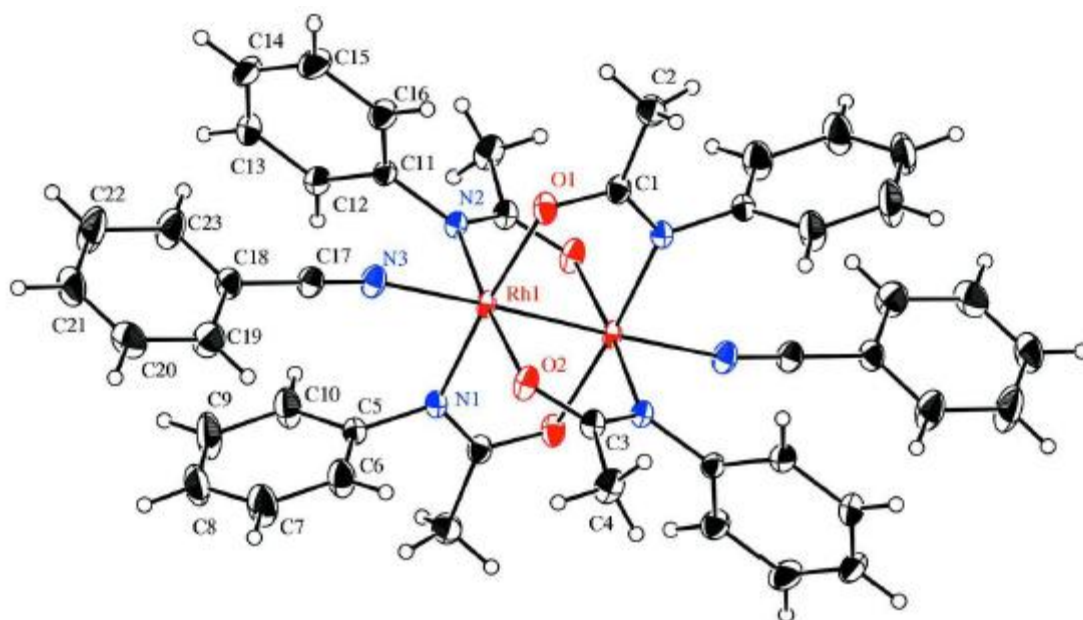


**Figure 3.51:** ORTEP of 2,2-*cis*-[Rh<sub>2</sub>(NPhCOCH<sub>3</sub>)<sub>4</sub>]·2NCC<sub>6</sub>H<sub>5</sub>

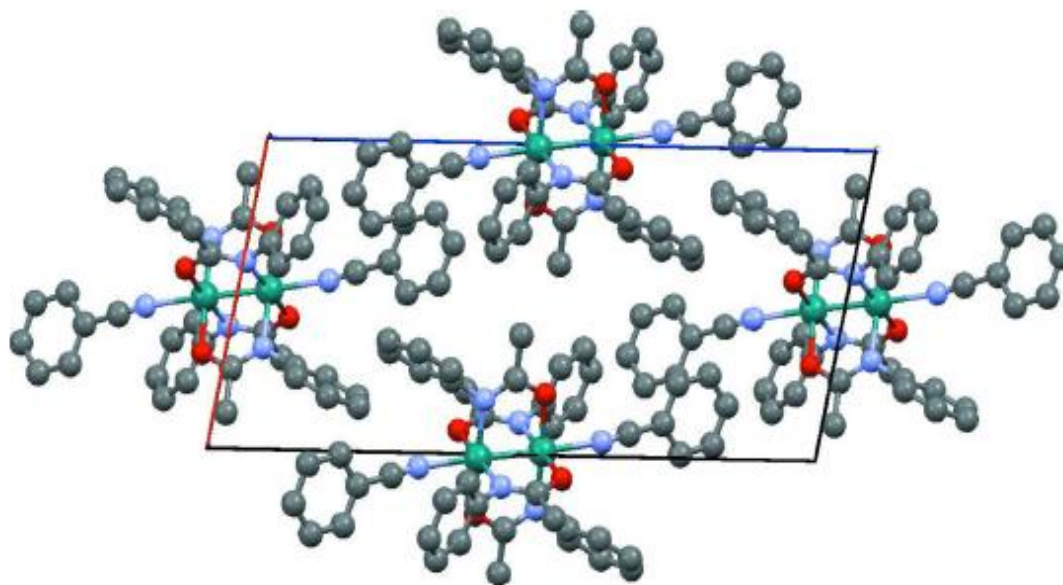


**Figure 3.52:** Packing diagram of 2,2-*cis*-[Rh<sub>2</sub>(NPhCOCH<sub>3</sub>)<sub>4</sub>]·2NCC<sub>6</sub>H<sub>5</sub> looking on the b-axis.

Hydrogen atoms are eliminated for clarity.

2, 2-*cis*-[Rh<sub>2</sub> (NPhCOCH<sub>3</sub>)<sub>4</sub>]·NC({2-CH<sub>3</sub>}C<sub>6</sub>H<sub>4</sub>)

*O*-TOLUNITRILE (One Equivalent)

A successful structure was solved using a crystal grown from methanol. Among all the other solvents used, methanol was the solvent that grew X-ray quality crystals. Some other solvents grew crystals but none of those crystals diffracted properly. H<sub>2</sub>O grew crystals that appeared to be of X-ray quality but the initial spots they showed were weakly diffracting. The interesting thing about this structure was that the nitrile attached to just one axial site instead of the two axial sites of the rhodium core when two equivalents of the nitrile were used in this complexation process.

Thus, in attempts to growing two equivalents, one equivalent of the nitrile was grown instead. See Experimental in Chapter 2 for details.

A single crystal was selected from the crystals obtained from methanol. This was done under a microscope of a magnification of 1. This crystal was then mounted on a Mitogen loop by using a mounting pin and securing the crystal unto goniometer in the diffractometer.

The X-ray data for the crystal was collected using Crystal Clear-SM Auto program and the structure was solved using Crystal Structure SM Auto program (SIR92).<sup>16,18</sup> The data were collected at a temperature of  $-50 \pm 1^\circ\text{C}$  and the crystal exposure time to the X-ray beam was 15 sec/°. After the initial structure was obtained it was refined using least squares until a goodness of fit of 1.028 and a maximum shift/error of 0.001 was attained.

From the Table 3.12 below, the structure solves in a triclinic crystal system and P-1 space group with the angles  $\alpha = 63.602(5)^\circ$ ,  $\beta = 79.518(6)^\circ$ ,  $\gamma = 69.225(5)^\circ$  and the sides  $a = 11.5088(8) \text{ \AA}$ ,  $b = 12.9628 \text{ \AA}$  and  $c = 14.3599(10) \text{ \AA}$ .

The  $R_1$  value is 3.74%. This shows that the model fits the data very well, thus the structure is a very good one.

**Table 3.12:** Crystallographic data of 2,2-*cis*-[Rh<sub>2</sub>(NPhCOCH<sub>3</sub>)<sub>4</sub>]·NC({2-CH<sub>3</sub>}C<sub>6</sub>H<sub>4</sub>)

Crystal Dimensions	
Crystal System	Triclinic
Space Group	P-1
Unit Cell Parameters	a = 11.5088(8) Å
	b = 12.9628(9) Å
	c = 14.3599(10) Å
	α = 63.602(5)°
	β = 79.518(6)°
	γ = 69.225(5)°
	V = 1793.4(3) Å <sup>3</sup>
Exposure Temperature	-50.0 °C
Exposure Rate	15.0 sec/°
R1	0.0374
R (All reflections)	0.0493
wR2 (All reflections)	0.0990
Goodness of Fit	1.028
Max Shift/Error	0.001

Figures 3.53 and 3.54 below show an ORTEP and packing diagram of 2,2-*cis*-[Rh<sub>2</sub>(N(C<sub>6</sub>H<sub>5</sub>)COCH<sub>3</sub>)<sub>4</sub>]·NC({2-CH<sub>3</sub>}C<sub>6</sub>H<sub>4</sub>) respectively. Hydrogen atoms are shown as small spheres.

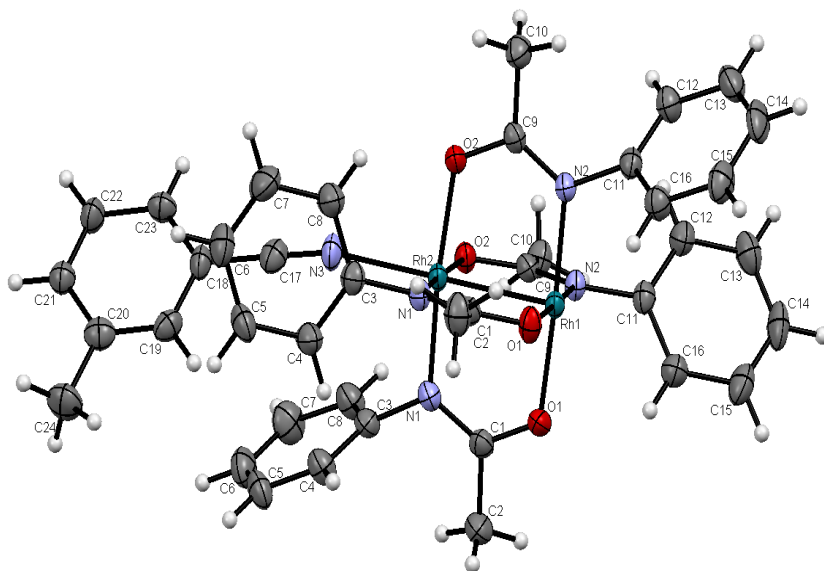


**Figure 3.53:** ORTEP of  $2,2\text{-}cis[\text{Rh}_2(\text{N}(\text{C}_6\text{H}_5)\text{COCH}_3)_4] \cdot \text{NC}(\{2\text{CH}_3\}\text{C}_6\text{H}_4)$

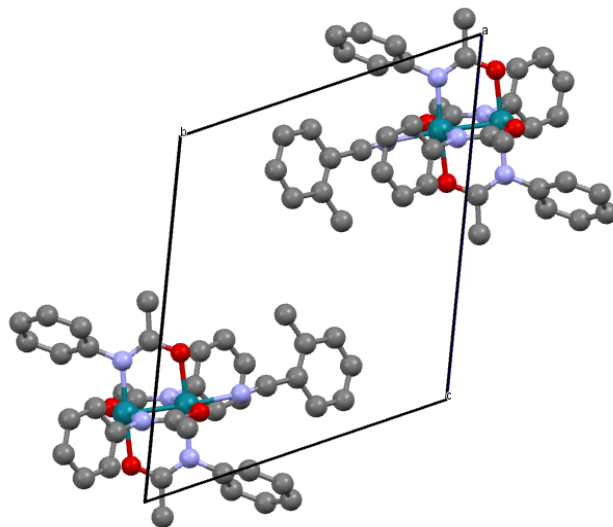


**Figure 3.54:** Packing diagram of  $2,2\text{-}cis\text{-}[\text{Rh}_2(\text{N}(\text{C}_6\text{H}_5)\text{COCH}_3)_4] \cdot \text{NC}(\{2\text{-CH}_3\}\text{C}_6\text{H}_4)$  looking on the  $b$ - axis. Hydrogen atoms are eliminated for clarity.

2, 2-*cis*-[Rh<sub>2</sub>(NPhCOCH<sub>3</sub>)<sub>4</sub>]·NC({2-CH<sub>3</sub>}C<sub>6</sub>H<sub>4</sub>)

*M*-TOLUNITRILE (One Equivalent)

A successful structure was solved using a crystal grown from methanol. Among all the other solvents used, methanol was the solvent that grew X-ray quality crystals. Some other solvents grew crystals but none of those crystals diffracted properly. H<sub>2</sub>O grew crystals that appeared to be of X-ray quality but they were extremely tiny and thin. This structure had the same interesting feature as that of *o*-tolunitrile above. The nitrile attached to just one axial site instead of the two axial sites of the rhodium core when two equivalents of the nitrile were used in the complexation.

Thus, in attempts to growing two equivalents, one equivalent of the nitrile was grown instead. See Experimental in Chapter 2 for details.

A single crystal was selected from the crystals obtained from methanol. This was done under a microscope of a magnification of 1. The single crystal was then mounted on a Mitogen loop by using a mounting pin and securing it unto a goniometer in the diffractometer.

The X-ray data for the crystal was collected using Crystal Clear-SM Auto program and the structure was solved using Crystal Structure SM Auto program(SIR 92).<sup>16,18</sup> The data were collected at a temperature of 20 ± 1°C and the crystal exposure time to the X-ray beam was 15 sec/°. After the initial structure was obtained it was refined using least squares until a goodness of fit of 1.058 and a maximum shift/error of 0.001 was attained.



From the Table 3.13 below, the structure solves in an orthorhombic crystal system and a Pnma space group with the angles  $\alpha = \beta = \gamma = 90^\circ$  and the sides  $a = 15.3319(14) \text{ \AA}$ ,  $b = 18.3248(16) \text{ \AA}$  and  $c = 12.9564(12) \text{ \AA}$ . The  $R_1$  value is 4.19%. This shows that the model fits the data very well.

**Table 3.13:** Crystallographic data of 2, 2-*cis*-[Rh<sub>2</sub>(NPhCOCH<sub>3</sub>)<sub>4</sub>]·NC({3-CH<sub>3</sub>}C<sub>6</sub>H<sub>4</sub>)

Crystal Dimensions	
Crystal System	Orthorhombic
Space Group	Pnma
Unit Cell Parameters	$a = 15.3319(14) \text{ \AA}$
	$b = 18.3248(16) \text{ \AA}$
	$c = 12.9564(12) \text{ \AA}$
	$\alpha = 90.000^\circ$
	$\beta = 90.000^\circ$
	$\gamma = 90.000^\circ$
	$V = 3640(6) \text{ \AA}^3$
Exposure Temperature	-50.0 °C
Exposure Rate	15.0 sec/°
R1	0.0419
R (All reflections)	0.0675
wR2 (All reflections)	0.0882
Goodness of Fit	1.058
Max Shift/Error	0.001

Figures 3.55 and 3.56 below show an ORTEP and a packing diagram of 2,2-*cis*- $[\text{Rh}_2(\text{N}(\text{C}_6\text{H}_5)\text{COCH}_3)_4] \cdot \text{NC}(\{3\text{-CH}_3\}\text{C}_6\text{H}_4)$  respectively. Hydrogen atoms are shown as small spheres.

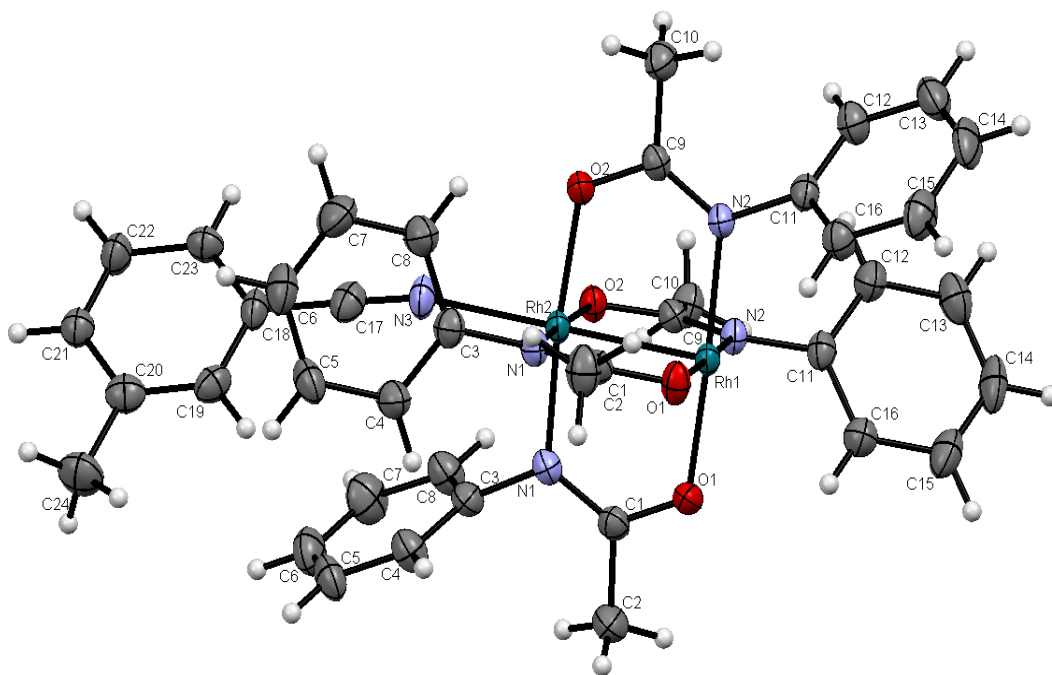


**Figure 3.55:** ORTEP of 2,2-*cis*- $[\text{Rh}_2(\text{N}(\text{C}_6\text{H}_5)\text{COCH}_3)_4] \cdot \text{NC}(\{3\text{-CH}_3\}\text{C}_6\text{H}_4)$

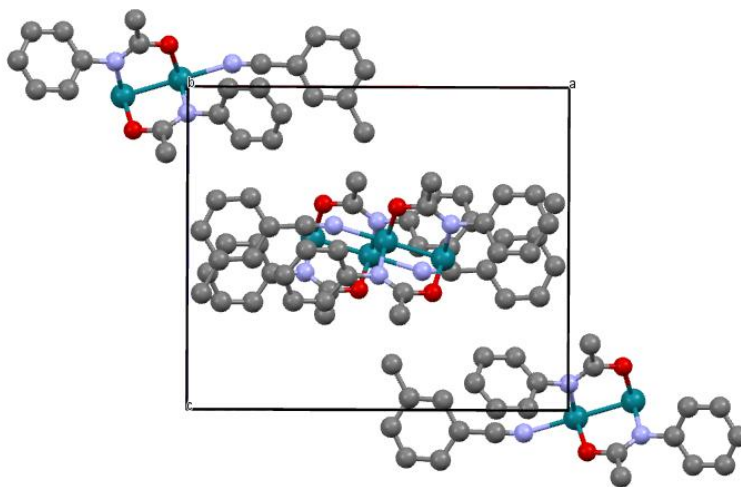


**Figure 3.56:** Packing diagram of 2,2-*cis*-[Rh<sub>2</sub>(N(C<sub>6</sub>H<sub>5</sub>)COCH<sub>3</sub>)<sub>4</sub>]·NC({3-CH<sub>3</sub>}C<sub>6</sub>H<sub>4</sub>) looking on the b- axis. Hydrogen atoms are eliminated for clarity.



*P*-TOLUNITRILE (Two Equivalents)

A successful structure was solved using a crystal grown from hexane. Among all the other solvents used, hexane was the solvent that grew X-ray quality crystals. Some other solvents grew crystals but none of those crystals diffracted properly. The nitrile attached to the two axial sites of the rhodium core similar to the benzonitrile when two equivalents of the nitrile were used in the complexation process.

A single crystal was selected from the crystals obtained from hexane. This was done under a microscope of a magnification of 1. This single crystal was then mounted on a Mitogen loop by using a mounting pin and securing the crystal unto a goniometer in the diffractometer.

The data for the crystal was collected using Crystal Clear-SM Auto program and the structure was solved using Crystal Structure SM Auto program (SIR92).<sup>16,18</sup> The data were collected at a temperature of  $-50 \pm 1^\circ \text{C}$  and the crystal exposure time to the X-ray beam was 15 sec/ $^\circ$ . After the initial structure was obtained it was refined using least squares until a goodness of fit of 0.918 and a maximum shift/error of 0.01 was attained.

From Table 3.14 below, the structure solves in a monoclinic crystal system and  $P2_1/c$  space group with the angles  $\alpha=\gamma= 90^\circ, \beta= 92.932(7)^\circ$  and the sides  $a= 14.5023(11) \text{ \AA}$ ,  $b=10.3868(8) \text{ \AA}$  and  $c=19.4877(15) \text{ \AA}$ .

The  $R_1$  value is 4.32%. This shows that the model fits the data very well, thus the structure is a very good one.

**Table 3.14:** Crystallographic data of 2, 2-*cis*-[Rh<sub>2</sub>(NPhCOCH<sub>3</sub>)<sub>4</sub>]·NC({4-CH<sub>3</sub>}C<sub>6</sub>H<sub>4</sub>)

Crystal Dimensions	
Crystal System	Monoclinic
Space Group	P2 <sub>1</sub> /c
Unit Cell Parameters	a = 14.5023(11) Å
	b = 10.3868(8) Å
	c = 19.4877(15) Å
	α = 90.000°
	β = 92.932(7)°
	γ = 90.000°
	V = 2931.6(4) Å <sup>3</sup>
Exposure Temperature	-50.0 °C
Exposure Rate	15.0 sec/°
R1	0.0432
R (All reflections)	0.0525
wR2 (All reflections)	0.1229
Goodness of Fit	0.916
Max Shift/Error	0.01

Figures 3.57 and 3.58 below show an ORTEP and a packing diagram of 2,2-*cis*-[Rh<sub>2</sub>(N(C<sub>6</sub>H<sub>5</sub>)COCH<sub>3</sub>)<sub>4</sub>]·NC({4-CH<sub>3</sub>}C<sub>6</sub>H<sub>4</sub>) respectively. Hydrogen atoms are shown as small spheres.

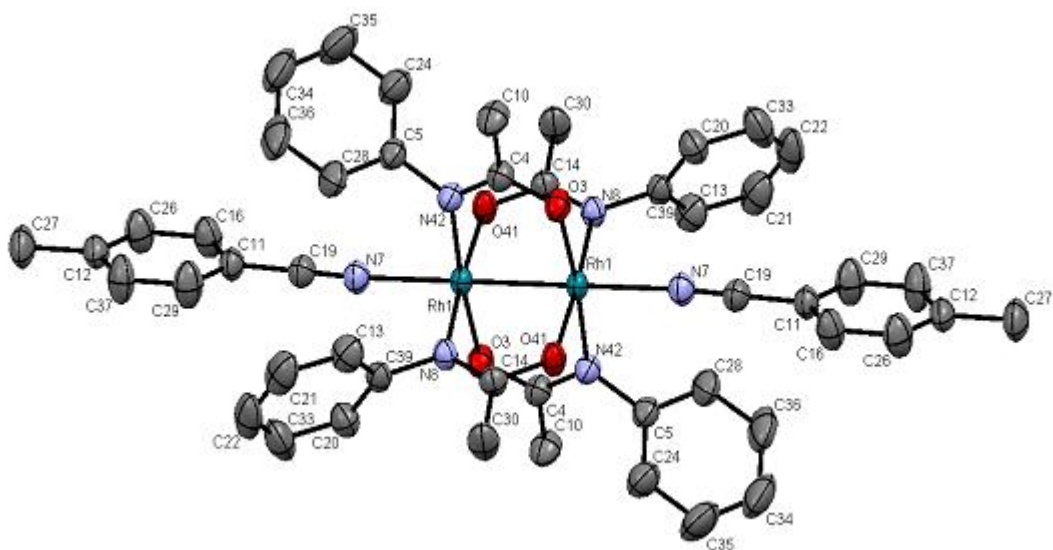


**Figure 3.57:** ORTEP of 2,2-*cis*-[Rh<sub>2</sub>(N(C<sub>6</sub>H<sub>5</sub>)COCH<sub>3</sub>)<sub>4</sub>]·NC({4-CH<sub>3</sub>}C<sub>6</sub>H<sub>4</sub>)

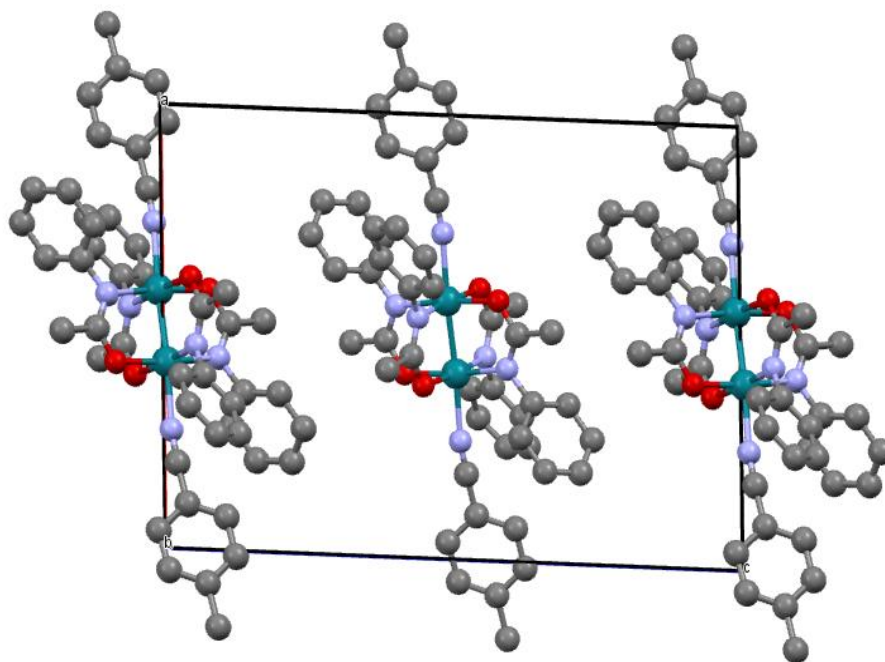


**Figure 3.58:** Packing diagram of 2,2-*cis*-[Rh<sub>2</sub>(N(C<sub>6</sub>H<sub>5</sub>)COCH<sub>3</sub>)<sub>4</sub>]·NC({4-CH<sub>3</sub>}C<sub>6</sub>H<sub>4</sub>) looking on the b- axis. Hydrogen atoms are eliminated for clarity.

2, 2- *cis*-[Rh<sub>2</sub>(NPhCOCH<sub>3</sub>)<sub>4</sub>]·NC({2-CH<sub>3</sub>}C<sub>6</sub>H<sub>4</sub>)

*O*-TOLUNITRILE (Two Equivalents)

A successful structure was solved using a crystal that grew from methanol. Among all the other solvents used, methanol was the solvent that grew X-ray quality crystals. Some other solvents grew crystals, but none of those crystals diffracted properly. The nitrile attached to the two axial sites of the rhodium core similar to the benzonitrile when 200 equivalents of the nitrile were used in the complexation process. The reason why 200 equivalents of nitrile were used before it attached to both axial sites can be explained with Le Chatelier's principle. That is, when more reactants are added, more products are formed which is indicative of the formation of diadducts.

A single crystal was selected from the crystals obtained from methanol. This was done under a microscope of a magnification of 1. This single crystal was then mounted on a Mitogen loop by using a mounting pin and securing the crystal unto a goniometer in the diffractometer.

The data for the crystal was collected using Crystal Clear-SM Auto program and the structure was solved using Crystal Structure SM Auto program (SIR92).<sup>16,18</sup> The data were collected at a temperature of  $-50 \pm 1^\circ \text{C}$  and the crystal exposure time to the X-ray beam was 15 sec/ $^\circ$ . After the initial structure was obtained it was refined using least squares until a goodness of fit of 1.070 and a maximum shift/error of 0.001 was attained.

From Table 3.15 below, the structure solves in a monoclinic crystal system and P2<sub>1</sub>/n space group with the angles  $\alpha = \gamma = 90^\circ$ ,  $\beta = 100.868(7)^\circ$  and the sides  $a = 10.3625(8) \text{ \AA}$ ,  $b = 10.0489(7) \text{ \AA}$  and  $c = 21.6110(16) \text{ \AA}$ .

The  $R_1$  value is 3.22 %. This shows that the model fits the data very well, thus the structure is a very good one.

**Table 3.15:** Crystallographic data of 2, 2-*cis*-[Rh<sub>2</sub>(NPhCOCH<sub>3</sub>)<sub>4</sub>]·NC({2-CH<sub>3</sub>}C<sub>6</sub>H<sub>4</sub>)

Crystal Dimensions	
Crystal System	Monoclinic
Space Group	P2 <sub>1</sub> /n
Unit Cell Parameters	a = 10.3625(8) Å
	b = 10.0489(7) Å
	c = 21.6110(16) Å
	$\alpha = 90.000^\circ$
	$\beta = 100.868(7)^\circ$
	$\gamma = 90.000^\circ$
	V = 2210.0(3) Å <sup>3</sup>
Exposure Temperature	-50.0 °C
Exposure Rate	15.0 sec/°
R1	0.0322
R (All reflections)	0.0399
wR2 (All reflections)	0.0726
Goodness of Fit	1.070
Max Shift/Error	0.001



Figures 3.59 and 3.60 below show an ORTEP and a packing diagram of 2,2-*cis*- $[\text{Rh}_2(\text{N}(\text{C}_6\text{H}_5)\text{COCH}_3)_4] \cdot \text{NC}(\{2\text{-CH}_3\}\text{C}_6\text{H}_4)$  respectively. Hydrogens are shown as small spheres.

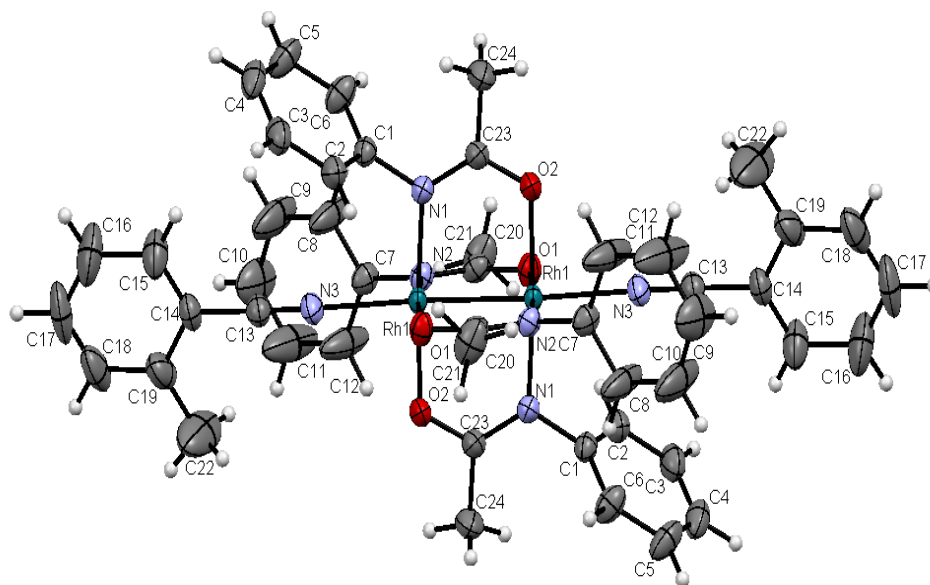


**Figure 3.59:** ORTEP of 2,2-*cis*- $[\text{Rh}_2(\text{N}(\text{C}_6\text{H}_5)\text{COCH}_3)_4] \cdot \text{NC}(\{2\text{-CH}_3\}\text{C}_6\text{H}_4)$

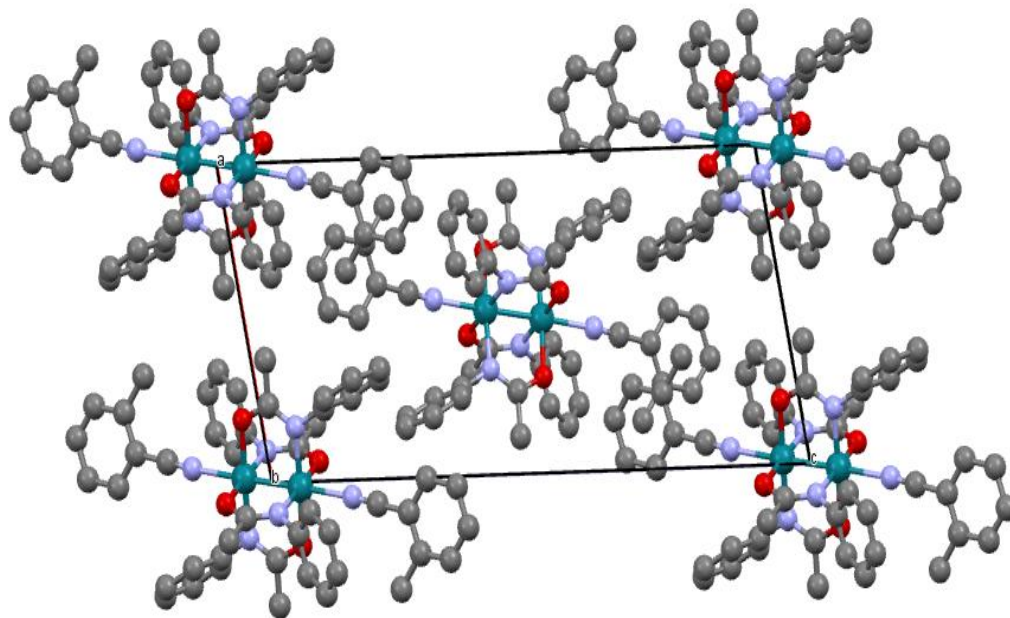


**Figure 3.60:** Packing diagram of 2,2-*cis*-[Rh<sub>2</sub>(N(C<sub>6</sub>H<sub>5</sub>)COCH<sub>3</sub>)<sub>4</sub>]·NC({2-CH<sub>3</sub>}C<sub>6</sub>H<sub>4</sub>) looking on the b-axis. Hydrogen atoms are eliminated for clarity.



*M*-TOLUNITRILE (Two Equivalents)

A successful structure was solved using a crystal that grew from methanol. Among all the other solvents used, methanol was the solvent that grew X-ray quality crystals. Some other solvents grew crystals but none of those crystals diffracted properly. The nitrile attached to the two axial sites of the rhodium core similar to the benzonitrile when 200 equivalents of the nitrile were used in the complexation process.

The reason why 200 equivalents of nitrile were used before it attached to both axial sites can be explained with Le Chatelier's principle. That is, when more reactants are added, more products are formed. This is indicative of the formation of diadducts. Thus when two equivalents of some nitriles are added, only one coordinates to the axial site. However, when a large excess of the nitrile is added, two nitriles coordinate; one to each axial site.

A single crystal was selected from the crystals obtained from methanol. This was done under a microscope of a magnification of 1. This single crystal was then mounted on a Mitogen loop by using a mounting pin and securing the crystal unto a goniometer in the diffractometer.

The data for the crystal were collected using Crystal Clear-SM Auto program and the structure was solved using Crystal Structure SM Auto program (SHELXL97).<sup>16,19</sup> The data were collected at a temperature of  $-50 \pm 1^\circ \text{C}$  and the crystal exposure time to the X-ray beam was 15 sec/°. After the initial structure was obtained it was refined using least squares until a goodness of fit of 1.077 and a maximum shift/error of 0.001 was attained.

From Table 3.16 below, the structure solves in a triclinic crystal system and P-1 space group with the angles  $\alpha=117.562(8)^\circ$ ,  $\beta=103.061(7)^\circ$ ,  $\gamma=101.562(7)^\circ$ , and the sides  $a=10.849(3) \text{ \AA}$ ,  $b=11.530(3) \text{ \AA}$  and  $c=12.259(3) \text{ \AA}$ .

The  $R_1$  value is 4.85 %. This shows that the model fits the data very well, thus the structure is a very good one.

**Table 3.16:** Crystallographic data of 2, 2-*cis*-[Rh<sub>2</sub>(NPhCOCH<sub>3</sub>)<sub>4</sub>]·NC({3-CH<sub>3</sub>}C<sub>6</sub>H<sub>4</sub>)

Crystal Dimensions	
Crystal System	Triclinic
Space Group	P-1
Unit Cell Parameters	a = 10.849(3) Å
	b = 11.530(3) Å
	c = 12.259(3) Å
	$\alpha = 117.562(8)^\circ$
	$\beta = 103.061(7)^\circ$
	$\gamma = 101.562(7)^\circ$
	V = 1238.9(6) Å <sup>3</sup>
Exposure Temperature	-50.0 °C
Exposure Rate	15.0 sec/°
R1	0.0485
R (All reflections)	0.0501
wR2 (All reflections)	0.1326
Goodness of Fit	1.077
Max Shift/Error	0.001

Figures 3.61 and 3.62 below show an ORTEP and a packing diagram of 2,2-*cis*- $[\text{Rh}_2(\text{N}(\text{C}_6\text{H}_5)\text{COCH}_3)_4] \cdot \text{NC}(\{3\text{-CH}_3\}\text{C}_6\text{H}_4)$  respectively. Hydrogen atoms are shown as small spheres.

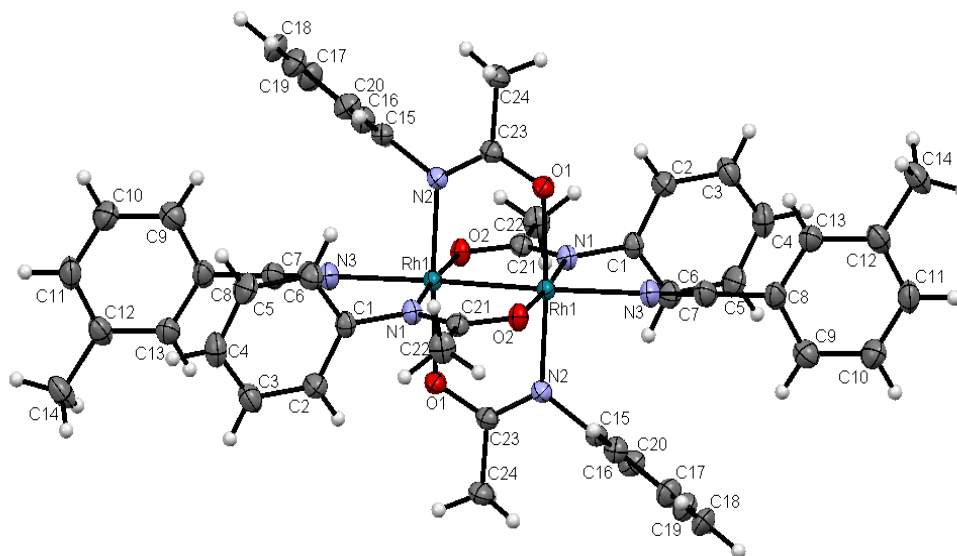


**Figure 3.61:** ORTEP of 2,2-*cis*- $[\text{Rh}_2(\text{N}(\text{C}_6\text{H}_5)\text{COCH}_3)_4] \cdot \text{NC}(\{3\text{-CH}_3\}\text{C}_6\text{H}_4)$

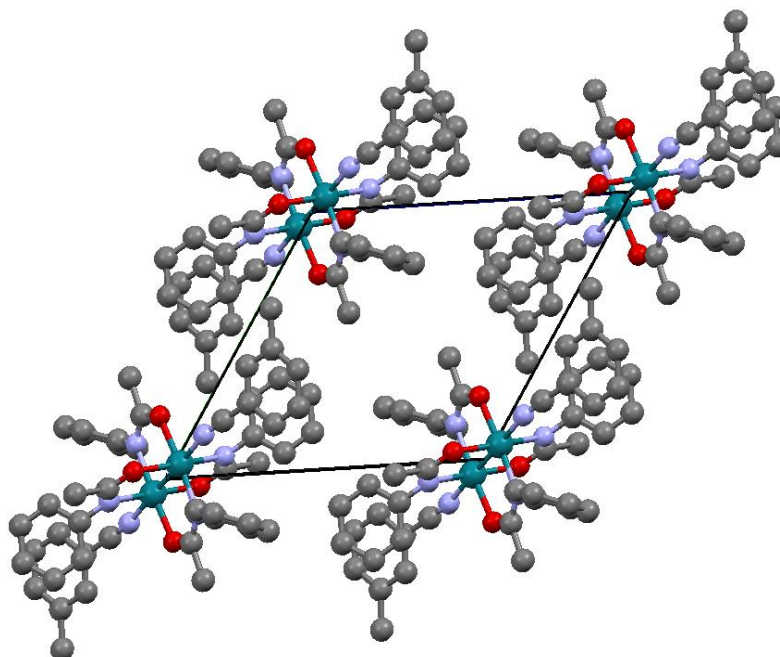


**Figure 3.62:** Packing diagram of 2,2-*cis*-[Rh<sub>2</sub>(N(C<sub>6</sub>H<sub>5</sub>)COCH<sub>3</sub>)<sub>4</sub>]·NC({3-CH<sub>3</sub>}C<sub>6</sub>H<sub>4</sub>) looking along the b-axis. Hydrogen atoms are eliminated for clarity.

The following observations are made from Table 3.16 below:

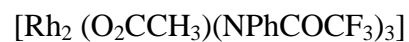
- The Rh-Rh bond distances of all the complexes are consistent (averaging 2.42Å) similar to Rh-Rh bond distances of other 2,2-*cis*-[Rh<sub>2</sub>(NPhCOCH<sub>3</sub>)<sub>4</sub>]·2NCC<sub>6</sub>H<sub>5</sub> complexes.
- The Rh-Rh-N bond angle of 1equivalent ortho- tolunitrile complex is smaller (176.03(8)°) than two equivalents ortho-tolunitrile (177.45(7)°), whereas that of the one equivalent meta-tolunitrile complex is larger (179.87(14)°) than the two equivalent meta-tolunitrile complex (178.04(7)°).
- All the complexes of two equivalents have similar Rh-Rh-N bond angles.
- The Rh-N-C bond angles of the one equivalent complexes of ortho-tolunitrile (162.5(3)°) and meta-tolunitrile (162.7(5)°) are smaller than their corresponding two equivalent complexes of ortho-tolunitrile (173.4(3)°) and meta-tolunitrile (164.5(5)°). Thus the bond angles for the complexes with two equivalents of nitriles are close to 180°. This is

indicative that there is a competition for the attachment of the nitriles when there are two equivalents but no competition for the attachment of the nitrile when there is one equivalent.  $\pi$ - back-bonding is coming out of the  $\pi^*$  orbital from the rhodium species.

- The C-N bond distances of the complexes with two equivalents of the nitriles are not distinctly different from each other (averagely about 1.137Å) but the C-N bond distances of the complexes of both ortho- tolunitrile and meta-tolunitrile with one equivalent of the nitrile are significantly longer; 1.153(6)Å and 1.150(8)Å respectively than the C-N bond distance of the complexes of ortho-tolunitrile (1.138(4)Å) and meta-tolunitrile (1.138(7)Å) with two equivalents of the nitrile.

**Table 3.17:** The bond angles and bond length of interest in complexes of 2,2-*cis*-Rh<sub>2</sub>(N(C<sub>6</sub>H<sub>5</sub>)COCH<sub>3</sub>)<sub>4</sub>

COMPLEX	Rh-Rh (Å)	Rh-Rh-N(°)	Rh-N-C(°)	C-N (Å)
Ortho-tolunitrile(1eq)	2.4078(4)	176.03(8)	162.5(3)	1.153(6)
Ortho-tolunitrile(2eq)	2.4342(3)	177.45(7)	173.4(3)	1.138(4)
Meta-tolunitrile(1eq)	2.4087(8)	179.87(14)	162.7(5)	1.150(8)
Meta-tolunitrile(2eq)	2.4249(6)	178.04(7)	164.5(5)	1.138(7)
Para-tolunitrile(2eq)	2.4342(4)	176.43(8)	171.6(3)	1.136(5)
Benzonitrile(2eq)	2.4322(3)	176.96(5)	167.14(15)	1.135(3)



[Rh<sub>2</sub>(O<sub>2</sub>CCH<sub>3</sub>)(NPhCOCF<sub>3</sub>)<sub>3</sub>] has been synthesized. The product that was isolated shows a synthesis of [Rh<sub>2</sub>(O<sub>2</sub>CCH<sub>3</sub>)(NPhCOCF<sub>3</sub>)<sub>3</sub>] instead of [Rh<sub>2</sub>(NPhCOCF<sub>3</sub>)<sub>4</sub>] after characterization by <sup>1</sup>HNMR and X-ray crystallography.

A successful structure was solved using a crystal that grew from hexane. Among all the other solvents used, hexane was the solvent that grew X-ray quality crystals. Some other solvents



grew crystals, but none of those crystals diffracted properly. The nitrile attached to the two axial sites of the rhodium core when two equivalents of the nitrile were used in the complexation process.

A single crystal was selected from the crystals obtained from hexane. This was done under a microscope of a magnification of 1. This single crystal was then mounted on a Mitogen loop by using a mounting pin and securing the crystal unto a goniometer in the diffractometer.

The data for the crystal were collected using Crystal Clear-SM Auto program and the structure was solved using Crystal Structure SM Auto program (SIR 92).<sup>16,18</sup> The data were collected at a temperature of  $-50 \pm 1^\circ \text{C}$ , and the crystal exposure time to the X-ray beam was 15 sec/ $^\circ$ .

The reason for the isolation of this product could be that this was the product that was crystallized successfully of the many products obtained after the reaction. Fractions one and two might have the tetra substituted product because that has been the trend of the rhodium phenylacetamide. In our case, crystals grew out of sample from fraction 15 (more polar), thus there is a likelihood that this synthesis produced a tetra substituted product but we were not able to crystallize it.

Various attempts have been made to solve this structure but the best results obtained so far shows that the R1 value is 8.50 that does not show a very good model to data fit.

However, upon further examination of the initial spots, the spots were too close together indicating perhaps twinning. It is a type of pseudo-merohedral twin. The crystal was also seen as split or cracked. It also looked like a system with two interpenetrating lattices. After the initial

structure was obtained it was refined using least squares until a goodness of fit of 0.976 and a maximum shift/error of 0.03 was attained.

From Table 3.17 below, the structure solves in a monoclinic crystal system and P2/m space group with unit cell dimensions:  $\alpha=90.000^\circ$ ,  $\beta= 107.113(8)^\circ$ ,  $\gamma= 90.000^\circ$ ,  $a=21.843(2) \text{ \AA}$ ,  $b=19.9797(19) \text{ \AA}$  and  $c=20.797(2) \text{ \AA}$ .

The  $R_1$  value is 8.50 %. This shows that the model fits the data but not very well, thus the structure is a fairly good one.

**Table 3.18:** Crystallographic data of  $[\text{Rh}_2(\text{O}_2\text{CCH}_3)(\text{NPhCOCF}_3)_3] \cdot 2\text{NCC}_6\text{H}_5$ 

Crystal Dimensions	
Crystal System	Monoclinic
Space Group	P2/m
Unit Cell Parameters	a = 21.843(2) Å
	b = 19.9797(19) Å
	c = 20.797(2) Å
	$\alpha = 90.000^\circ$
	$\beta = 107.113(8)^\circ$
	$\gamma = 90.000^\circ$
	V = 8674.3(15) Å <sup>3</sup>
Exposure Temperature	-50.0 °C
Exposure Rate	15.0 sec/°
R1	0.0850
wR2 (All reflections)	0.2638
Goodness of Fit	0.976
Max Shift/Error	0.03

Figures 3.63 and 3.64 below show an ORTEP and a packing diagram of  $[\text{Rh}_2(\text{O}_2\text{CCH}_3)(\text{NPhCOCF}_3)_3] \cdot 2\text{NCC}_6\text{H}_5$  respectively. Hydrogen atoms are shown as small spheres

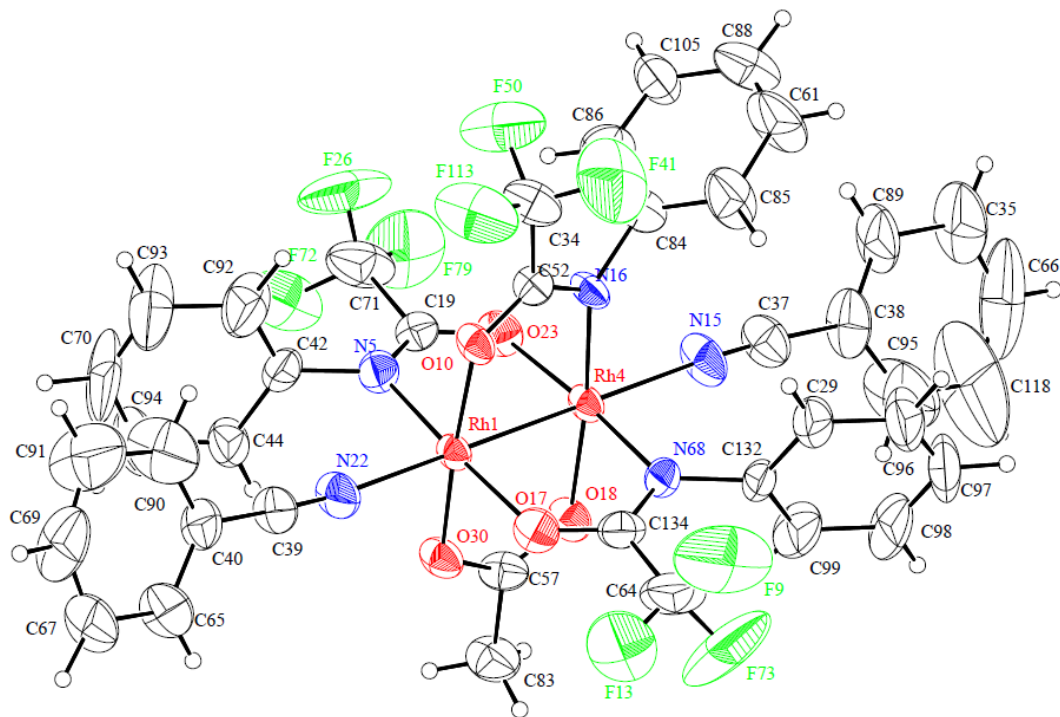


**Figure 3.63:** ORTEP of  $[\text{Rh}_2 (\text{O}_2\text{CCH}_3)(\text{NPhCOCF}_3)_3] \cdot 2\text{NCC}_6\text{H}_5$ .

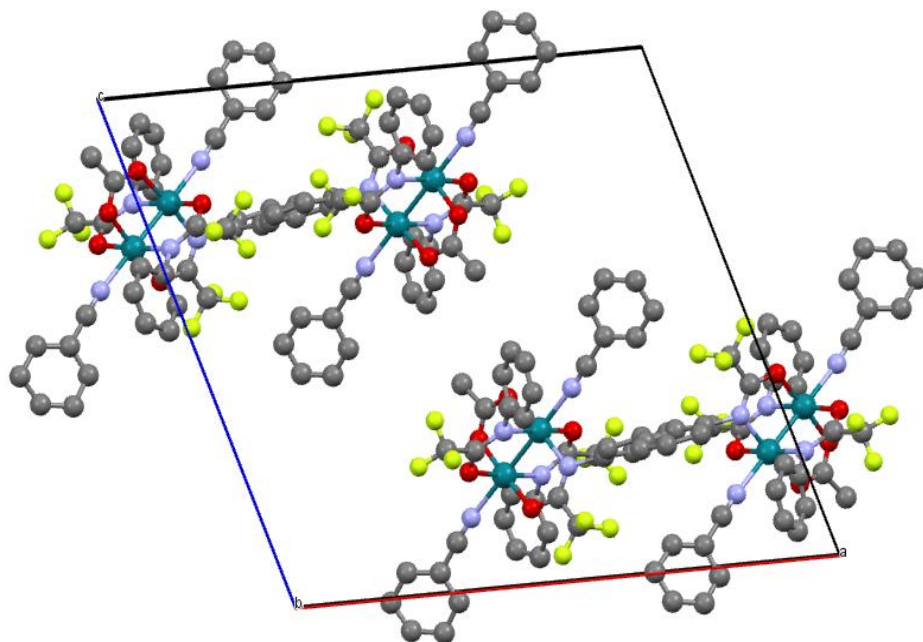


**Figure 3.64:** Packing diagram of  $[\text{Rh}_2 (\text{O}_2\text{CCH}_3)(\text{NPhCOCF}_3)_3] \cdot 2\text{NCC}_6\text{H}_5$  looking along the b-axis.

## CHAPTER 4

### CONCLUSION

Five new compounds ( $2,2\text{-cis-}[\text{Rh}_2(\text{NPhCOCH}_3)_4]\cdot 2\text{NCC}_6\text{H}_5$ ;  $2,2\text{-cis-}[\text{Rh}_2(\text{NPhCOCH}_3)_4]\cdot \text{NC}(\{2\text{-CH}_3\}\text{C}_6\text{H}_4)$ ;  $2,2\text{-cis-}[\text{Rh}_2(\text{NPhCOCH}_3)_4]\cdot \text{NC}(\{3\text{-CH}_3\}\text{C}_6\text{H}_4)$ ;  $2,2\text{-cis-}[\text{Rh}_2(\text{NPhCOCH}_3)_4]\cdot \text{NC}(\{4\text{-CH}_3\}\text{C}_6\text{H}_4)$ ;  $[\text{Rh}_2(\text{O}_2\text{CCH}_3)(\text{NPhCOCF}_3)_3]\cdot 2\text{NCC}_6\text{H}_5$ ) have been successfully synthesized and characterized by NMR, IR, and X-ray crystallography.

The interesting thing about the structures was that when two equivalents of the nitrile were used in this complexation process for  $2, 2\text{-cis-}[\text{Rh}_2(\text{NPhCOCH}_3)_4]\cdot \text{NC}(\{2\text{-CH}_3\}\text{C}_6\text{H}_4)$  and  $2, 2\text{-cis-}[\text{Rh}_2(\text{NPhCOCH}_3)_4]\cdot \text{NC}(\{3\text{-CH}_3\}\text{C}_6\text{H}_4)$  complexes, the nitrile attached to just one axial site instead of the two axial sites of the rhodium core. However, when 200 equivalents of the nitrile was used in the complexation process, the nitrile attached to both of the axial sites of the rhodium core. The reason for this can be explained with Le Chatelier's principle. That is, when more reactants are added, more products are formed, which is indicative of the formation of diadducts.

In an attempt to synthesize  $[\text{Rh}_2(\text{NPhCOCF}_3)_4]\cdot 2\text{NCC}_6\text{H}_5$ ,  $[\text{Rh}_2(\text{O}_2\text{CCH}_3)(\text{NPhCOCF}_3)_3]\cdot 2\text{NCC}_6\text{H}_5$  was synthesized. We believe this is because this was the product that was crystallized successfully of the many products obtained after the reaction. As stated earlier in the discussion, fractions one and two might have had the tetra substituted product because that has been the trend of the rhodium phenylacetamide. In our case, crystals grew from fraction 15 (more polar), thus there is a likelihood that this synthesis produced a tetra substituted product, but we were not able to crystallize it.

Comparison of the bond angles and bond lengths of interest in complexes of 2,2-*cis*-[Rh<sub>2</sub>(N(C<sub>6</sub>H<sub>5</sub>)COCH<sub>3</sub>)<sub>4</sub>] also revealed similarities as well as significant differences between complexes with one equivalent of nitrile as opposed to complexes with two equivalents of nitriles.

These similarities and differences are listed below:

- The Rh-Rh bond distances of all the complexes were consistent (averaging 2.42Å) similar to Rh-Rh bond distances of other 2,2-*cis*-[Rh<sub>2</sub>(NPhCOCH<sub>3</sub>)<sub>4</sub>]·2NCC<sub>6</sub>H<sub>5</sub> complexes.
- The Rh-Rh-N bond angle of 1equivalent ortho- tolunitrile complex was smaller (176.03(8)°) than 2 equivalents ortho-tolunitrile (177.45(7)°) whereas that of the 1 equivalent meta-tolunitrile complex was larger (179.87(14)°) than the 2 equivalent meta-tolunitrile complex (178.04(7)°).
- All the complexes of 2 equivalents had similar Rh-Rh-N bond angles.
- The Rh-N-C bond angles of the 1 equivalent complexes of ortho-tolunitrile (162.5(3)°) and meta-tolunitrile (162.7(5)°) were smaller than their corresponding 2 equivalent complexes of ortho-tolunitrile (173.4(3)°) and meta-tolunitrile (164.5(5)°). Thus the bond angles for the complexes with two equivalents of nitriles were close to 180°. This is indicative that there is a competition for the attachment of the nitriles when there are two equivalents but no competition for the attachment of the nitrile when there is one equivalent.  $\pi$  back- bonding is coming out of the  $\pi^*$  orbital from the rhodium species.
- The C-N bond distances of the complexes with 2 equivalents of the nitriles were not distinctly different from each other (averagely about 1.137Å) but the C-N bond distances of the complexes of both ortho- tolunitrile and meta-tolunitrile with 1 equivalent of the nitrile were significantly longer; 1.153(6) Å and 1.150(8) Å respectively than the C-N

bond distance of the complexes of ortho-tolunitrile (1.138(4) Å) and meta-tolunitrile (1.138(7) Å) with 2 equivalents of the nitrile.

This information together with the library of data we are collecting for nitriles of the other isomers of  $[\text{Rh}_2(\text{NPhCOCH}_3)_4]$  may be used in successful understanding of the reaction between  $\text{Rh}_2\text{L}_4$  complexes and compounds that are capable of  $\sigma$  and  $\pi$ -back-bonding.

## REFERENCES

1. Cotton, F. A.; Murillo, C. A.; Walton, R. A., *Multiple bonds between Metal Atoms*. Springer Science and Business Media Inc.: 2005; p 37.
2. Cotton, F. A.; Murillo, C. A.; Walton, R. A., *Multiple bonds between Metal Atoms*. 3rd ed.; Spring Science and Business media Inc.: 2005; p 13.
3. Toreki, R. Organometallic Hypertextbook.
4. Cotton, F. A.; Murillo, C. A.; Walton, R. A., *Multiple bonds between Metal Atoms*. 3rd ed.; Spring Science and Business media Inc.: 2005; p 465.
5. Davies, H. M. L.; Beckwith, R. E. J., High Symmetry Dirhodium(II) Paddlewheel Complexes as Chiral Catalysts. *Chem.Rev.* **2003**, *103*, 2861-2903.
6. Doyle, M. P.; Zhou, Q. L.; Raab, C. E.; Roos, G. H. P.; Simonsen, S. H.; Lynch, V., Synthesis and Structures of (2,2-cis)-Dirhodium(II) Tetrakis[methyl 1-acyl-2-oxoimidazolidin-4(S)-carboxylates]. Chiral Catalysts for Highly Stereoselective Metal Carbene Transformations. *Inorg Chem* **1996**, *35*, 6064.
7. Timmons, D. J.; Doyle, M. P., Catalyst Selection for Metal Carbene Transformations. *J. Organomet. Chem.* **2001**, *617-618* (0), 98-104.
8. Brad, P. C., *Catalytic Enantioselective Insertion Of Rhodium-carbenoids into aliphatic C H bonds*. **2006**; pp 25-26.
9. (a) Dennis, A. M.; Howard, R. A.; Lançon, D.; M., K. K.; L., B. J., A Dirhodium(II) Complex with Trifluoroacetamido Ligands. *Chem. Commun.* **1982**, 399; (b) Kadish, K. M.; Lançon, D.; Dennis, A. M.; Bear, J. L., Electrochemistry of (TPP)Mo(O)(OCH<sub>3</sub>) and (TPP)Mo(O) in Dichloromethane. *Inorg. Chem.* **1982**, *21* (8), 2987.



10. Bear, J. L.; Zhu, T. P.; Malinski, T.; Dennis, A. M.; Kadish, K. M., Electrochemical Characterization of a Rhodium(II) Dimer with N-phenylacetamido Bridging Ligands. *Inorg. Chem.* **1984**, *23* (6), 674.
11. Eagle, C. T.; Farrar, D. G.; Holder, G. N.; Pennington, W. T.; Bailey, R. D., Structural and Electronic Properties of (2,2-trans)-dirhodium(II) tetrakis(N-phenylacetamidate). *J. Organomet. Chem.* **2000**, *596* (1–2), 90-94.
12. Doyle, M. P.; Raab, C. E.; Roos, G. H. P.; Lynch, V.; S.H., S., (4,0)-Dirhodium(II) Tetrakis[methyl 1-acetyl-2-oxoimidazolidin-4(S)-carboxylate]. Implications for the Mechanism of Ligand Exchange Reactions. *Inorg Chim Acta* **1997**, *266*, 13.
13. Zink, L. C., *Synthesis of N-(substituted phenyl) acetamides*. East Tennessee State University: **2012**.
14. Eagle, C. T.; Farrar, D. G.; Pfaff, C. U.; Davies, J. A.; Kluwe, C.; Miller, L.,  $\pi$ -Back Bonding in Bis(isonitrile) Complexes of Rhodium(II) Acetate: Structural Analogs for Rhodium Carbenoids. *Organometallics* **1988**, *17*, 4523.
15. Sands, D. E., *Introduction to Crystallography*. Dover Publications, Inc.: Mineola, NY., 1994; p 127.
16. Rigaku *Crystal Structure Analysis Package*, CrystalStructure 4.0; New Trails Dr. The Woodlands **2000-2010**.
17. Burla, M. C.; Caliendo, R.; Camalli, M.; Carrozzini, B.; Cascarona, G. L.; De Caro, L.; Giocovazzo, C.; Polidori, G.; Spagna, R. *SIR 2004*, **2005**.
18. Altomare, A.; Cascarona, G.; Giocovazzo, C.; Guagliardi, A.; Burla, M.; Polidori, G.; Camalli, M. *SIR 92*, **1994**.

19. Sheldrick, G. M. *SHELX97*, Cambridge university, **1997**.

## VITA

### FREDRICKA FRANCISCA QUARSHIE

- Personal Data:** Date of Birth: February 23, 1981  
Place of Birth: Saltpond, Central Region, Ghana, West Africa  
Marital Status: Widowed
- Education:** M.S. Chemistry, East Tennessee State University (ETSU), Johnson City, Tennessee 2013  
B.Sc Chemistry, University of Cape Coast, Ghana, West Africa 1999-2013
- Professional Experience:** Graduate Teaching Assistant, College of Arts and Sciences, East Tennessee State University, Johnson City Tennessee, 2012-Present  
Water Treatment Chemist, Tema Oil Refinery LTD, Ghana, 2005-2011  
Chemist, Azar Chemical Industry LTD, Ghana, 2004-2005
- Publications:** Eagle, C. T.; Quarshie, F.; Ketron, M. E.; Atem-Tambe, N. "Cis-tetrakis[ $\mu$ -N-(phenyl)acetamidato]-K<sup>4</sup>N:O;K<sup>4</sup>O:N bis[(benzonitrile-KN) dirhodium(II)] (Rh-Rh)"  
Eagle, C.T.; Atem-Tambe, N.; Kpogo, K.K.; Tan, J.; Quarshie, F. "Trans-tetrakis[ $\mu$ -N-(phenyl)acetamidato]-K<sup>4</sup>N:O;K<sup>4</sup>O:N-bis[(3-methylbenzonitrile-KN) dirhodium(II)] (Rh-Rh)" Accepted with revision.
- Honors and Awards:** 2013 Outstanding Masters in Chemistry Student (ETSU)